THE EXPLORATION OF THE VALIDITY OF QUANTITATIVE *2-DEOXY-2-[FLUORINE-18] FLUORO-D-GLUCOSE* (^{18}F-FDG) POSITRON EMISSION TOMOGRAPHY/COMPUTED TOMOGRAPHY (PET/CT) TO ASSESS LUNG INFLAMMATION

LAURENCE DOMINIC VASS

Wolfson College

and

Division of Experimental Medicine and Immunotherapeutics

Department of Medicine

University of Cambridge

This thesis is submitted for the degree of

Doctor of Philosophy

November 2020

DECLARATION

This thesis is the result of my own work and includes nothing which is the outcome of work done in collaboration except as declared in the Preface and specified in the text. It is not substantially the same as any that I have submitted, or, is being concurrently submitted for a degree or diploma or other qualification at the University of Cambridge or any other University or similar institution except as declared in the Preface and specified in the text. I further state that no substantial part of my thesis has already been submitted, or, is being concurrently submitted for any such degree, diploma or other qualification at the University of Cambridge or any other University or similar institution except as declared in the Preface and specified in the text. It does not exceed the prescribed word limit for the relevant Degree Committee.

Laurence Vass

ABSTRACT

The exploration of the validity of quantitative 2-deoxy-2-[fluorine-18] fluoro-D-glucose (^{18}F-FDG) Positron Emission Tomography/Computed Tomography (PET/CT) to assess lung inflammation

Laurence Dominic Vass

Lung diseases are one of the leading causes of death in the UK; responsible for 20% of all deaths each year. Inflammation is thought to be an important driver of the pathogenesis and progression of several lung diseases. Positron emission tomography/computed tomography (PET/CT) is an imaging modality capable of providing functional and molecular imaging through detection of trace quantities of a radioactive tracer. ^{18}F-FDG is the most widely available tracer and in several small studies has been used to investigate diffuse lung diseases such as chronic obstructive pulmonary disease (COPD). These studies rely on quantification of the PET image.

Static acquisitions provide information on the biodistribution of the tracer at a single time point after administration, the standardised uptake value (SUV) is the most widely used measure of ^{18}F-FDG uptake. Dynamic acquisitions provide information on the spatial *and* temporal distribution of the tracer; linear and non-linear modelling techniques allow estimation of the metabolic rate of ^{18}F-FDG in the lung. Previous studies have used a linear method called Patlak graphical analysis, whilst non-linear compartmental models have been used more recently to estimate metabolism. However, these contending measures of pulmonary ^{18}F-FDG uptake, which are putative biomarkers of lung inflammation, have so far been disparately applied. Further, there is nascent understanding that these imaging endpoints are affected by pulmonary air and blood volume; the importance of this effect will likely depend on the disease and its severity. These issues are exacerbated by the presence of respiratory motion and the low signal- to-noise ratio achieved in PET studies. This has led to questions regarding the utility of quantitative ^{18}F-FDG PET to assess lung inflammation.

In this work, prospective and retrospective clinical studies were used to assess the clinical, biological and technical validity of ^{18}F-FDG PET imaging endpoints in several clinically relevant diseases. The central hypothesis was that pulmonary inflammation can be assessed using quantitative ^{18}F-FDG.

Using retrospective data from two complementary imaging studies, pulmonary ^{18}F-FDG uptake was investigated in COPD patients, α_1ATD patients, smokers without COPD and heathy non-smokers. The results demonstrate that the different ^{18}F-FDG imaging endpoints produce disparate findings, and this is exacerbated by the presence of varying blood and air volumes due to emphysema. Nevertheless, measures derived from Patlak analysis revealed elevated uptake consistent with the pathophysiological understanding of the disease process and further demonstrated correlation with other putative markers of inflammation hence, one could speculate that it relates to inflammation. Further, ^{18}F-FDG imaging outcomes assessed using Patlak analysis were shown to be more reliable than compartmental modelling outcomes. However, the Patlak outcomes are composite measures, not only driven by inflammation but also by pulmonary blood and air. In circumstances where differences in pulmonary blood and air volume between subjects are substantial, it may not be a suitable biomarker of inflammation, but it could be a useful marker of disease activity. Further tissue validation and independent measures of pulmonary blood are required to support its role as a marker of inflammation.

In a prospective study, dynamic ^{18}F-FDG PET scans were used to evaluate pulmonary inflammation in sarcoidosis patients and healthy controls. The results show that ^{18}F-FDG uptake was increased in sarcoidosis using Patlak analysis, whilst no difference was found using SUV or compartmental models. Preliminary findings suggest that the signal relates to inflammatory cell counts (macrophages and lymphocytes were most numerous) rather than any one specific cell line; however, further evidence is required to determine if ^{18}F-FDG uptake is driven by underlying inflammation. Consistent with previous findings, mismatch in CT and PET lung images has substantial effect on the quantitative ^{18}F-FDG outcomes; notably, Patlak outcomes were less influ-

enced than compartmental modelling.

In summary, the observations made in this work demonstrate the substantial challenges of using ^{18}F-FDG PET/CT to assess diffuse lung disease. Given the incongruity between the different imaging outcomes, these data highlight that future studies should be carefully planned with particular justification of the acquisition and analysis methods. The results of this work suggest that Patlak measures may have the most utility in diffuse lung disease. However, differences in Patlak measures should be interpreted judiciously, as they may be driven by differences in pulmonary blood and air along with inflammation; further study is required to determine if it may be a useful marker of disease activity. In contrast, no differences in pulmonary ^{18}F-FDG uptake between patients and controls were found using compartmental modelling across all studies. Equally, the SUV was found to have poor utility across studies. Future efforts to expedite the use of novel tracers that are more specific to inflammation combined with the development of improved noise reduction techniques may improve the utility of quantitative PET/CT in the context of lung inflammation.

LIST OF ABBREVIATIONS

6MWD	6 minute walk distance
α_1ATD	Alpha anti-trypsin deficiency
μ	Linear attenuation coefficient
AA	Ascending aorta
AC	Attenuation correction
ACE	Angiotensin converting enzyme
ADE	Advanced destructive emphysema
ALI	Acute Lung Inflammation
ARDS	Acute respiratory distress syndrome
BAL	Bronchoalveloar lavage
Bq	Bequerel
CF	Cystic Fibrosis
CLE	Centrilobular emphysema
CM	Compartmental modelling
COPD	Chronic obstructive pulmonary disease
COR	Coefficient of repeatability
COV	Coefficient of variation
CT	Computed tomography
DA	Descending aorta
EANM	European Association of Nuclear Medicine
EBC	Exhaled breath condensates
EGF	Epidermal growth factor
emeans	Estimated marginal means
EVOLUTION	An Evaluation Of Losmapimod in Patients With Chronic Obstructive Pulmonary Disease (COPD) With Systemic Inflammation Stratified Using Fibrinogen
EVOLVE	Evaluation of arterial inflammation in obstructive sleep apnoea hypopnoea syndrome (OSAHs) and chronic obstructive pulmonary disease
EU	European union
FBP	Filter back projection
FDG	Flourodeoxyglucose
FEV_1	Forced expiratory volume in 1 second
FOV	Field of view
FVC	Forced vital capacity
GOLD	Global initiative for chronic obstructive lung disease
GE	General Electric
HRCT	High resolution computed tomography
hsCRP	High sensitivity C-reactive protein
HU	Hounsfield unit
IDIF	Image derived input function
IFN	Interferon
IL	Interleukine
ILD	Interstitial lung diseases
IPF	idiopathic pulmonary fibrosis
IQR	Interquartile range
K_{im}	Metabolic rate constant (compartmental modelling)
K_{ip}	Rate of FDG uptake (patlak analysis)
LLOA	Lower limit of agreement
LV	Left ventricle

MAPK	p38 mitogen-activated protein kinase
MIG	Monokine induced by gamma interferon
MMP	Matrix Metallo-Proteinases
MR	Magnetic resonance
NE	Neutrophil elastase
nK_i	Normalised K_{ip} (patlak analysis)
NOS	Nitric oxide synthase
nsHV	Never smokers (healthy volunteers)
p.a.	Post-administration
Perc15	15th percentile of Hounsfield Units distribution
PDGF	Platelet-derived growth factor
PET	Positron emission tomography
PGA	Patlak graphical analysis
PLE	Panlobular emphysema
POB	Plasma over blood
PSE	Paraseptal emphysema
r	Correlation coefficient
ROI	Region of interest
SAD	Small airways disease
SD	Standard deviation
sHV	Smokers (healthy volunteers)
SMC	Smooth muscle cell
SPECT	Single positron emission tomography
SUV	Standardised uptake value
Sv	Sievert
t	Time
TAC	Time activity curve
TDL	The Doctors Laboratory
TGF	Transforming growth factor
TNF	Tumour necrosis factor
UK	United kingdom
ULOA	Upper limit of agreement
V_a	Fractional air volume
V_b	Fractional blood volume (compartmental modelling)
V_{ss}	Steady state volume of distribution (patlak analysis)
VEGF	Vascular endothelial growth factor
WCC	White blood cell count
WBC	White blood cell
WRSS	Weights residual sum of squares

PUBLICATIONS

L Vass et al. 'Advances in PET to assess pulmonary inflammation: A systematic review.' In: European Journal of Radiology 130 (2020), p. 109182. issn: 0720-048X. *doi: https://doi.org/10.1016/j.ejrad.2020.109182* http://www.sciencedirect.com/science/article/pii/S0720048X20303715.

L Vass et al. 'Reproducibility of compartmental modelling of ^{18}F- FDG PET/CT to evaluate lung inflammation.' In: EJNMMI Physics 6.1 (2019), p. 26. issn: 2197-7364. *doi: 10.1186/s40658-019-0265-8* https://doi.org/10.1186/s40658-019-0265-8.

D L Chen... **L Vass** et al. 'Consensus recommendations on the use of (18)F-FDG PET/CT in lung disease.' eng. In: Journal of nuclear medicine : official publication, Society of Nuclear Medicine (2020). issn: 1535-5667 (Electronic). *doi: 10.2967/jnumed.120.244780*

D L Chen...**L Vass** et al. 'Quantification of Lung PET Images: Challenges and Opportunities.' In: Journal of Nuclear Medicine 58.2 (2017), pp. 201-207. issn: 0161-5505. *doi: 10.2967/jnumed.116.184796* http://jnm.snmjournals.org/lookup/doi/10.2967/jnumed.116.184796.

L Vass et al. 'Compartmental modelling of ^{18}F- FDG to assess Pulmonary Inflammation'. Best clinical abstract in conference Medical Image Understanding and Analysis (MIUA) 2018 (Southampton).

ACKNOWLEDGMENTS

There are many people I would like to thank, without whom, this work would not have been possible.

Foremost, I am indebted to my supervisor Prof. Ian Wilkinson, his sage advice from grant application through to publications, generous support and pithy observations have been instrumental in driving me to complete this work. Equally, I am extremely grateful to Fred Wilson, my industry supervisor, his insights, help navigating the logistical complexities, tremendous support, and fantastic sense of humour have helped keep me on track throughout the project.

Special mention goes to Dr Joseph Cheriyan; his advice, guidance and countless discussions with me, often at all hours, were invaluable. Also, for all our many discussions regarding the technical details, I would like to thank Dr Sarah Lee, without her helpful suggestions doubtless I would have been much more frustrated with MATLAB. A big thanks to Dr Kasia Maki-petaja for all our informal chats, keeping me laughing and making my time during the PhD the most enjoyable experience. Equally, a special thanks to Dr Marie Fisk for all her insights and explanations about lung diseases, for helping me regardless of how busy she was, and generally for being one of the most agreeable people with which to work. I am also grateful to the countless times that Liz Husband and Beverley Reynolds helped me keep organised and for knowing what I was looking for before I did, without them my studies would not have run so smoothly, and they always made me smile. So many people from the wider department deserve thanks: Dr Carmel McEniery, the nurses who were consummate professionals, Dr Nick Bird and all the radiographers in PET/CT for helping the imaging visits run smoothly and all those at the Papworth hospital particularly Dr Muhunthan Thillai for his infectious enthusiasm.

Finally, to my family, for putting up with me working at unearthly hours and who have been nothing but supportive over the last 4 years.

THESIS OVERVIEW

Chapter 1 provides an overview of diffuse lung diseases and the role of inflammation. More detailed information is provided on the two principal diseases under investigation in this work: chronic obstructive pulmonary disease (COPD) and sarcoidosis. Existing clinical measures of pulmonary disease and inflammation are introduced with emphasis on their shortcomings and the need for new biomarkers of pulmonary inflammation. A summary of the imaging methods used in diffuse lung diseases is provided. Finally, I reproduce my recently published systematic review of PET imaging of lung inflammation.

Chapter 2 details the mathematical and physics background required to understand quantitative ^{18}F-FDG PET. Each method used to estimate ^{18}F-FDG uptake is described with the mathematical derivations, where relevant. Importantly, it describes the influence of pulmonary blood and air on the ^{18}F-FDG PET imaging endpoints. The hypotheses and aims of this work are summarised at the end of the chapter.

Chapter 3 describes the methodology which is common throughout this work, including clinical measurements, image acquisition, image analysis and statistics. It includes a description of the bespoke analysis pipeline that I developed to evaluate the quantitative ^{18}F-FDG imaging endpoints. Further, I performed all statistical comparisons, as described in this chapter, in all further chapters containing data. Methods which only apply to a specific chapter are detailed in the relevant chapter.

Chapter 4 discusses the results of quantitative ^{18}F-FDG PET lung imaging in a large cohort of COPD subjects from two retrospective complementary imaging studies; which I analysed using the bespoke pipeline that I developed. Further, ^{18}F-FDG uptake is compared to α_1ATD patients, current smokers without COPD and healthy never smokers. The different quantitative ^{18}F-FDG PET imaging outcomes are compared and contrasted by evaluating their variability, repeatability, reproducibility and

relationship to clinical measurements.

In chapter 5 I hypothesised that COPD subtypes defined by visual and quantitative CT are associated with varying degrees of pulmonary inflammation as assessed by ^{18}F-FDG PET. To accomplish this, I established a collaboration with lung specialists including a thoracic radiologist from the Royal Brompton Hospital to categorise the patients using their CT scans; I then reanalysed and interpreted the PET imaging endpoints in these groups. Further, the impact of different ^{18}F-FDG PET outcomes are investigated in a COPD sub-type with the confounding influence of emphysema minimised, and compared to smokers and never-smokers.

Chapter 6 describes a prospective study of sarcoidosis patients that I designed. I was involved in all elements of this study including writing the grant application, study design, protocol development, imaging manual and optimising the PET/CT acquisition, completing the required IRAS and ARSAC documentation, completing case report forms (CRFs), attending/arranging subject visits, image analysis and interpretation. The pulmonary ^{18}F-FDG signal in sarcoidosis patients is compared to healthy controls; notably, this includes comparing ^{18}F-FDG uptake derived from both static and dynamic acquisitions, which has yet to be performed in pulmonary sarcoidosis. Further, the biological validity of the imaging biomarkers of inflammation is assessed by comparing these against clinical measures of inflammation obtained from inflammatory cell counts in bronchoalveolar lavage fluid (BALf) and plasma biomarkers of inflammation. In addition, the technical validity of ^{18}F-FDG imaging outcomes is explored by investigating the influence of respiratory motion on quantitative ^{18}F-FDG in sarcoidosis patients.

Finally, chapter 7 provides a discussion and my conclusions given the results of the studies undertaken in this work. Speculations are made on the future directions of PET/CT imaging of pulmonary inflammation and suggestions for future work are given.

CONTENTS

LIST OF FIGURES

LIST OF TABLES

1

BACKGROUND

1.1 DIFFUSE LUNG DISEASES

Respiratory disease represents a considerable burden to the healthcare system: chronic obstructive pulmonary disease (COPD) alone is the third largest cause of mortality in the UK and the percentage of deaths worldwide is predicted to rise from 6.6 to 8.6% in the next decade [1]. The costs of healthcare and lost productivity due to COPD is equally remarkable: in the EU it is estimated to be a staggering €48.4 billion. Asthma - a condition which results in few deaths but causes significant morbidity within the population - costs €33.9 billion according to the same research. The causes of many respiratory diseases are often preventable: approximately half the economic burden is attributable to smoking and poor air quality [1]. Despite considerable effort, treatment options remain limited: the probability of a drug successfully entering the market for lung indications has been estimated as 16%, the lowest of the major indications [2]. The reasons are multi-factorial and partly due to the lack of sensitive biomarkers which accurately reflect underlying disease. Clinical manifestations and severity of lung diseases vary widely, there is a need for biomarkers which identify phenotypes that exhibit rapid progression or patients who respond more effectively to novel therapies.

Sections 1.2.1 and 1.2.2 provide more in-depth discussion of the two principal diffuse lung diseases investigated in this work: COPD and sarcoidosis.

1.2 THE ROLE OF INFLAMMATION IN DIFFUSE LUNG DISEASE

Persistent inflammation is thought to be the driving factor in many diseases [3]. In the lung, inflammation is thought to be the underlying cause of several diseases; im-

plicated in the pathogenesis, progression and severity. The pathophysiology of lung inflammation can be broadly categorised into focal or diffuse with further refinement into those affecting the airways or parenchyma [4].

Inflammation is a response to an invading pathogen or endogenous signals from damaged cells; the consequences are tissue repair or pathology. Understanding the inflammatory response is challenging owing to the complex interactions of molecular, immunological and physiological processes. In several diseases including cancer and atherosclerosis, inflammation is now considered an important driver of the disease process [3]. The profile of the inflammatory response is dependent on the disease and the tissue involved. Indeed, within the spectrum of lung diseases the initiation, sequence of events and resolution can vary widely. For example, asthmatic patients suffer from inflammation of the airways which develops from a predominantly eosinophilic response after an allergic reaction to an inhaled substance [5]. However, asthma is a heterogenous disease; in fact, it is considered an umbrella term covering many endotypes and phenotypes [6], it is now realised that management must be individualised to the phenotypic characteristics of each patient [7].

One distinction that is often made is between acute and chronic pulmonary inflammation. When the resolution of an acute response is incomplete, the lung exhibits a chronic response which aims to clear the debris, prevent infections and repair lung tissue. Table 1.1 is a summary of the immune mechanisms in common respiratory diseases as outlined in [8]. The key components include macrophages, neutrophils and lymphocytes; with cytokines dictating the extent and type of response. Typically, Th2 cytokines play a major role in chronic inflammation leading to fibrosis.

In summary, the immune response in respiratory disease involves a complex interplay of cells, cytokines and other mediators. Despite substantial efforts to unravel the key inflammatory components involved in diffuse lung disease, the mechanisms by which inflammation causes lung dysfunction remain uncertain and further work is needed to understand the drivers of the disease progression. Measurements which

Table 1.1: Overview of main components of inflammatory response in some common lung diseases.

Disease	Pathology	Cells	Mediators
COPD	Alveolar apoptosis	Macrophage	MMP12,8,9
	poor phagoctosis of apoptotic neutrophils → necrosis →↑ NE release	Neutrophil	cathepsin; S,L,G, NE, IFN-γ, MIG
	↓ VEGF	CD8+ T cell	TGF-β, EGF,
	Chronic parenchymal and airway inflammation	Airway epithelial cell	PDGF
Asthma	Airway inflammation, Fibrosis and SMC	Eosinophil	↓ IL-10
	hyperplasia, ↓ tolerogenic immune response	Mast Cell	TGF-β
		Neutrophil	↑ IL-17
		Macrophage, DC	IL-4,5,9,13
		Airway SMC	
		Epithelial cell	
		Fibroblast	
		CD4+ T cells	
		Basophil	
IPF	Epithelial→mesenchymal transition, injury→	Fibroblast,	IL-8, TNF-α,
	mediator release: fibrosis, ↑ angiogenesis, damaged basement membrane	Airway epithelial cell	TGF-β, IL-4, 5, 13
		Type II pneumocyte	

Adapted from [8].
COPD = Chronic obstructive pulmonary disease, EGF = epidermal growth factor, IFN = interferon, IL = interleukine, IPF = idiopathic pulmonary fibrosis, MIG = Monokine induced by gamma interferon, MMP = matrixmetalloproteinases, NE = Neutrophil elastase, PDGF = platelet-derived growth factor,SMC = smooth muscle cell, TGF = transforming growth factor, TNF = tumour necrosis factor, VEGF = vascular endothelial growth factor.

could complement the existing clinical measures of lung disease and are specific to inflammatory processes are needed to help address these concerns.

1.2.1 *Chronic Obstructive Pulmonary Disease*

COPD is the leading cause of mortality in non-malignant respiratory diseases [9]; it is an umbrella term which covers a complex set of conditions. COPD is characterised by an abnormal inflammatory response which occurs as a result of inhaled stimuli. The pattern of inflammation seen in COPD patients can vary dependent on the nature of the stimulus. Nevertheless, there is a characteristic pattern with increased numbers of neutrophils, macrophages, T and B Lymphocytes [10–12] (see figure 1.1 and table 1.1). Interestingly, this pattern is common in smokers without airflow limitation but the response in COPD is amplified. The molecular mechanisms are still unknown,

but if they could be understood might provide an explanation of which smokers go on to develop airway obstruction. Patients exhibit progressive airflow limitation due to remodelling of the small airways and destruction of lung parenchyma. Computed tomography (CT) scans indicate that small-airway obstruction occurs prior to the development of emphysema [13].

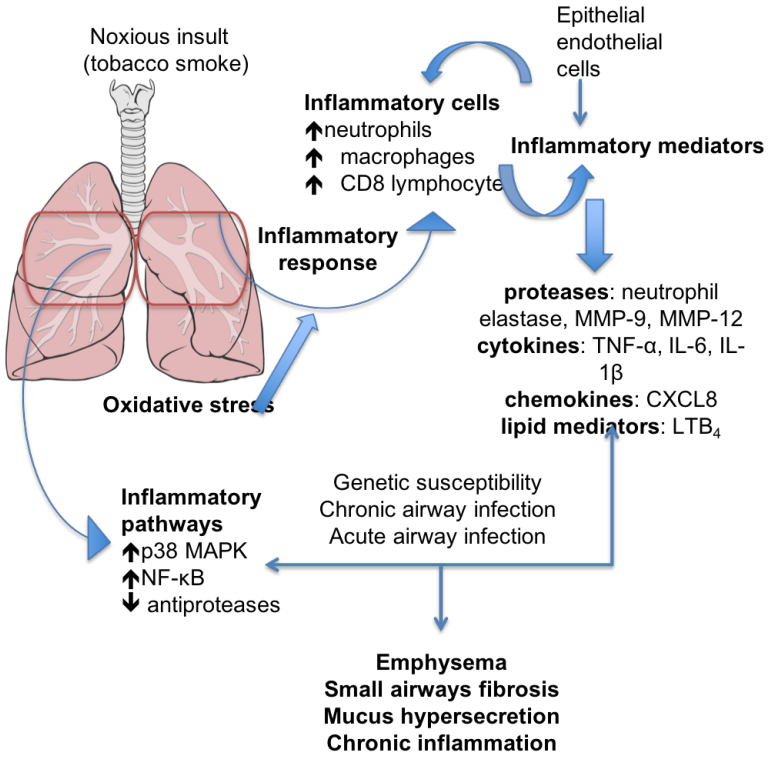

Figure 1.1: **Pathophysiological mechanisms of COPD.**

One of the ongoing challenges has been to define clinically meaningful phenotypes, several suggestions have been made but these phenotypes have proved difficult to identify in different populations with no link to any underlying mechanism. The lack of progress with phenotypes of COPD restricts the ability to deliver specific therapies: recognising that coexisting mechanisms may be interacting in complex ways paves the way for identifying responder phenotypes [14].

COPD is also associated with systemic inflammation; the picture is far from clear whether increased systemic inflammation is a consequence of lung inflammation or if related to a co-morbid disease that affects the lung as well [15].

Periods of acute increased inflammation occur during exacerbations, but the relationship with clinical outcomes and disease progression remains poorly understood [16]. Clinical trials need to address the challenge that large numbers of patients need to be studied over long follow-up periods. Biomarkers capable of assessing disease activity (or surrogate markers) could help facilitate the development of efficacious anti-inflammatory drugs. Indeed, if treatments are to become targeted to certain phenotypes then biomarkers that can target specific pathways might be needed.

1.2.2 *Pulmonary Sarcoidosis*

Sarcoidosis is a multi-organ granulomatous disease of unknown aetiology which most commonly affects the lungs [17]. An antigen is phagocytosed primarily by macrophages and through a complex series of interactions leads to the formation and accumulation of granulomas. Eventually, the granulomas may mature and become encased in fibroblasts and collagen leading to distortion of organ architecture and function. Although in a proportion of patients the disease may resolve itself, others will go on to develop progressive pulmonary fibrosis. There is a poor understanding of which patients will require long term therapy and therapeutic options have not convincingly shown prevention of progression or fibrosis [18, 19]. Patients often experience restrictive ventilatory capability according to spirometry readings with reduced forced expiratory volume in one second (FEV_1) and forced vital capacity (FVC); in at least 50% of patients the ratio of FEV_1 to FVC is also reduced [19].

Sarcoidosis is diagnosed using compatible clinical and radiological features, radiographic chest findings are often confirmed by tissue biopsy. Recently, endobronchial ultrasound (EBUS) has gained in popularity, it allows clinicians to biopsy chest lymph nodes to confirm the presence of granulomas with lower risk than the traditional transbronchial biopsy. Sarcoidosis remains a disease of exclusion [17]; no single marker or test has proven robust enough to provide a definitive diagnosis. Serum angio-tensin converting enzyme (ACE) reflects the total granuloma burden in sarcoidosis [20]. However, there is some debate around its diagnostic and prognostic usefulness [21] .

1.3 CLINICAL MARKERS OF PULMONARY INFLAMMATION

There are several measurements which are used in a clinical and research setting to assess pulmonary disease, very few of these provide a direct measure of underlying inflammation. Spirometry is the mainstay of evaluating disease severity in diffuse respiratory diseases. Although FEV_1 and FVC are not a direct measures of lung dysfunction nor direct indictors of inflammation, they are commonly used for diseases such as COPD and they are widely used as the primary endpoints in clinical trials of respiratory disease. However, spirometry has well recognised limitations [22]. Spirometry is a global measurement therefore, may mask any regional changes in disease; further it exhibits a long interval - typically, months to years - before a change in disease can be identified.

Bronchoalveolar Lavage (BAL) fluid provides a picture of the cellular constituents within the lung and has been used in an experimental model of lung inflammation to correlate against imaging markers [23, 24]. This provides a picture of the intra-alveolar cellular environment; differential cell counts are taken to reveal the make-up of the inflammatory response. However, it is an invasive procedure and therefore carries risk of complications. Sputum collection allows quantitative assessment of the cells in the upper respiratory tract. Sputum collection has a number of methodological challenges, these have led to poor repeatability [25].

There is some evidence that circulating plasma levels of inflammatory cells may be elevated in pulmonary disease; however, the origin of the increase is not well understood. The relationship with pulmonary inflammation depends on the pathological origins of the disease in question. In COPD, plasma fibrinogen, a soluble protein, has been found to be elevated compared to healthy controls and further elevated levels are associated with increased risk of exacerbation and death [26]. However, fibrinogen has also been used as a marker of cardiovascular disease (CVD) and this is a comorbidity in COPD hence may not relate directly to lung disease, further there is no direct evidence that there is a link between fibrinogen levels and pulmonary inflammation. Moreover, there is some controversy regarding the role of fibrinogen as

a putative biomarker in other indications; studies indicate that it does not correlate well with disease prognoses in coronary heart disease [27] or in lung cancer [28]. Systemic markers may be complementary to the disease or represent a comorbidity; in either case, parenchymal disease activity may be compartmentalised, therefore systemic markers may not be truly reflective of lung inflammation.

There is considerable interest in whether chemicals in exhaled breath could be indicative of disease, so called Exhaled Breath Condensates (EBC). In asthma, exhaled nitric oxide (NO) has transitioned from research into clinical practice as a marker of airways inflammation and helps to inform diagnosis [29]. However, it is still too early to draw firm conclusions about EBC in inflammatory lung conditions and further work will need to be performed to verify the relationship between EBC and inflammatory burden.

1.4 IMAGING INFLAMMATION IN DIFFUSE LUNG DISEASES

Imaging has many benefits over other measures of pulmonary disease. Imaging can provide whole lung measurements and regional information relating to disease; this can be at the level of an individual image voxel or combined into any larger region size (e.g. lobes). Imaging techniques are largely non-invasive and the images can be analysed to generate biomarkers of disease; such putative imaging biomarkers could be applied [30]

1. In early-phase clinical pharmacodynamic studies of anti-inflammatory therapies
2. As a complement to functional spirometry and other forms of imaging
3. As a tool to improve our understanding of the pathogenic mechanisms of these complex lung diseases

Changes in the structure and function of the lung occur in an unpredictable manner and reflect different stages of inflammation. Imaging techniques aid in the appreciation of such stages: CT can characterise the secondary pulmonary lobule and delineate

morphology, to a lesser extent magnetic resonance imaging (MRI) is used to depict morphology and provide additional functional information.

Nuclear medicine techniques encompass planar imaging, single photon emission computed tomography (SPECT) and positron emission tomography (PET). The subsequent sections focus on 3D imaging techniques (i.e. SPECT and PET) rather than planar images which are less quantitative. SPECT and PET are non-invasive functional imaging modalities which enable quantification of underlying molecular and cellular processes. They are designed to obtain an image of the biodistribution of radioactive tracers (herein, called a tracer). In principle, any metabolic substrate, receptor, or drug can be labelled for use as a tracer. Therefore, the potential to explore pathophysiological processes is vast [31]. However, novel tracers are challenging to develop: a time-consuming, multi-disciplinary process which often results in failure. Nevertheless, nuclear medicine imaging techniques are appealing as they have the potential to demonstrate target engagement and in-vivo efficacy of a drug. Further, they can interrogate mechanisms directly related to disease activity and so, be able to detect changes at an earlier stage than CT alone. Since respiratory diseases exhibits distinct differences in inflammatory cell involvement [8], an ideal tracer will be specific, labelling only the molecular target responsible for disease progression. SPECT imaging suffers from poorer spatial resolution and is less quantitative than PET imaging, which may explain the predominance of the latter in the context of lung inflammation. Given that PET is the principal modality under investigation in this work, a detailed review is devoted to the role of PET tracers in inflammatory lung disease, whereas an overview is provided for the other modalities.

1.4.1 *Computed Tomography*

CT is the pre-eminent technique to characterise lung disease in the clinic, it provides a detailed picture of lung anatomy based on the differential attenuation of x-rays by tissue; radiographic contrast is high in the lung due to the large proportion of air. Despite density changes caused by respiration, inflammatory processes are recognised by an increase in density compared to normal tissue. Although the density changes are not

specific for inflammation, their appearance and distribution are valuable to help with differential diagnoses [32]. A review of the role of CT imaging in non-infectious inflammatory diseases categorises the conditions as airways, vascular or interstitial predominant [33]. Currently, high resolution CT (HRCT) is capable of delineating down to the 8th generation of the airways and characteristic patterns are observable on HRCT. For example, in airways disease: areas of debris, fluid, inflammatory cells and bacterial pneumonia cause opacities and consolidation. In HRCT scans of interstitial lung diseases (ILDs) progressive fibrosis leads to honeycombing whereas non-specific pneumonias manifest as ground-glass opacities. In a study of smoking related inflammation, it was found that cumulative and current smoking were associated with high attenuating areas on CT due to inflammatory changes [34].
In summary, inflammation appears in predictable patterns on CT scans which are useful to distinguish different causes of lung inflammation. Since CT cannot delineate disease activity, quantification of inflammatory burden is limited especially in conditions where inflammation is widespread.

1.4.2 *Magnetic Resonance Imaging*

Currently, MRI has a limited role in diffuse lung diseases; the low density of protons and susceptibility artefacts at the air/lung interface result in a low signal-to-noise ratio. Contrast-enhanced MRI using intravenous administration of paramagnetic contrast agents or inhaled hyperpolarised gases has improved the situation [35]. Gadolinium leads to enhancement of signal in tissues either through interstitial or intravascular enhancement, in previous studies of ILDs, early enhanced lesions were indicative of active disease [36] whereas fibrotic lesions were characterised by late enhancement [37]. As a tool to investigate pulmonary ventilation and microstructure, the hyperpolarised gases ^{3}He and ^{129}Xe have emerged as a promising technique in MRI. For example,^{129}Xe MRI has shown both structural and functional information on fibrotic change and gas exchange in IPF [35]. However, a recent systematic review acknowledged that there was only weak evidence for the use of MRI in the assessment of ILD [38]. Although, MRI of the lung is challenging, the non-ionising radiation makes it appealing in conditions which afflict younger patients. MRI may have a role in cystic

fibrosis (CF) where unlike CT, it is capable of providing additional functional information such as perfusion, pulmonary haemodynamics and ventilation. Nevertheless, quantitative MRI is limited in this context due to the low SNR, non-linearity of contrast media to MR signal and inhomogeneities due to the physical set-up [39]. In conditions with loss of tissue due to parenchymal destruction and consequent restricted blood flow, the corresponding loss in MR signal creates an even more challenging situation. Similar to CT, the role of MR in such conditions may be limited to functional parameters and respiratory dynamics [40]. Although limited principally to morphological changes and perfusion defects in ILD, there has been some evidence to indicate its use for assessment of inflammation: only recently has it been possible to achieve suitable image quality with MRI in ILD, and this has allowed inflammatory lesions to demonstrate a hyperintense MR signal [36]. Doubtless, further improvements in image quality will continue to be made; motion correction and development of advanced MR sequences will contribute to this end.

1.4.3 *SPECT*

There are a number of SPECT tracers which target inflammatory activity. ^{67}Ga-Citrate localises in inflammatory areas, it has been suggested that the tracer binds to neutrophils predominantly [41]. However, there are only very few studies that have investigated its use in diffuse lung diseases [41, 42] and none within the last decade indicating that it has been supplanted by other techniques. ^{111}In was used in an early animal model of pulmonary inflammation, providing the first evidence of migration of immune cells in inflammatory conditions [43] but several factors have limited its further use in the lung including poor image quality.

In-vitro cell labelling has had some promising initial findings: a study of COPD patients demonstrated increased neutrophil accumulation and retention compared to healthy controls using ^{99m}Tc labelled neutrophils [44]. The authors noted the critical importance of labelling technique to avoid the neutrophils become activated. In asthma, a condition characterised by eosinophilic inflammation, labelling of eosinophils with ^{99m}Tc revealed an increase in 24 hour accumulation compared to healthy controls [45]. The findings are suggestive that eosinophil labelling could be an imaging

biomarker for the disease, specifically for monitoring response to therapy. Although cell labelling has much potential, its widespread use may be limited by the expertise and facilities needed for the careful preparation of the labelled immune cell [44].

Matrix-metalloproteinases (MMPs) are a family of proteinases thought to play an important role in the repair of alveoli. Investigation of the pathogenesis of COPD has led many investigators to explore the role of MMPs [46]. Although still in the early pre-clinical stages of development, ligands which target MMP activation using ^{99m}Tc have been tested in a murine model [47]. The authors demonstrated a correlation between lung uptake of the tracer and CD68 expression, suggesting that MMP activation reflects the macrophage content. This is consistent with previous findings investigating vascular inflammation [48, 49], but further studies are needed to validate this in humans. Equally, there has also been a few studies of PET tracers targeting MMPs albeit in pre-clinical models (discussed in section 1.4.4). Molecular imaging of MMPs may serve as a valuable tool in a range of human diseases.

1.4.4 *Positron Emission Tomography*

In a recent review article, the literature was searched to identify the current status and future direction of PET tracers to assess inflammatory lung disease [50]. The diseases under investigation were heterogenous across studies therefore, the literature is summarised below according to tracer ligand.

Fluorodeoxyglucose

^{18}F-FDG is the most widely used tracer clinically. Whilst it is a non-specific indicator of inflammation, activated immune cells are known to increase their glucose turnover. Thus, investigators have reasoned that accumulation of ^{18}F-FDG may be reflective of increased inflammatory activity. Several other excellent reviews have highlighted the role of ^{18}F-FDG PET in the context of inflammatory lung diseases alongside other imaging modalities and clinical biomarkers [22, 32, 51]. With a focus on quantitative ^{18}F-FDG PET, a collaboration of specialists reviewed current approaches to evaluate

pulmonary inflammation using ^{18}F-FDG PET [30].

Human studies of lung diseases using ^{18}F-FDG PET are summarised in [30]; its non-specific nature has allowed it to be utilised in several lung diseases including Cystic Fibrosis (CF), Acute Respiratory Distress Syndrome (ARDS), Acute Lung Inflammation (ALI), Interstitial Lung Diseases (ILDs), COPD and Asthma.
Several small studies have shown that pulmonary uptake of ^{18}F-FDG is increased in COPD, asthma and ILDs when compared to control subjects [52–62]. In COPD, ^{18}F-FDG uptake has been shown to correlate well with clinical markers of disease severity [54] and is associated with disease progression [56]. In asthma, regional ^{18}F-FDG uptake may serve as a predictive biomarker and help distinguish phenotypes [58]. In CF, it has been suggested that ^{18}F-FDG uptake may help to identify more aggressive phenotypes [63, 64]. Using an established model of acute inflammation in healthy volunteers, several studies have highlighted that ^{18}F-FDG uptake could serve as a reliable method to evaluate response to anti-inflammatory drugs [23, 24, 65]. Taken together, the data summarised in [30] are compelling and support the use of ^{18}F-FDG for monitoring inflammation and potentially for phenotyping patients. However, careful thought needs to be given to the methodological differences in the analysis and the origin of the ^{18}F-FDG signal before firm conclusions can be drawn [66] (see chapter 2). Further, clinical validation has yet to be performed.

Understanding the origin of increased ^{18}F-FDG signal remains challenging: neutrophils, macrophages, lymphocytes, eosinophils and structural cells have all been implicated in ^{18}F-FDG scans of inflammatory processes [57–59]. Consequently, ^{18}F-FDG PET lung images probably reflect an integrated inflammatory response. Interpretation of ^{18}F-FDG lung imaging is confounded by the substantial proportions of air and blood in the lung; quantification is similarly affected with several correction strategies reported in an attempt to more accurately assess the lung tissue signal (detailed discussion in chapter 2). Although static measures are simpler to apply clinically, dynamic acquisitions allow greater scope for robust correction of these confounding factors. The proportions of air, blood and tissue will vary with disease and as a consequence of disease progression. To improve reproducibility in ^{18}F-FDG PET, standardisation

of acquisition and analysis protocols are of paramount importance [30, 67]. To that end, a wide-ranging group of experts recently provided recommendations on optimal protocols [68]. Although this will no doubt improve reliability of imaging endpoints, further studies providing technical and clinical validation of quantitative ^{18}F-FDG PET could foment more widespread confidence in the technique. Furthermore, the cohorts studied so far have typically been small; larger studies will be required to help establish the clinical relevance of increased uptake of ^{18}F-FDG PET in lung disease.

Due to its wide availability, ^{18}F-FDG PET will likely remain the principal tracer for investigation of lung diseases; despite its shortcomings, it has shown promise in identifying suspected inflammatory disease and correlates well with clinically relevant markers of disease.

Nitrous Oxide Synthase (NOS)

Nitrous Oxide Synthase (NOS) comes in several forms; only inducible NOS (iNOS) is excreted during the inflammatory response and repair process. iNOS is an important substrate expressed in a variety of inflammatory diseases; thus, it represents a desirable target for a PET label. A few pilot studies have investigated the feasibility of ^{18}F-NOS, an inhibitor of NOS which binds primarily to iNOS [69, 70]. Following initial promising results in a murine endotoxin challenge model, the feasibility and dosimetry of ^{18}F-NOS was assessed in cardiac transplantation patients [70]. In the first application of ^{18}F-NOS in the lung, Huang et al [71] experimentally induced lung inflammation in a cohort of healthy volunteers (n=7) using a well-established endotoxin model [23]. Baseline scans were compared with scans post endotoxin challenge (taken approximately 12 hours post challenge). The PET signal was correlated against immunohistochemical staining of BAL fluid cells and exhaled nitric oxide measurements. A modest but statistically significant difference was detected in the exposed lung between baseline and follow-up scan (distribution volume ratio (DVR): 0.42 ± 0.07 vs 0.54 ± 0.12; $p < 0.05$); the control lungs exhibited no difference. Unlike ^{18}F-FDG, ^{18}F-NOS is a reversible tracer and therefore unable to take advantage of localised tissue retention which may explain the low uptake compared to simi-

lar protocols with ^{18}F-FDG [23, 65]. Despite seemingly disappointing uptake, a lack of change in exhaled nitric oxide measurement does indicate that ^{18}F-NOS may be sensitive enough to identify mild regional changes undetected by whole lung measurements. The authors recognised that changes in radiochemistry may improve the clinical applicability: specifically, the presence of metabolites and rapid clearance. Further, it is reasonable to assume that the expression of iNOS may be greater in diseased individuals than healthy controls which may improve the signal. Further human studies in relevant disease cohorts will be able to ascertain the clinical utility of ^{18}F-NOS. Investigators are further exploring ^{18}F-NOS to provide an imaging endpoint in a trial evaluating lung inflammation in e-cigarette users, cigarette smokers and healthy volunteers (ClinicalTrials.gov reference: NCT03721822).

Animal Studies

The paucity of tracers used in human studies to assess lung inflammation is clear from the preceding section. Indeed, the significant challenges in developing novel tracers has led to few crossing the gap from animal to human studies. Hence, to present a comprehensive picture of emerging PET tracers, the preclinical studies undertaken to assess lung inflammation are summarised below.

Matrix Metallo-Proteinases (MMPs) inhibitors

As introduced earlier, MMPs likely play an important role in diseases such as COPD, substrates which act as MMP inhibitors have been developed based on NFR receptors [72]. The first reported PET tracer synthesised targeting MMPs was *(R)-N1-((S)-1-(((S)-1-amino-6-(4-([18F]fluorobenzamido)-1-oxohexan-2-yl)amino)-1-oxo-3-phenyl propan-2-yl)-N4-hydroxy-2-isobutylsuccinamide* (called [^{18}F]-FB-ML5) [73]; it was administered to mice after using cigarette smoke (CS) exposure to induce lung inflammation (n=6) and compared to an unexposed control group (n=5). Despite a generally low uptake in the lung, a two-fold increase was observed (90 minutes p.a.) in the CS exposed group. However, in ex-vivo lung samples, no difference was observed between groups - it is unclear if methodological issues confounded the result: a BAL procedure was

performed immediately prior to the ex-vivo biodistribution study.

Observing the unfavourable target to background ratio of [^{18}F]-FB-ML5, Kondo et al undertook further development work for ligands targeting MMPs [74]. They evaluated several target substrates and identified ^{18}F-IPFP as a candidate with the highest binding affinity for MMP-12 and MMP-5. Biodistribution data indicated a four-fold increase in the lungs of CS exposed mice (n=18) compared to unexposed controls (n=18). However, PET imaging data in the murine lungs were less encouraging: uptake between exposed and control mice proved unremarkable; interestingly, the opposite was observed with [^{18}F]-FB-ML5. One explanation, posited by the authors, may be due to the poor relative expression of MMPs in the CS exposed group compared to control group. Accurate models of chronic lung disease such as COPD remain limited: previous work has shown CS induced models may not reflect the same pattern of inflammatory response as in humans [75]. In future human studies, it would be reasonable to expect increased MMP expression in COPD patients [76]. Further, it is not clear why kinetic analyses were not attempted given that dynamic acquisitions were undertaken, since this may have proven helpful to overcome the low target to background ratios [22]. Given the nascent understanding of the role of MMPs to the disease process, PET tracers targeting MMPs could serve as a source of selective biomarkers when evaluating synthetic inhibitors of MMPs.

Trans-locator protein (TSPO) receptor

Trans-locator protein (TSPO), originally known as peripheral benzodiazepine receptor (PBR), is expressed on the mitochondrial outer membrane of several cells, notably monocytes and neutrophils [42], and has been widely explored as a marker of neuroinflammation [77–82], several groups have synthesised PET ligands that target TSPO.

The first substrate to be explored to assess pulmonary inflammation was *(R)-[1(2-chlorophenyl)-N-methyl-N-(1-methylpropyl)-3-isoquinoline carboxamide]* labelled with Carbon-11 (herein, ^{11}C(R)-PK11195). Hardwick et al [83] experimentally induced lung inflammation in mice and compared ^{11}C(R)-PK11195 uptake to controls. Although there was

a statistically significant increase in lung signal between LPS treated (n =3) and control mice (n =3), the signal in exposed lungs was small and highly variable. In hindsight, this is perhaps not surprising, given the shortcomings of PK11195 in neuroinflammation- including high nonspecific binding and low signal- which have been subsequently highlighted [84]. Kumata et al [85] later developed a series of ligands intended to improve on the limitations of ^{11}C(R)-PK11195. The most promising was an oxopurine analog, N-Ethyl-N-(4-pyridinylmethyl)-2-(-7-[11C]methyl-8-oxo-2-phenyl-7,8-dihydro-9H-purin-9-yl)acetamide, the authors named 11C[3a]. To assess the feasibility of this tracer, PET images of rats exposed to LPS (n =4) were compared to unexposed control rats (n=4). Imaging revealed a 2.5-fold increase in the exposed lung compared to controls (at 30 minutes p.a.). Biodistribution studies confirmed the imaging findings, with a 2.1-fold increase in lung uptake compared to controls. However, the presence of a significant metabolite and the requirement for ^{11}C limits places limitations on its broader applicability.

Building on this and previous work [86–88], Hatori et al used the novel tracer *N-benzyl-N-methyl-2-[7,8-dihydro-7-(2-[18F]fluoroethyl)-8-oxo-2-phenyl-9H-purin-9-yl*]acetamide, known as [^{18}F]FEDAC, to quantify lung inflammation [89]. Further, they examined the relationship of imaging data with TSPO expression and cells. Using the same model of LPS exposed rats, they compared uptake against ^{11}C(R)-PK11195 and controls (n=4 for each group). At 24 hours p.a, quantitative PET revealed a 50% increase in signal using [^{18}F]FEDAC compared to 11C(R)-PK11195 in LPS exposed lung. Pre-treatment with unlabelled ("cold") PK11195 showed negligible uptake of [^{18}F]FEDAC indicating excellent in-vivo specific binding for TSPO, consistent with the ex-vivo measurements of radioactivity performed post dissection. The contribution of the pulmonary blood to the signal rather than lung tissue alone is unclear, methods capable of providing an estimate of blood volume such as wet-to-dry ratios or further imaging methods may be helpful in future studies [90, 91]. Nevertheless, ^{18}F-FEDAC seems a promising candidate for imaging inflammation: it has been suggested that it may have a role in predicting therapeutic effect in rheumatoid arthritis [92] and monitoring hepatic fibrosis [93].

Future studies should aim to provide validation in human subjects. In neuroinflammation, promising tracers continue to be investigated and may provide further options for future lung studies [94, 95]. Additionally, these prior studies have demonstrated the importance of histological validation for TSPO ligands, including a genetic predisposition for different affinity binding patterns across individuals [96]. When designing future studies it may be necessary to incorporate genotyping to stratify subjects into low, moderate and high affinity binders. The specificity for particular immune cells still needs to be addressed; although macrophages and neutrophils have been shown to express TSPO, many other cells including bronchial/bronchiole epithelium also express TSPO [97]. Lessons learned from ^{18}F-FDG studies are helpful here: future human studies should be designed to identify the cellular origins of any changes in signal.

N-formylpeptide receptor

Neutrophils are thought to be a key driver of the response of the immune system, active in the early stages of the immune response; in-vivo detection of neutrophils would allow early investigation of acute response. The antagonist, *cinnamoyl-F-(D)L-F-(D)L-F* (cFLFLF), was identified early as a peptide probe which binds with high affinity to the neutrophil N-formylpeptide receptor (FPR) [98]; improved radiochemistry was achieved with the compound cFLFLF-PEG-DOTA labelled with ^{64}Cu [99]. Evaluation of this tracer in a murine model of bacterial inflammation (n=6) revealed a 5 fold increase in signal in infected lungs compared with control lungs (n=4)[100]. Immunohistochemical staining indicated that in the infected mice (42 hours p.a.), there was a substantial neutrophilic burden with few macrophages; this contrasted dramatically with the control lungs which exhibited only normal alveolar wall structure. The tracer also has an affinity for macrophages, so has been investigated and compared to ^{18}F-FDG imaging in type 2 diabetic patients; demonstrating stronger PET signal in the macrophage containing pancreatic islets [101]. Future studies would require more desirable properties of the radioisotope however, DOTA can also chelate to more common radioisotopes such as ^{68}Ga with improved availability and half-life.

Chemokine receptors

Given the promising results with peptide receptors targets, coupled with the evidence that these receptors are over expressed on inflammatory cells (particularly neutrophils), other institutions have explored different peptide probes. Chemokine receptor 2 (CCR2) is found on monocytes and macrophages amongst other cells [102, 103]; it is up-regulated in lung diseases such as Asthma and COPD [104, 105]. The recent identification of a peptide inhibitor, called extracellular loop 1 inverso (ECL1i), which binds to CCR2, led to the development of a tracer called ^{64}Cu-DOTA-ECLi [106]. Subsequently, this was shown to have a high affinity for macrophages and monocytes in a lung transplantation study [107]. Further investigation of the feasibility of this tracer to detect lung inflammation was undertaken using human tissue and animal models [108]. Using an established model of acute lung injury in mice, intratracheal LPS was administered prior to PET imaging (n=7) and compared to a control group of phosphate buffered saline (PBS) treated mice (n=5). ^{64}Cu-DOTA-ECL1i uptake was assessed using the percentage injected dose (ID) per gram of tissue and peaked at 24 hours p.a. The LPS group demonstrated an approximate four-fold increase in pulmonary signal compared to the control group. This confirmed the findings of the biodistribution study. Sensitivity of the tracer to LPS was assessed in three groups receiving low (n=3), intermediate (n=7) or high doses (n=3) revealing that the tracer could distinguish low from intermediate or high doses.

Specificity was evaluated using competitive blocking with "cold" ECL1i (n=4), CCR2-deficient mice (n=3) and treatment naive wild-type mice (n=3). The lung signal was at similarly low levels in these three groups (mean <0.63% ID); compared to the LPS treated group (mean 4.43%ID per gram). However, in resected human lung tissue from COPD patients, CCR2 immunostaining revealed a lack of specificity, with a wide range of cells CCR2-positive. Although overall the percentage of CCR2 expression was increased in the COPD group relative to the donor group, there was substantial overlap between them. The well documented heterogeneity of the COPD population may provide an explanation for this finding [109]. Nevertheless, autoradiography of the tracer in COPD tissue sections demonstrated increased binding in human tissue with high

numbers of CCR2 positive cells compared to those with low numbers. CCR2 based imaging with DOTA-ECL1i appears promising; further expanded radiochemistry to enable ^{18}F labelling would make the ligand more desirable for clinical use. Human studies are underway and will provide important information on the utility of this tracer (ClinicalTrials.gov reference: NCT03492762).

Summary of PET tracers

PET tracers can be targeted to specific cells and pathways to provide accurate measures of disease activity. Thus, their use in appropriately-designed studies could improve our understanding of the role of inflammation in lung diseases. Development of novel anti-inflammatory drugs has been stifled by the lack of robust, sensitive clinical measurements [22]; PET derived imaging biomarkers have the potential to facilitate the development of targeted therapies.

Development of novel tracers is a highly challenging process [31], reflected by the paucity of tracers which have translated from bench to human studies. Indeed, it is probable that ^{18}F-FDG will remain the most widely utilised tracer in inflammatory lung diseases; the existing data is compelling and supports continued use of ^{18}F-FDG for monitoring inflammation in a variety of diseases. However, existing studies have used disparate acquisition and analysis methods, and there remains several unanswered questions concerning the validity of the analysis methodology and clinical relevance of the imaging endpoints [30, 66, 67].

Considerable work has gone into developing tracers targeting specific causes of inflammation; those summarised in this review demonstrate the breadth of potential targets. Although the low signal-to-noise ratio is a challenge which impedes all PET tracer development in the lung, several tracers have demonstrated the potential for monitoring inflammation in experimental animal models. Whether these promising results translate into human studies remains to be seen, but they are encouraging and warrant further investigation, for example, studies using ^{64}Cu-DOTA-ECLi and ^{18}F-NOS are currently underway in humans. The imaging endpoints and correlative data

provided in the animal studies are disparate, efforts to exclude confounding factors such as blood volume changes and in-vivo specificity would be helpful to improve confidence. The majority of studies were small in scope which makes it difficult to make any firm conclusions about the future clinical utility of these tracers; larger studies in disease cohorts are needed. In future human studies, correlation with clinical measures of disease severity would also improve knowledge of the clinical utility of PET derived biomarkers.

2

QUANTITATIVE POSITRON EMISSION TOMOGRAPHY

2.1 INTRODUCTION

The previous chapter discussed the clinical background of diffuse pulmonary diseases, in this chapter the theory behind PET is provided; quantifying a PET image is a powerful method to estimate biological and physiologic information.

2.1.1 *Positron Emission*

Unstable nuclei undergo radioactive decay in order to reduce their energy state toward a more stable configuration, prior to decay the nucleus is called the parent, the products of the decay are the daughter nuclei. If the nucleus has an excess of protons then decay may occur by spontaneously emitting a positron. Seldom occurring in isolation, positron emission from a radioisotope may be accompanied by other forms of radioactive decay (e.g. gamma emission). An example of a radioactive decay scheme is shown figure 2.1. In PET, the decay of the radioisotope should: (i) be to a stable daughter where no further radioactive decay is expected, (ii) have a relatively short half-life (iii) be via positron emission with a high probability.

Positrons are emitted with a range of energies, the maximum energy is characteristic of the radioisotope. The distance the positron travels in a medium before annihilation is determined by the medium's density and the positron's energy. The positron range is increased when traversing a lower density medium and when it has a higher energy. Both of these affect the spatial resolution achievable in a PET image. The emitted positrons interact with matter principally through scattering collisions, it subsequently loses energy until it eventually annihilates with an electron. Annihilation results in the conversion of the electron-positron pair into two gamma photons emitted at 180° to each other, the energy of each photon is $511keV$ - this is a common feature of all

positron emission regardless of radioisotope. Detection of the resulting pair of gamma photons is fundamental to the process of image formation.

The positron-emitting radioisotopes are labelled to biologically functional compounds; this radiotracer is then administered to a patient. The radiotracer preferentially accumulates in regions where the compound is metabolised. The time-varying distribution of the radiotracer provides a non-invasive way of determining pathophysiologic and biologic information.

Figure 2.1: **Decay scheme for Fluorine-18.**

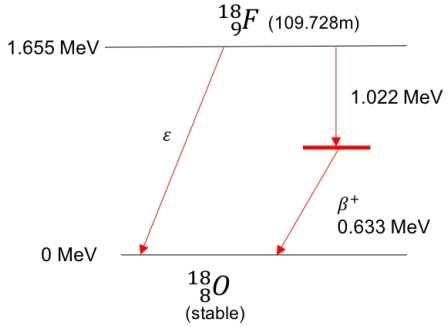

The main mode of emission is positron decay (β^+) with a branching probability of 96.86%. Decay may also occur via electron capture (ϵ) with a probability of 3.14%. *m = minute, MeV = mega-electron volt.*

2.1.2 *PET scanners and image formation*

At the core of the PET scanner are a series of rings which contain scintillation detectors coupled to photomultiplier tubes. The purpose of this arrangement is to detect as many true coincidence events as possible i.e. co-linear photon pairs from the scanned portion of the body. In human tissue, positrons annihilate within the body, a short distance from the radiotracer and a proportion of the resulting photon pairs are absorbed in the detector rings. When the two photons are detected within a short coincidence time window (typically 1-10 ns), the joint detection forms a parallelpiped region called a tube of response. The true-coincidence rate is proportional to the total amount of radiotracer in the tube of response, this fundamental tenet allows an accurate 3D image of the distribution of the radiotracer. Even in well designed systems the resulting images are dominated by noise due to the paucity of true coincidence events detected. The density of the detectors, count-rate capabilities, the duration of acquisition and

the amount of injected radiation determine the noise level.

Modern PET scanners are usually combined with a complementary image modality which can provide a more detailed picture of anatomy. A computed tomography scanner is the most common modality to be combined with PET as PET/CT; an additional benefit is access to an attenuation correction map provided by the CT image (discussed in section 2.1.3. More recently, technological advances have allowed magnetic resonance scanners to be combined into PET/MR scanners; the MR scanner produces excellent soft-tissue contrast and allows additional functional imaging. However, some challenges remain such as obtaining an accurate attenuation map.

The main aim of PET image reconstruction is to achieve an accurate distribution of the radiotracer, this relies on algorithms which are usually proprietary and vary widely amongst scanner manufacturers. The resulting images exhibit different noise and image characteristics, which will depend on various factors such as the choice of filters or any *a priori* assumptions [110] . These algorithms may be analytical or iterative, the main example of the former is filtered back projection (FBP). Iterative methods have become widespread in clinical practice and can produce improved signal-to-noise ratios compared to FBP. Accurate noise modelling in the reconstruction process is desirable due to the dominant appearance of noise in PET; however, for frequently-used iterative image reconstruction algorithms the noise distribution is seldom known. Further work is needed to establish the optimal reconstruction algorithm for PET lung images [68]. In addition, various corrections for physical effects are needed in order to obtain an accurate image of radiotracer distribution.

2.1.3 *Physical Effects and Corrections in PET*

The relationship between the number of true-coincident events and radioactivity is subject to corrections for several confounding physical effects. These include corrections for attenuation, randoms, scatter, patients' movements, geometric variations in efficiency, detector dead-time and radioisotope decay. A full description of these effects is provided in [111]. These effects must be estimated prior to applying the correc-

tion. Gamma photons are attenuated by tissue on route to the detectors; CT provides an estimate of this attenuation based on the reduction of x-ray intensities through the patient. Although the x-rays used in CT are of lower energy than the $511keV$ photons in PET, a bi-linear transformation is commonly utilised to correct this discrepancy.

In the lung, respiratory motion results in inaccuracies in qualitative and quantitative PET images. The duration of PET scans makes respiratory motion unavoidable, this contrasts with CT scans which can be obtained in a single breath hold of a patient. The major effects of respiration on PET images include blurring leading to shape distortion and loss of signal. Further, CT is used to generate an attenuation correction (AC) map which is applied to the PET scan, the mismatch between the CT-AC and PET images leads to inaccuracies in quantitative PET due to this mismatch. A number of methods have been suggested to minimise the mismatch [68]. One advantageous method uses cine-CT to generate a time averaged CT-AC that more closely mimics the lung image from the PET acquisition [112, 113]. In a previous study of IPF patients using cine-CT, investigators found significant errors were introduced to quantitative PET as a result of motion and density mismatch between CT and PET [114]. A further development of this approach phase matches the CT and PET scans using respiratory gating; however, this results in noisier PET images. Alternative approaches have been suggested which minimise blurring and mismatch without the noise increase [115]. The disease under investigation and its severity are likely to impact the extent of density changes in the lung during respiration, and therefore, magnitude of error introduced in quantitative PET. As mentioned previously (see chapter 1), interpretation of PET lung images is further confounded by the large proportion of air and tracer concentration in pulmonary blood (detailed discussion provided in section 2.2).

2.2 QUANTITATIVE PET

With the appropriate corrections in place, quantitative studies of tracer uptake can be performed. PET allows both relative (i.e. one tissue region compared to another) and absolute quantification. Methods to quantify the tracer uptake vary in complexity

from static measures taken at a single time point post-injection to mathematical modelling of the tracer dynamics. In the following sections, the different methods which can been applied in diffuse lung diseases are discussed; given that ^{18}F-FDG is the most commonly utilised tracer, I focus on techniques developed primarily for this radiotracer.

A major challenge in quantifying ^{18}F-FDG in the lung is the poor signal-to-noise ratio; the low basal uptake of ^{18}F-FDG is a consequence of the low density of lung tissue (due to large proportions of air). Indeed, this is likely to be a challenge for all PET tracers targeting lung parenchyma and airways. A PET image can be considered a superposition of different layers of signal corresponding to tissues or cells within the region of interest (ROI); untangling the contribution of individual layers provides an accurate means to assess the target tissue. Indeed, interpretation of lung PET images is confounded by pulmonary blood; which in the healthy lung is substantially larger (typically 15-20%) than other organs, e.g. the brain (typically 5%). The ROI may be defined anatomically, e.g.the entire lung or individual lobes, it may be selected to encompass a relevant disease process or a voxel-by-voxel approach may be adopted.

2.2.1 *Static measures*

Perhaps the simplest method to obtain an estimate of the tracer concentration relies on delineating a ROI at single time point typically. Clinical ^{18}F-FDG PET imaging protocols are designed to give a favourable tissue-to-background ratio and optimal patient throughput [116]. Typically intervals of between 45-60 minutes between administration of the tracer and the start of the acquisition are used (although optimal protocols continue to be refined [117]). The most widely used metric is the Standardised Uptake Value (SUV):

$$\mathrm{SUV} = \frac{C(t_o)}{A \times W} \tag{2.1}$$

where $C(t_o)$ is the concentration of the tracer at time, t_o, A is the administered activity and W is the weight of the patient. Although often normalised by total body

weight, recent evidence from oncology patients indicate that lean body mass may be more reproducible [118]. Currently, there is no evidence to suggest this may be appropriate in the lung. Static measures, such as the SUV, are likely to be heavily influenced by pulmonary blood and air, this has led to the exploration of alternative methods that account for these effects [114].

2.2.2 *Dynamic measures*

Dynamic scans involve continuous data acquisition from the time of injection until a late time-point (typically 60-90 minutes for ^{18}F-FDG). The acquisition is divided into a series of time frames with varying duration; typically, initial frames have a short duration (e.g. 10 seconds), these are followed by longer frames later in the scan (e.g. 10 minutes). This type of acquisition allows the estimation of physiologic or biologic parameters. Although static measurements are simpler to obtain, dynamic measurements may be more sensitive when overall tracer uptake is low [119].

2.2.2.1 *Compartmental Models*

Kinetic modelling has traditionally be regarded as the gold standard method of quantification in PET studies; well established applications include estimation of cerebral metabolic rate (CMR) and neurological receptor binding (a general framework for kinetic modelling is described in [120]). In compartmental models, the tracer is exchanged between a series of compartments; the rate of exchange is governed by the rate constants. The concentration of the tracer within a compartment at a specified time can be found by solving ordinary differential equations. Modelling the time varying distribution of the tracer using a series of compartments allows one to isolate the signal of interest. Typically the models comprise one, two or three compartments depending on the pharmocokinetics of the tracer and the disease. Such a model requires an input function; the concentration of the tracer as a function of time in the blood or plasma of an artery usually serves this purpose. These models are necessarily simplifications of complex biologic and physiologic processes with assumptions that must be satisfied. The accuracy of these models needs to be assessed and periodically revisited to ensure the conditions of the model are still met.

2.2.2.2 *^{18}F-FDG Compartmental Model of Lung Inflammation*

In the lung, provided there is not significant oedema, the two-compartment irreversible model [121] has been widely adopted to model the kinetics of ^{18}F-FDG in pulmonary inflammation [122] (see Figure 2.2).

The concentration of ^{18}F-FDG measured in a ROI within the lung can be described by:

$$C_m(t) = V_b C_b(t) + (1 - V_a - V_b) C_T(t, K_1, k_2, k_3, V_b) + V_a C_a(t) \tag{2.2}$$

where $C_m(t)$ is the concentration of ^{18}F-FDG in the ROI; $C_b(t)$ and $C_T(t)$ are the concentrations of ^{18}F-FDG in the pulmonary blood vessels and lung cells respectively; V_a and V_b are the fractional volumes of air and blood respectively, and K_1, k_2 and k_3 are the microparameters of the model [120]. The concentration of radioactivity in air, $C_a(t)$, is assumed negligible. V_a can be estimated as described in section 2.2.2.4.

The metabolic rate constant of ^{18}F-FDG is then given by

$$K_{im} = K_1 k_3 / (k_2 + k_3) \tag{2.3}$$

Figure 2.2: **Irreversible two-compartmental model describing the kinetics of ^{18}F-FDG used to evaluate lung inflammation.**

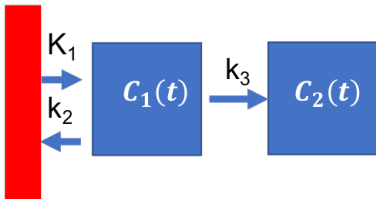

In the absence of significant oedema, the concentration of ^{18}F-FDG in a ROI in the lung can be described by three compartments [122]: a blood compartment $C_b(t)$, an extravascular pre-cursor pool $C_1(t)$ and phosphorylated ('trapped') ^{18}F-FDG compartment $C_2(t)$. The relationships between the concentration of tracer in a compartment is described by the rate constants (i.e. K_1, k_2, k_3). *ROI = Region of Interest*

The time varying concentration in the compartments of this model can be described by

$$\frac{dC_1(t)}{dt} = K_1 C_p(t) - k_2 C_1(t) - k_3 C_1(t) \tag{2.4}$$

$$\frac{dC_2(t)}{dt} = k_3 C_1(t) \tag{2.5}$$

where $C_p(t)$ is the concentration of ^{18}F-FDG in the plasma, the tissue concentration is then $C_T(t) = C_1(t) + C_2(t)$, solving these equations yield:

$$C_1(t) = K_1 e^{-(k_2+k_3)t} \otimes C_p(t) \tag{2.6}$$

$$C_2(t) = \frac{K_1 k_3}{(k_2+k_3)}(1 - e^{-(k_2+k_3)t}) \otimes C_p(t) \tag{2.7}$$

Rearranging and simplifying gives

$$C_T(t) = \frac{K_1 k_3}{(k_2+k_3)} \otimes C_p(t) + \frac{K_1 k_2}{k_2+k_3} e^{-(k_2+k_3)t} \otimes C_p(t) \tag{2.8}$$

The microparameters and V_b are estimated by minimising the weighted residual sum of squares (WRSS):

$$WRSS = \sum_{i=1}^{N} W_i (Y(i) - C_m(i))^2 \tag{2.9}$$

where N is the number of time frames of the dynamic scan, i is the frame number and W_i is the weighting factor for each frame, $C_m(i)$ is the estimated concentration of ^{18}F-FDG fitted from the compartmental model in frame i (i.e. equation 2.2) and $Y(i)$ is

the measured concentration from the PET scanner.

As discussed in Chapter 1, additional compartments may provide a more accurate picture of ^{18}F-FDG kinetics when there is significant oedema [119].

2.2.2.3 *Input Function*

An essential requirement of this approach is an accurate input function ($C_p(t)$) [123]; this can be obtained from discrete blood samples from a peripheral vein during the PET scan. Alternatively, an input function can be measured from the dynamic PET images by delineating a ROI within a vessel in the field of view, referred to as an Image Derived Input Function (IDIF). Optimal positioning of the blood vessel ROI has been discussed extensively in application to ^{18}F-FDG tumour kinetics [124] and cardiac metabolism [125]; IDIFs derived from several different vessels were found to be comparable to arterial samples. In pulmonary ^{18}F-FDG kinetics, several regions have been explored including the ascending & descending pulmonary aorta, left & right ventricles, vena cava and aorta [126, 127]. The TAC extracted from the blood pool ROI is then modelled as a continuous curve to reduce noise: models based on an initial linear rise followed by a sum of exponentials have been proposed in tumour kinetics [128], followed by correction to a plasma input function. In the brain, extensive effort has been made to improve input function modelling including those based on reference regions [129] and methods using carotid or other blood vessels with one or more manual samples [130–132] with voxel based approaches also feasible [133]. In the lung, there remains a need for optimisation of input function modelling.

Early studies of kinetic models of cerebral blood flow (CBF) demonstrated the importance of correcting the input function for time delay [134] (i.e. the time taken for the tracer to travel between the sampling site and the tissue of interest). Methods to estimate the delay between blood sample point and the tissue ROI are largely based on these earlier observations in neurological PET [135, 136]. More recently, inaccuracies in time delay were shown to cause significant deviations in the microparameters of a CMR kinetic model in rodents [137]. This applies equally to pulmonary compartmental models of ^{18}F-FDG: incorporating a regional lung time delay has been shown

to improve the fit to the experimental data compared to no delay in acute lung injury (ALI) [138]. Further corrections such as accounting for the partial volume effect (PVE) and spill-over in pulmonary ^{18}F-FDG scans may be important [127] but the impact of this approach on kinetic parameter estimation in humans has yet to be explored. Dispersion of a tracer alters the shape of the input function, parameters estimated from compartmental modelling are affected by dispersion but there is evidence that graphical analyses (such as Patlak) are largely insensitive to dispersion [139].

2.2.2.4 *Fractional Air Volume*

In order to solve equation 2.2, an estimate of the fractional air volume, V_a, in the ROI needs to be obtained. Fortunately, CT has been shown to give an accurate measure of the volume of air compared to other methods [140]. Following the correction outlined by [53], V_a is given by:

$$V_a = \frac{HU_{lung} - HU_A}{HU_t - HU_A} \tag{2.10}$$

where HU_{lung}, HU_A and HU_t are the Hounsfield units for the lung, air and soft tissue respectively. This methodology was originally devised to attempt to correct SUV in the lung for the air fraction [53].

2.2.3 *Graphical Methods*

Compartmental modelling with PET data is non-trivial and is sensitive to noise particularly in the initial frames; alternative methods can overcome these issues. Patlak graphical analysis (PGA) is a widely adopted technique applicable when irreversible tracers are used. The seminal paper developing the mathematics was produced by Patlak and the technique bears his name [141]. PGA is derived from a general compartmental model which makes no assumptions regarding the number of compartments through which the tracer can be exchanged. Although originally intended for neurological studies [141], it has been applied in diffuse pulmonary diseases (see chapter 1).

Applying PGA to the compartmental model of pulmonary inflammation (figure 2.2), we return to equation 2.8 and simplify further (following the approach in [66])

$$C_t(t) = \frac{K_1 k_3}{(k_2 + k_3)} \int_0^t C_p(\tau) d\tau + \frac{k_2}{k_2 + k_3} C_1(t) \tag{2.11}$$

Using K_{im} as defined in equation 2.3, substitution of equation 2.11 into 2.2 and dividing by $C_p(t)$ yields

$$\frac{C_m(t)}{C_p(t)} = V_b + (1 - V_b - V_a)(K_{im} \frac{\int_0^t C_p(\tau) d\tau}{C_p(t)} + \frac{k_2}{k_2 + k_3} \frac{C_1(t)}{C_p(t)}) \tag{2.12}$$

A key assumption is that the tracer reaches steady state after a time, t^*, post-injection thereby,

$$\frac{C_1(t)}{C_p(t)} = \frac{K_1}{k_2 + k_3} \tag{2.13}$$

$$\frac{C_m(t)}{C_p(t)} = V_b + (1 - V_b - V_a)(K_{im} \frac{\int_0^t C_p(\tau) d\tau}{C_p(t)} + \frac{K_1 k_2}{(k_2 + k_3)^2}) \tag{2.14}$$

If $V_{ss}^c = \frac{K_1 k_2}{(k_2 + k_3)^2}$ then the above simplifies further to

$$\frac{C_m(t)}{C_p(t)} = V_b + (1 - V_b - V_a) V_{ss}^c + (1 - V_b - V_a)(K_{im} \frac{\int_0^t C_p(\tau) d\tau}{C_p(t)}) \tag{2.15}$$

Patlak's method plots this equation in the form of a straight line thus

$$\frac{C_m(t)}{C_p(t)} = K_{ip} \cdot \frac{\int_0^t C_p(\tau) d\tau}{C_p(t)} + V_{ss}^c \tag{2.16}$$

Where $C_m(t)$ is the concentration of the tracer in the lung ROI, $C_p(t)$ is the plasma input function and V_{ss}^c is the steady state volume of distribution of the tracer. Measurement of $C_p(t)$ is described in section 2.2.2.3; note that it is derived from a blood

vessel which requires correction from $C_b(t)$ to $C_p(t)$ (the implications of this correction are discussed in chapter 4, see limitations in section 4.6). Equation 2.16 is that of a straight line with a slope of K_{ip} and an intercept equal to V_{ss}. Comparing equations 2.15 and 2.16 leads to the following observations:

$$K_{ip} = (1 - V_b - V_a)K_{im} \tag{2.17}$$

$$V_{ss} = (1 - V_b - V_a)V_{ss}^c + V_b \tag{2.18}$$

In an attempt to correct for the affect of lung density, a normalised parameter, nK_i was suggested [55]:

$$nK_i = \frac{K_{ip}}{V_{ss}} = \frac{(1 - V_b - V_a)K_{im}}{(1 - V_b - V_a)V_{ss}^c + V_b} \tag{2.19}$$

This mathematical proof shows that in the lung, estimates of ^{18}F-FDG uptake using either K_{ip} or nK_i are influenced by the blood and air contributions. The benefits of PGA lie in its relative simplicity compared to compartmental modelling and its ability to cope with noise (due to its regression over many time points). The rationale for normalising the metabolic rate defined by equation 2.19 has been questioned previously [23]. Nevertheless, PGA may provide a composite measure of disease activity and correlates well with measures of disease severity [54]; indeed, it continues to be reported as a surrogate measure of pulmonary inflammation in humans [24].

2.3 SUMMARY OF QUANTITATIVE PET

The complex architecture of the lung and the small proportion of tissue - even in healthy lung - compounded with the substantial tidal motion make quantifying radiotracer concentration in diffuse lung diseases challenging. Currently, a great deal of effort has been spent investigating and refining quantitative ^{18}F-FDG as a marker of

Figure 2.3: **Patlak graphical plot derived from an ^{18}F-FDG PET scan.**

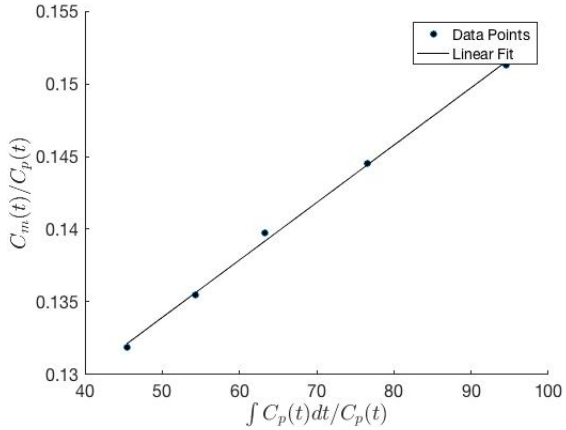

This data was taken from a ROI around the whole lung of a COPD patient scan.
COPD = chronic obstructive pulmonary disease, ROI = Region of Interest

pulmonary inflammation. Despite this, no consensus on the most appropriate method has been reached with static and dynamic approaches still routinely applied. Quantities such as V_b and V_a vary significantly with disease and severity, which could lead to different conclusions depending on the analysis method [66].

2.4 HYPOTHESES AND AIMS

In this project, the principal hypothesis was that quantitative ^{18}F-FDG PET/CT can be used to assess pulmonary inflammation in diffuse lung diseases. In order to test this hypothesis, prospective and retrospective clinical studies were used to assess the clinical, biological and technical validity of ^{18}F-FDG PET imaging endpoints. These were performed in clinically relevant diseases including COPD, α_1ATD associated COPD, sarcoidosis and compared to positive and negative controls.

Hypothesis 1 (Chapter 4): COPD patients, α_1ATD patients and smokers will have elevated pulmonary inflammation as measured by ^{18}F-FDG PET.

The aims of the studies described in Chapter 4 include:

1. To compare regional and whole lung inflammation in COPD participants, α_1ATD participants, current smokers without COPD and healthy never smokers using quantitative ^{18}F-FDG PET.
2. To compare and contrast the different quantitative ^{18}F-FDG PET imaging outcomes, evaluating their variability, repeatability, reproducibility and relationship to clinical measurements.

Hypothesis 2 (Chapter 5): COPD subtypes defined by visual and quantitative CT will be associated with varying degrees of pulmonary inflammation as assessed by ^{18}F-FDG PET.

The aims of the study described in Chapter 5 include:

1. To compare lung inflammation (using quantitative ^{18}F-FDG PET) between radiologic sub-types of COPD and to explore associations between emphysema severity and disease activity using ^{18}F-FDG PET.
2. To investigate whether differences in treatment response could be identified in these subtypes of COPD using longitudinal ^{18}F-FDG PET scans.

3. To assess the different ^{18}F-FDG PET outcomes in a single subtype defined by the mildest disease- thus minimising the confounding influence of emphysema- and compared to smokers and never-smokers.

Hypothesis 3 (Chapter 6): Sarcoidosis patients will have an increased pulmonary ^{18}F-FDG PET signal compared to healthy controls; dynamic measures of ^{18}F-FDG will further improve the distinction between these groups.

The aims of the study described in Chapter 6 include:

1. To compare the pulmonary ^{18}F-FDG signal in sarcoidosis patients to healthy controls; this includes comparing both static and dynamic measures of uptake.
2. To assess biological validity by comparing these quantitative measures against clinical measures of inflammation obtained from inflammatory cell counts in bronchoalveolar lavage fluid (BALf) and plasma biomarkers of inflammation.
3. To explore the technical validity of ^{18}F-FDG imaging outcomes by investigating the influence of respiratory motion on quantitative ^{18}F-FDG in sarcoidosis patients.

3

METHODS

This chapter describes the methodology which is common for the study protocols and analysis methods used throughout this work. This includes a detailed description of the clinical markers of pulmonary disease, PET/CT acquisition protocols, image analysis methods and statistical tests used. Individual chapters describe additional methods, which only pertain to the work undertaken in those chapters.

3.1 CLINICAL MARKERS

3.1.1 *Blood Based Biomarkers*

Venous blood samples were collected according to a standard operating protocol for the studies: a 4.7ml serum gel tube for full lipid profile, renal function and high sensitivity C reactive protein (hsCRP); fibrinogen was analysed via the Clauss method using a 2.7ml sodium citrate sample tube; standard haematology was evaluated using a 2ml EDTA sample tube. Samples were processed either at accredited departments within NHS hospitals or The Doctors Laboratory (TDL, London).

3.1.2 *Pulmonary Function Tests*

Spirometry was performed using the CareFusion MicroLab Spirometry (San Diego, USA) according to joint American Thoracic Society and European Respiratory guidelines [142] and the best-performed procedure out of at least three attempts was recorded. In COPD patients alone, spirometry was performed after inhaled bronchodilator medication. The forced expiratory volume in 1 second (FEV_1) is the amount of air exhaled in 1 second after maximum inspiration; forced vital capacity (FVC) is the total exhaled volume after maximum inspiration. A value of $FEV_1/FVC < 0.7$ indicates airflow ob-

struction, % predicted values (based on age, gender and height) of FEV_1 and FVC were recorded.

3.2 PET/CT ACQUISITION PROTOCOL

Scans were performed at the PET/CT Unit of Addenbrookes Hospital, Cambridge using the GE 690 Lightspeed Discovery VCT scanner (Milwaukee, Wisconsin) or Invicro ltd (formerly Imanova), London using the Siemens mCT Biograph (Munich, Germany). The acquisition protocols were matched as closely as possible.

Subjects were required to fast for 6 hours prior to the scan and told to avoid strenuous exercise in accordance with the standard guidance from the European Association of Nuclear Medicine (EANM) for ^{18}F-FDG oncology imaging [143]. A blood glucose level of $< 11 mmol/g$ was required for the subject to proceed to the scanner. Positioning aids were used to ensure the subject was comfortable: knee wedges and arm straps were used. All subjects underwent a topogram - a low dose, full body image - to aid in the positioning of the FOV in other scans. Further CT scans were performed as described in the relevant chapters.

3.2.1 *PET*

After CT scans were completed, the subject was positioned in the PET scanner. ^{18}F-FDG was administered into the antecubital vein followed by a flush of saline (10ml). The dynamic acquisition was initiated immediately prior to the administration; data were acquired in list mode for 60 minutes post-administration (p.a.). Framing schedules were study specific and described in the relevant chapters. Images were reconstructed using proprietary algorithms: either the discrete Fourier transform (DIFT; Siemens) or 3D Fourier rebinning filter back projection (FORE-FBP; GE). The FORE-FBP algorithm was used (rather than an iterative reconstruction algorithm) in the prospective study (see Chapter 6, all scans acquired on the GE 690 PET/CT scanner). The rationale behind this choice was: (1) to ensure consistency with the retrospective

data (chapter 4) and (2) to mitigate other identified issues such as bias found in the iterative ordered subset expectation maximisation (OSEM) reconstruction algorithm [144]. All PET images were corrected using an attenuation map formed from the CT scan.

Discrete venous blood samples were acquired during the scan from the contralateral arm; these samples were used to provide a plasma to blood ratio. Samples were spun in centrifuge at 3000 revolutions per minute (rpm) for 5 minutes; 0.5ml of plasma and whole blood were pipetted into a vial. Samples were measured three times in a gamma counter for 60 seconds; the average value was used in calculations.

All scans were reported by consultant radiologist or nuclear medicine physician using a static scan reconstructed in the final 15 mins (45-60mins).

3.3 PET/CT IMAGE ANALYSIS

3.3.1 *Overview of the analysis pipeline*

The goal of analysing PET/CT lung scans was to estimate pulmonary ^{18}F-FDG uptake. In this work several outcomes were used to estimate ^{18}F-FDG uptake and these were taken as surrogate markers of inflammation. These include the SUV, K_{ip} and nK_i obtained from Patlak graphical analyses and finally K_{im} obtained from compartmental modelling. The SUV is obtained from static acquisitions whereas the other outcomes incorporate information on the time course of the tracer from the dynamic acquisition. In order to estimate these outcomes, an analysis pipeline was developed; an overview of the pipeline is shown in figure 3.1. This pipeline was implemented primarily in MATLAB [145] (version R2016b). Below is a more detailed description of the stages involved.

Figure 3.1: **Overview of the Analysis Pipeline for ^{18}F-FDG PET/CT Lung Images.**

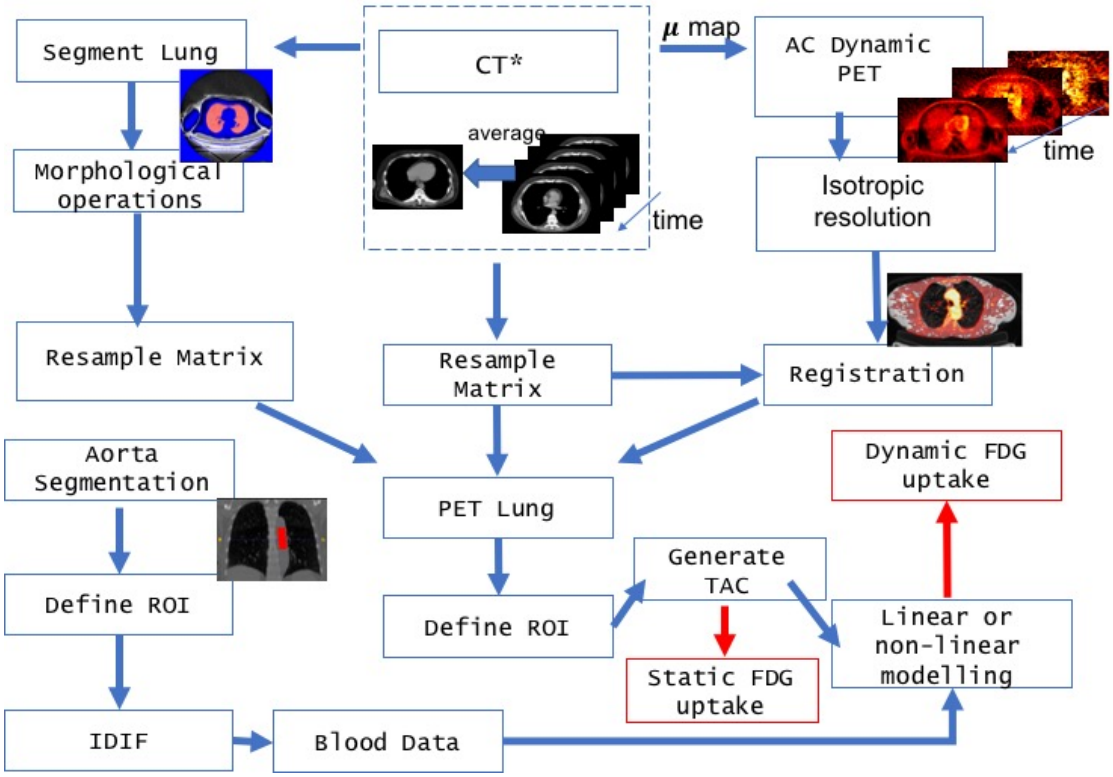

A schematic overview of the different stages of the analysis pipeline and their relationships.
** CT refers to either standard resolution chest CT or cine-CT.*
AC = attenuation correction, CT = computed tomography, PET = positron emission tomography, IDIF = image derived input function, ROI = Region of Interest, TAC = time activity curve, μ = linear attenuation coefficient.

3.3.2 *Image registration*

The alignment of the PET and CT scans is inherent in hybrid scanners. Visual inspection of the registered PET and CT scans were made using viewing ITK-snap [146], particular attention was paid to the heart and vessels as these are more readily observable than structures within the lung. Attempts were made to correct gross patient movement using simple translation operations.

3.3.3 *Lung and Vessel Segmentation*

The purpose of segmentation was to extract a region of interest from an image (i.e. sections of lungs or vessels), the output of segmentation is a binary mask whose value is 1 in the ROI and 0 for all other points in the image. After a period of exploratory work,

whole lung segmentations were undertaken using a semi-automated technique within ITK-SNAP software [146]. The CT image is first pre-processed: a threshold based on CT numbers of $>$ -1022 and $<$ 300 excludes soft tissue, blood vessels and bone from the image leaving mainly lung airways and parenchyma. Next, an active contouring method delineates the contours from a set of user defined seed points, major air vessels were not included. The lung mask was manually inspected and corrected when necessary.

Morphological operations were then performed: erosion with a disc shaped structural element with a radius of 3 pixels followed by an opening operation. The resulting whole lung masks were then visually inspected: the first 5 minutes of the ^{18}F-FDG PET scan was summed and overlaid on the lung mask. Spillover of the ^{18}F-FDG signal from the heart and diaphragm were manually corrected, if required.

The lungs were further subdivided into twelve equal volume ROIs to investigate regional difference in ^{18}F-FDG uptake as has been performed in previous analysis pipelines [66]. An example of these regions is shown in figure 3.2. These regions were combined into larger volumes which more anatomical relevance: the upper, middle and lower lung (by combining left and right, anterior and posterior segments).

The descending aorta (DA) was chosen as the vessel for the input function. The rationale for using the DA is based on previous work which revealed it to be preferable in estimating kinetic rate constants [127]. A circular ROI was manually delineated and positioned in the centre of the DA to minimise the partial volume effect, unless otherwise stated a 5 pixel diameter was used. The ROIs were drawn over 25 axial slices; the most superior slice was chosen in the aortic bifurcation. A summed ^{18}F-FDG PET image (0-5 minutes) was generated and used as guide to help with the placement of the ROI and assess gross patient movement.

Figure 3.2: **Example of a regional lung segmentation for a subject.**

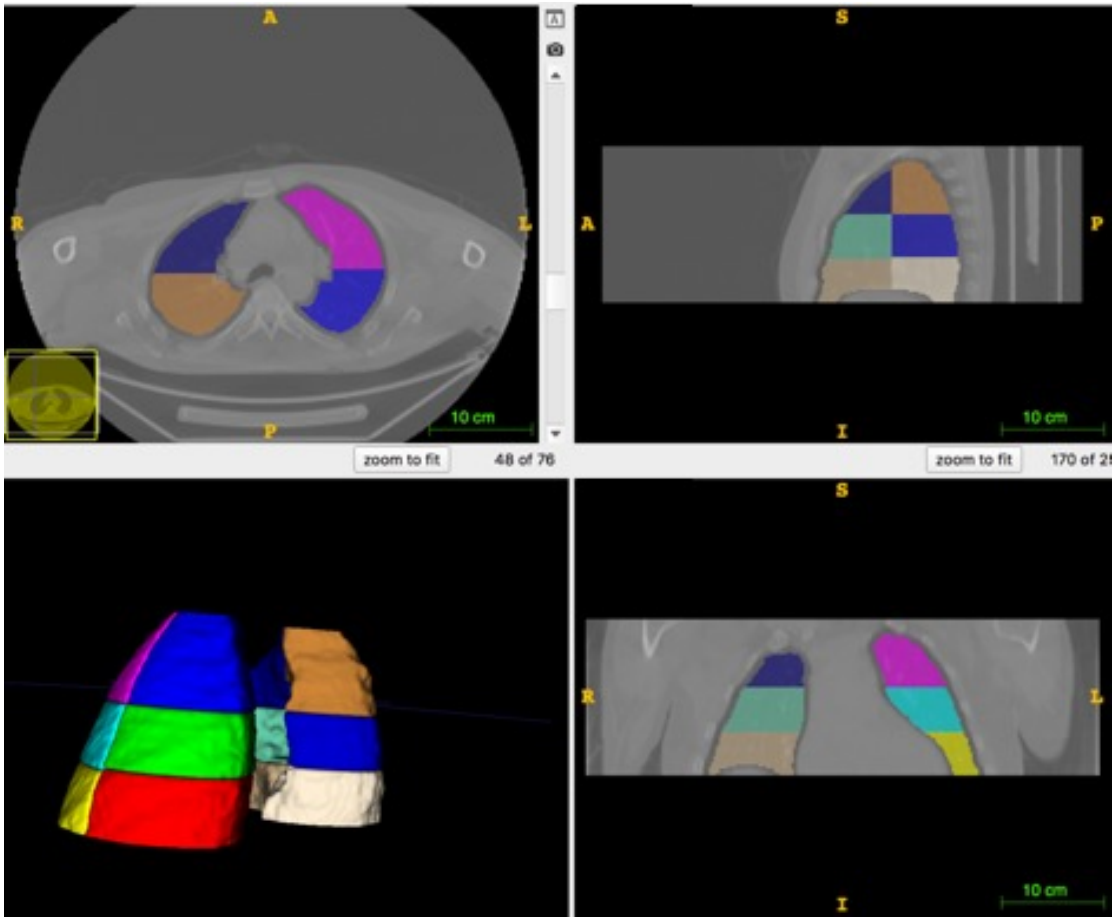

Each lung was divided into 6 equal volume regions. These regions were combined to give larger lung regions of interest.

3.3.4 *Lung TACs and IDIF*

For each subject, the binary mask obtained from the lung segmentations was applied to the registered PET scan to obtain lung time activity curves (TACs). TACs represent the concentration of ^{18}F-FDG over time in the ROI. Blood TACs were obtained using the vessel segmentation.

The blood TACs were first smoothed to minimise noise by fitting a function to the data points. In general, the blood TAC was modelled by basis functions with a varying number of exponentials with an initial linear slope as described in [147] ; the exponential model that best fits the blood TAC was found using a least squares algorithm.

Next a correction was introduced for the time delay, τ, between the bolus injection of the tracer and the arrival time in the lung ROI. Unless otherwise stated, to estimate the time delay, a one-compartmental model was fitted to the first 5 minutes of the smoothed blood TAC and lung TAC. Then a delay of $\pm$ 50 seconds in one second increments was introduced and the delay was estimated by finding the minimum value of the residual sum of squares on the model fit [66].

The clearance of a tracer is assumed from the plasma rather than blood in keeping with previous studies and general kinetic modelling principles [66, 147] hence, the blood TAC was converted into a plasma TAC using the plasma-over-blood (POB) ratio. The POB ratio was calculated for each subject using the ratio of counts in the plasma and blood from the discrete venous blood samples. The limitations of this correction are presented in detail in Chapter 4 (see Discussion).

3.3.5 *Outcome Measures*

For each subject, whole or regional ^{18}F-FDG uptake in the lung was estimated using the lung TAC and IDIF. An overview of the process to estimate the outcomes is shown in figure 3.3. The SUV was calculated using equation 2.1 as the mean value in the ROI (unless otherwise stated) where, $C(t)$ was the average decay corrected concentration from the final 30 minutes of the PET scan.

Patlak graphical analysis was used to estimate the rate of uptake of ^{18}F-FDG in the lung, K_{ip}, and the steady state volume of distribution, V_{ss}, using equation 2.16. $C_m(t)$ and $C_p(t)$ were obtained from the lung TAC and the IDIF, using time points $t > 10$mins. Further, the normalised uptake, nK_i, described by equation 2.19 was also calculated.

Compartmental modelling was used to estimate the metabolic rate constant (K_{im}). The Sokoloff irreversible two-compartment model was used to describe the kinetics of ^{18}F-FDG in the lung [121]. The fractional blood volume, V_b, is a parameter that is

Figure 3.3: **Overview of analysis steps to estimate pulmonary ^{18}F-FDG outcomes.**

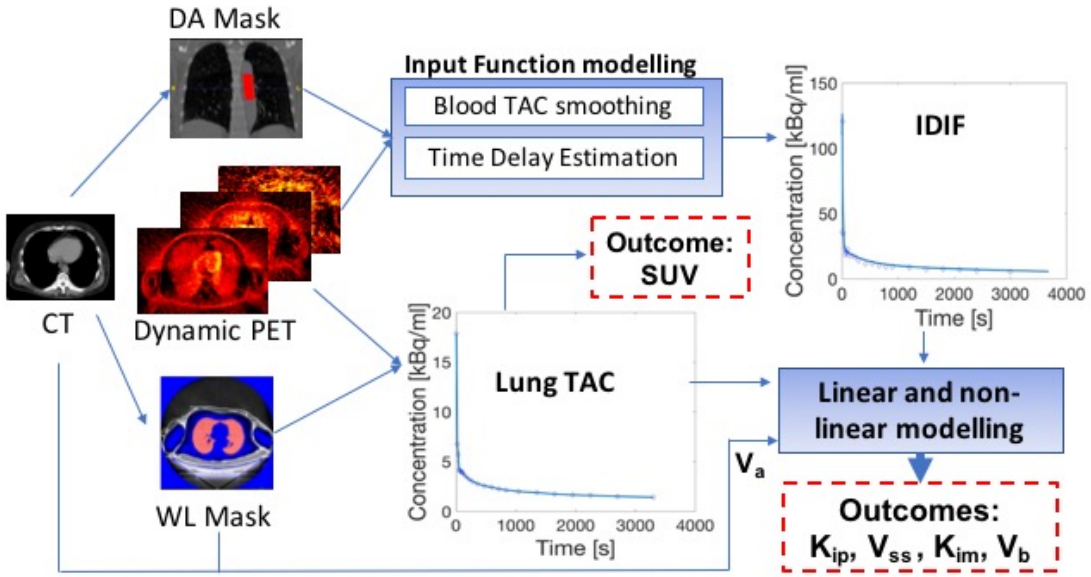

Modelling of the lung TAC and the IDIF gives estimates of the dynamic measures of ^{18}F-FDG uptake (i.e. K_{ip}, V_{ss}, K_{im} and V_b). The SUV is calculated using the average of the final time points of the lung TAC.
CT = computed tomography, PET = positron emission tomography, IDIF = image derived input function,SUV = standardised uptake value, TAC = time activity curve, V_a = fractional air volume), V_b = fractional blood volume), WL = whole lung

estimated in this model and is also reported as an outcome measure along with K_{im}. These outcomes were obtained by solving equation 2.2.

In order to solve equation 2.2 and arrive at estimates of K_{im} and V_b, a number of inputs are required. $C_p(t)$ was defined by the IDIF and the measured concentration of ^{18}F-FDG in the lung was given by the lung TAC (i.e. Y_i in equation 2.9). V_a was estimated using the CT-AC and equation 2.10.

The WRSS (equation 2.9) was minimised using the simulated annealing global optimisation method; this was implemented in a bespoke automated pipeline using the MATLAB optimisation toolbox (version 7.5). A start point is required by the optimisation algorithm, which is an initial guess of the parameters (i.e. K_1, k_2, k_3 and V_b), multiple start points were used and obtained using the MultiStart function within the

toolbox. The weighting factors, W_i, were calculated based on the duration of the frame length given by:

$$W_i = \frac{\sqrt{t_d(i)}}{\sum_i \sqrt{t_d(i)}} \tag{3.1}$$

3.4 STATISTICS

Statistics were analysed using R version 3.0.0 with R studio version 0.98.953 [148]. Medians, means, inter-quartile ranges and correlations were used. When longitudinal study measures were compared, changes from baseline were analysed using linear regression model covariates included systemic markers of inflammation (e.g. WBCs, Fibrinogen, hsCRP).

P-values < 0.05 were considered significant for all statistical analyses, except when the Bonferroni correction was applied. All data are presented as mean $\pm$ standard deviation (SD), percentages, or with 95% confidence intervals.

Bland-Altman plots were used to compare the different outcome variables as a measure of repeatability and reproducibility. The Bland-Altman coefficient of repeatability is given by $2\times$ SD; we expect 95% of the difference to be less than this value. We also reported the coefficient of variation (COV) as a further measure of repeatability.

Histogram plots were used to assess whether a normal distribution was observed in a variable. To investigate group differences the Hedge's g effect was used, as a further complementary measure to the unpaired t-test .

Additional study specific statistical tests are discussed in the relevant chapters.

4

^{18}F-FDG PET/CT IN CHRONIC OBSTRUCTIVE PULMONARY DISEASE

4.1 BACKGROUND

Chronic obstructive pulmonary disease (COPD) is a complex condition characterised by a range of pathological changes including bronchitis and emphysema. Although the molecular origins of the disease have yet to be fully elucidated, it is postulated that inhalation of tobacco smoke (or other toxic air particulates) can trigger an abnormal exuberant inflammatory response which may persist even when the trigger is removed. Inflammation is a driver of disease progression and is characterised by increased lymphocytes, macrophages and neutrophils in the lung [11, 149–151]. For COPD patients, current treatment options remain limited, leading to many remaining symptomatic and experiencing moderate to severe exacerbations, despite being on optimal therapy [149]. Development of alternative therapies has been unduly slow and can be explained, in part, by the lack of biomarkers reflective of disease phenotypes, progression or severity. Whilst Forced Expiratory Volume in 1 second (FEV_1), assessed by spirometry, is used to diagnose COPD, this measure does not relate well to systemic inflammation or indeed to the impact of the condition on symptoms [152]. Doubtless, the difficulty of establishing clinically relevant phenotypes and endotypes in COPD has contributed to the challenge of finding efficacious treatments.

Since glucose utilisation is increased in inflammatory cells, COPD patients should exhibit increased pulmonary uptake of ^{18}F-FDG, despite emphysematous loss of lung tissue [153]. To date, only a handful of studies have used ^{18}F-FDG in COPD patients: a small study found whole lung uptake of ^{18}F-FDG could distinguish COPD participants from healthy controls and asthmatics [55]. In later work, the rate of ^{18}F-FDG uptake in COPD participants correlated with disease severity assessed using FEV_1 [54].

Regional analyses of the lung also revealed that ^{18}F-FDG uptake had a heterogenous distribution which may be related to the emphysematous burden. One of the most widely reported ^{18}F-FDG PET imaging outcomes, taken as a surrogate of lung inflammation, is the normalised rate of uptake, nK_i, derived from Patlak graphical analysis (PGA) [43]. However, alternative methods have been used to quantify pulmonary ^{18}F-FDG uptake, with the lung signal in each influenced to varying degrees by blood and air content. Indeed, preliminary findings suggests that an extemporaneous choice of ^{18}F-FDG PET imaging endpoint could lead to different conclusions [66]. To ensure confidence in ^{18}F-FDG PET as a research tool which could advance pathophysiological understanding and therapeutics development in COPD, further work is urgently needed to understand the limitations of these quantitative ^{18}F-FDG outcomes.

In this chapter, ^{18}F-FDG PET/CT scans from two parallel imaging studies are used to compare and contrast the utility of quantitative ^{18}F-FDG PET/CT imaging endpoints in a substantially larger dataset of COPD subjects (n = 85) than previously reported. The clinical relevance of ^{18}F-FDG uptake was investigated in relation to validated markers of systemic inflammation and disease severity. Further, imaging outcomes were compared in cohorts of α_1ATD patients, healthy smokers (sHV) and healthy non-smokers (nsHV). Finally, the technical validity was assessed by measuring repeatability and reproducibility of the different ^{18}F-FDG PET imaging outcomes.

4.2 HYPOTHESES

COPD patients, α_1ATD patients and current smokers will have elevated pulmonary inflammation as measured by ^{18}F-FDG PET compared to never-smokers.

4.3 AIMS

The primary aim was to compare regional and whole lung inflammation in COPD participants, α_1ATD patients, current smokers without COPD and healthy never smokers using quantitative ^{18}F-FDG PET. The different methods were compared and con-

trasted, evaluating their variability, repeatability, reproducibility and relationship to clinical measurements.

4.4 METHODS

4.4.1 *Study Design*

All subjects provided written informed consent in keeping with the Declaration of Helsinki. Subject data analysed in this work arise from two parallel imaging studies: the EVOLUTION clinical trial and an observational study (EVOLVE) (*REC 13/EE/0165, UK CRN ID 1513*).

EVOLUTION was a double-blinded, placebo controlled, randomised control trial investigating a novel, unlicensed compound in Phase II drug development, Losmapimod (a p38 MAPK inhibitor), in COPD participants [154]- the primary outcome of this study was the assessment of vascular inflammation, which is reported together with methodology elsewhere [155]. A favourable ethics opinion was granted from Cambridgeshire South Research Ethics Committee and the study is registered with ClinicalTrials.gov (**NCT01541852**). The trial flow chart is reproduced in figure 4.1. Longitudinal data are reported as baseline and follow-up ^{18}F-FDG PET/CT scans; the interval was approximately 16 weeks.

COPD participants were randomised equally to receive either losmapimod or placebo. The longitudinal data from the participants receiving placebo were used to investigate repeatability of ^{18}F-FDG PET/CT over 4 months.

EVOLVE was an observational, cross-sectional study of COPD participants, α_1ATD participants, healthy smokers and healthy never-smokers. Identical study assessments were performed in both studies (see chapter 3). A single cross-sectional ^{18}F-FDG PET/CT was performed on participants in this study.

Figure 4.1: **The EVOLUTION trial flow chart.**

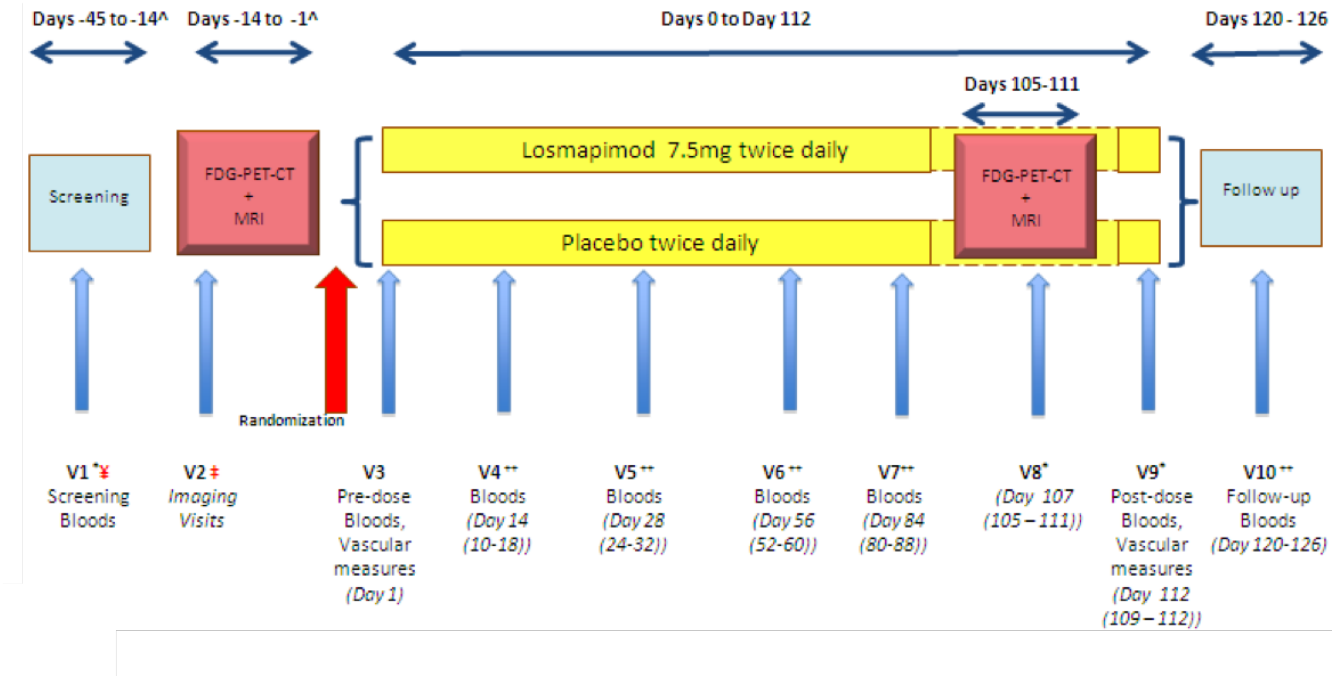

A baseline and follow-up pulmonary ^{18}F-FDG PET/CT scans occurred approximately 16 weeks apart. More details of the trial are available [154]. *MRI = Magnetic resonance imaging.*

4.4.2 *Quantitative PET/CT Protocol*

The subjects underwent the PET/CT protocol as described in chapter 3. For COPD and α_1ATD participants a single HRCT was performed, in the longitudinal study this was performed only at the baseline scan. Subjects were scanned in the supine position with arms raised above their heads; at full inspiration, where possible. The FOV covered the apex to the base of the lungs, with the subjects lungs centred in the FOV. Table 4.1 summarises the protocols used for HRCT scans for the scanners used in this study, images were reconstructed using a sharpening algorithm. The effective dose for the HRCT was estimated as 3.8mSv using the impact dose calculator. Emphysema burden was calculated from the HRCT scan using the Perc15 score, that is, the 15th percentile of Hounsfield Units distribution as described previously [156].

Prior to the PET scan, a low dose CT-AC scan, covering a single bed position with the subject breathing freely was performed. The whole lung fractional air volume, V_a, was calculated from the CT-AC. A bolus of approximately 240MBq ^{18}F-FDG was ad-

Figure 4.2: **Flow diagram for participants.**

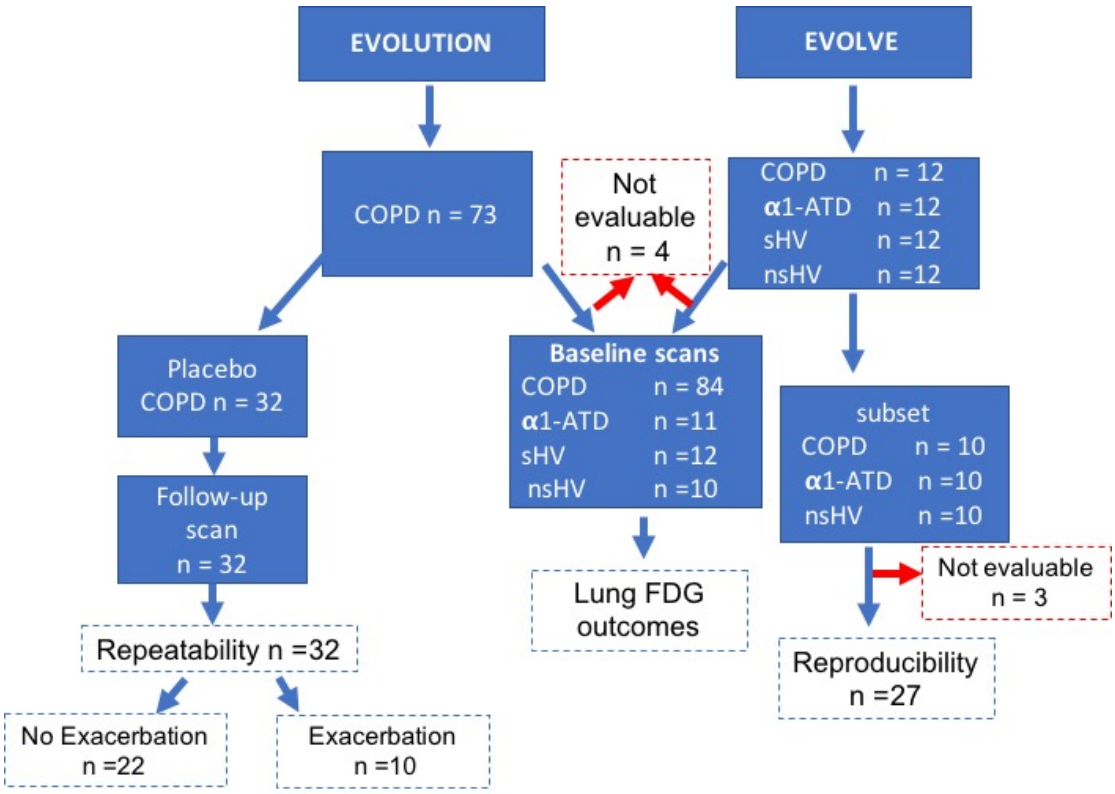

Summary diagram explaining the subject numbers for each of the experiments in this chapter. *COPD = Chronic Obstructive Pulmonary Disease, α_1ATD = Alpha-1-anti-trypsin deficiency, sHV = Healthy Volunteer smokers, nsHV = Healthy Volunteer never smokers.*

Table 4.1: Acquisition parameters for high resolution CT (HRCT) scans of the lungs for the two scanners used in this study.

Parameter	Scanner A	Scanner B
Tube voltage (kVp)	130	120
Tube current (mA)	170	440 (max)
Effective exposure (mAs)	70	440 (max)
Reconstruction	B70s	Body filter
Slice thickness (mm)	2	1.25

ministered at the start of the scan; the scan duration was 60 minutes.

4.4.3 *Image Analyses*

In this chapter, the pipeline described in chapter 3 was used for all subsequent analyses except for the reproducibility study (described in section 4.4.4).

In the reproducibility study, either pipeline A or pipeline B was used, given these labels to distinguish them from the pipeline used in the rest of this thesis. Hence, when reference to pipeline A or B is made, it should be understood that these have been used only in the reproducibility study (i.e. results in section 4.5.5); the differences between the pipelines are described in section 4.4.4.
^{18}F-FDG uptake was evaluated using SUV, nK_i, K_{ip} and K_{im} as surrogate markers of pulmonary inflammation. Unless otherwise stated SUV refers to the mean SUV in the ROI. Further outcomes from the ^{18}F-FDG imaging analyses included V_{ss} and V_b.

4.4.4 *Reproducibility of analysis*

A subset of 30 age and gender matched patients from the EVOLVE study were included in this evaluation: ten patients with COPD (age= 66 ± 9; 8M/2F), ten patients with α_1ATD (age= 63 ± 8; 7M/3F) and ten healthy never smokers (age= 68 ± 8; 9M/1F). For the initial analysis, subject data were analysed by operator A (as described in [66]) using a Molecular Imaging and Kinetic Analysis Toolbox (MIAKAT^{TM} [157]; Version no: 4.2.6) based pipeline - referred to as pipeline A. Operator B (LV) independently analysed the same dataset using the pipeline based on that described in chapter 3 - referred to as pipeline B. However, again note that the initial pipeline B is not identical to that described in chapter 3 (the differences are highlighted shortly).

The pipelines shared common procedures for pre-processing: the segmentation of the whole lung and blood vessels were performed using ITK-SNAP [158], plasma TACs were obtained from an ROI manually delineated within the descending aorta (DA); drawn in the centre of the vessel to minimise the partial volume effect. The principle differences between the pipelines are outlined in table 4.2. In pipeline A, subsequent analysis was performed using a MIAKAT based pipeline: MIAKAT software was modified for lung ^{18}F-FDG kinetics by operator A. Importantly, both pipelines used the same underlying models to obtain the ^{18}F-FDG PET imaging outcomes (e.g. K_{im},K_{ip} etc.), see chapter 2.

In order to understand the drivers of any differences in the results, operator B investigated the salient parts of the analysis methodology, which led to any differences, and adjusted elements of pipeline B (described later) to improve agreement.

Table 4.2: Comparison of two analysis pipelines used to estimate metabolic rate of ^{18}F-FDG to assess pulmonary inflammation.

Parameter	**Pipeline A**	**Pipeline B: Initial**	**Pipeline B: Final**
Vessel ROI size	Circular, 5 pixel diameter, aortic arch to variable end	Circular, 8 pixel diameter, 25 slices beginning aortic arch	As pipeline A
Lung ROI closing/erosion operation	5 pixel diameter disc	3 pixel diameter disc	As pipeline B initial
Input function model	Exponential basis functions	Tri- or Bi- exponential fits	As pipeline A
Time Delay Estimation	Outside compartmental model optimisation	Inside compartmental model optimisation	As pipeline A
Time Delay Fitting	Delays spanning -50 to 50 seconds using 1-compartmental model fitted for first 5 minutes-lowest residual sum of squares	Additional parameter within estimation of rate constants	As pipeline A
Optimisation*	Local optimum	Global optimum	As pipeline A
Start point of Optimisation*	K_1 = 0.5, k_2 = 0.2, k_3 = 0.3, V_b = 0.1	Multiple start points generated finds best guess (lowest objective function value)	As pipeline A

The table highlights the key differences between the implementations primarily of the compartmental model. Parameters not included below were identical between the analysis pipelines.
Columns "Pipeline B: Initial" and "Pipeline B: Final" describes the parameters which were used in the initial evaluation and the final settings used following adjustments to pipeline B respectively.
** Apply only to compartmental modelling.*
ROI = Region of Interest

4.4.5 *Statistics*

In addition to the methods outlined in chapter 3, the intra-observer repeatability was assessed using the coefficient of variation (COV) by operator B using pipeline B. Spearmans correlation coefficient was calculated. Bland Altman plots were inspected for

bias following the approach suggested in [159], data were log transformed. The upper and lower levels of agreement (uloa and lloa)were calculated as the mean difference $\pm 2\times$ standard deviation of the difference. In the reproducibility experiment, as a further complementary measure to the unpaired t-test, group differences were investigated using the Hedge's g effect.

4.5 RESULTS

Table 4.3 shows the demographics, lung function tests, systemic markers and quantitative CT outcomes for the groups. The total number of evaluable cross-sectional scans in each subject group was 84 COPD participants, 11 α_1ATD participants, 12 nsHV and 10 sHV. Four participants (1 COPD, 1 α_1ATD and 2 sHV) were excluded due to excessive movement on the PET/CT scan.

There was no difference in the smoking pack-years between COPD participants and smokers (40 ± 26 vs 37 ± 19 pack-years respectively, $p = 0.36$); α_1ATD participants had smoked significantly less than both these groups (19 ± 11 pack-years, $p < 0.001$).

A significant difference was found in the FEV_1 and hsCRP between COPD and α_1ATD subjects compared to never smokers. V_a was significantly higher in the COPD and α_1ATD subjects compared to smokers and never smokers; there was no difference between smokers and never smokers.

Table 4.3: Demographics, clinical and CT imaging measures of the disease and control groups.

	COPD (n = 84)	**α_1ATD (n =11)**	**Smokers (n = 12)**	**Never Smokers (n =10)**
Gender (%male)	67	73	58	83
Age (years)	68 ± 8	$62 \pm 8^*$	$62 \pm 6^*$	69 ± 7
FEV_1 (L)	$1.37 \pm 0.6^{***}$	$1.47 \pm 0.4^{***}$	2.84 ± 0.56	2.88 ± 0.6
Fibrinogen (g/L)	$3.4 \pm 0.7^*$	3.1 ± 0.6	2.8 ± 0.6	2.7 ± 0.5
hsCRP (mg/L)	$5.2 \pm 7.0^*$	$3.3 \pm 2.3^*$	2.1 ± 1.4	1.2 ± 0.6
WCC ($\times 10^9$ /L)	6.54 ± 1.83	7.01 ± 2.72	7.28 ± 2.02	5.84 ± 1.31
Neutrophils ($\times 10^9$ /L)	4.43 ± 3.6	4.68 ± 2.47	4.53 ± 1.45	3.63 ± 1.11
Perc15 (HU)	-889 ± 54	-942 ± 18	NA	NA
V_a	$0.80 \pm 0.05^{**}$	$0.83 \pm 0.03^{**}$	0.73 ± 0.03	0.72 ± 0.04

FEV_1 = *forced expiratory volume in 1 second, hsCRP = high sensitivity C-reactive protein, Perc15 = 15th percentile of Hounsfield units distribution, NA = not applicable,* V_a *= fractional air volume, WCC = white cell count.*
****p<0.001, **p<0.01, *p<0.05 significant difference compared to never-smokers.*

4.5.1 *Whole lung ^{18}F-FDG PET imaging endpoints*

Patlak graphical analysis outcomes

nK_i was increased in COPD participants, α_1ATD participants and smokers compared to never smokers (see figure 4.4a). There was no statistical difference in whole lung nK_i between COPD, α_1ATD participants or smokers. Grouping COPD participants by smoking history revealed that nK_i was modestly elevated in COPD participants who were current smokers compared to those who were ex-smokers ($4.2 \pm 0.1 \times 10^{-3}$ vs $3.7 \pm 0.1 \times 10^{-3} ml \cdot cm^{-3} \cdot min^{-1}$, respectively; $p = 0.049$) despite no significant difference in FEV_1 between them (mean FEV_1 % predicted: $47 \pm 18\%$ vs $50 \pm 22\%$, respectively).

K_{ip} and V_{ss} were elevated in the smokers without COPD and never-smokers compared to the COPD and α_1ATD participants, there was a modest indication that K_{ip} was elevated in the smokers compared to never smokers (p=0.048). There was no difference in K_{ip} between COPD and α_1ATD participants.

Compartmental modelling outcomes

In contrast to nK_i, the group differences in K_{im} did not reach significance between any of the cohorts compared to the never-smoker control group (see figure 4.5a). An elevated K_{im} was observed in smokers compared to COPD participants ($p = 0.007$) but no other significant differences were found. COPD and α_1ATD participants had decreased V_b when compared to smokers and never smokers; there was no statistical difference in V_b between smokers and never smokers.

SUV

The SUV was increased in the smokers and never smokers groups compared to the COPD and α_1ATD cohorts (see figure 4.5); there was no significant difference between the smokers and never smokers. The SUV was significantly elevated in the COPD participants compared to the α_1ATD subjects (0.43 ± 0.13 vs 0.31 ± 0.086; $p = 5.0 \times 10^{-4}$).

Figure 4.3: **Whole lung nK_i, K_{ip} and V_{ss} in disease and control groups.**

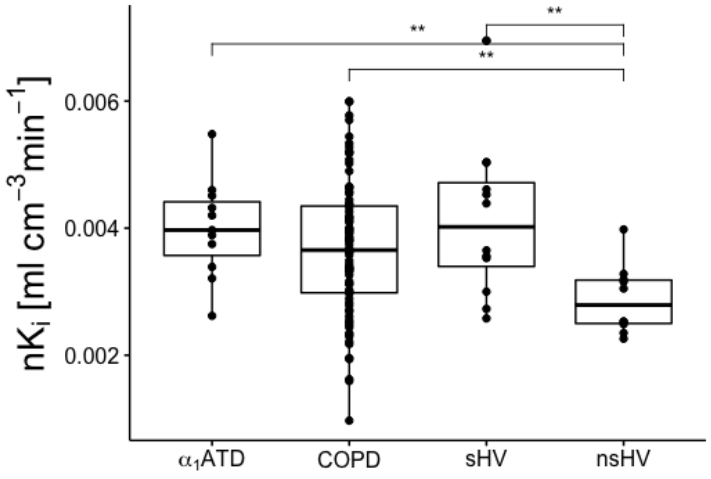

(a) **Whole lung nK_i.**

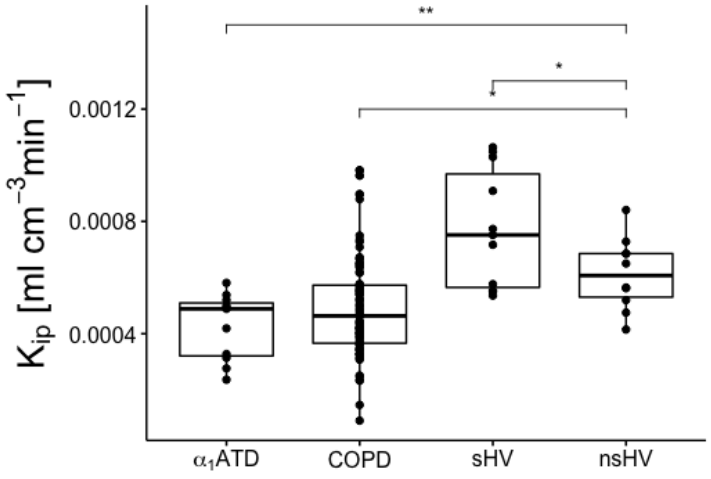

(b) **Whole lung K_{ip}.**

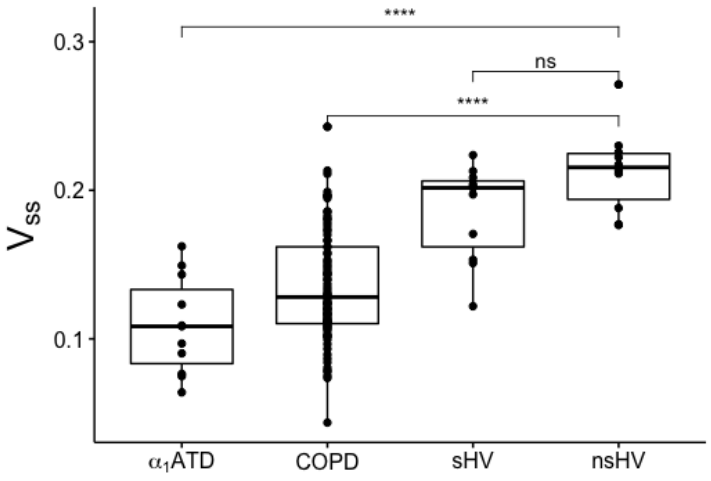

(c) **Whole lung V_{ss}.**

Individual values are shown along with median, first and third quartile values. SUV is the average value from the final 30 minutes of the scan. *COPD = Chronic Obstructive Pulmonary Disease, α_1ATD = Alpha-1-anti-trypsin deficiency, sHV = Healthy Volunteer smokers, nsHV = Healthy Volunteer never smokers.* * *p-value* < 0.05, ** *p-value* < 0.01, *** *p-value* < 0.001, **** *p-value* < 0.0001

Figure 4.4: **Whole lung K_{im} and V_b in disease and control groups.**

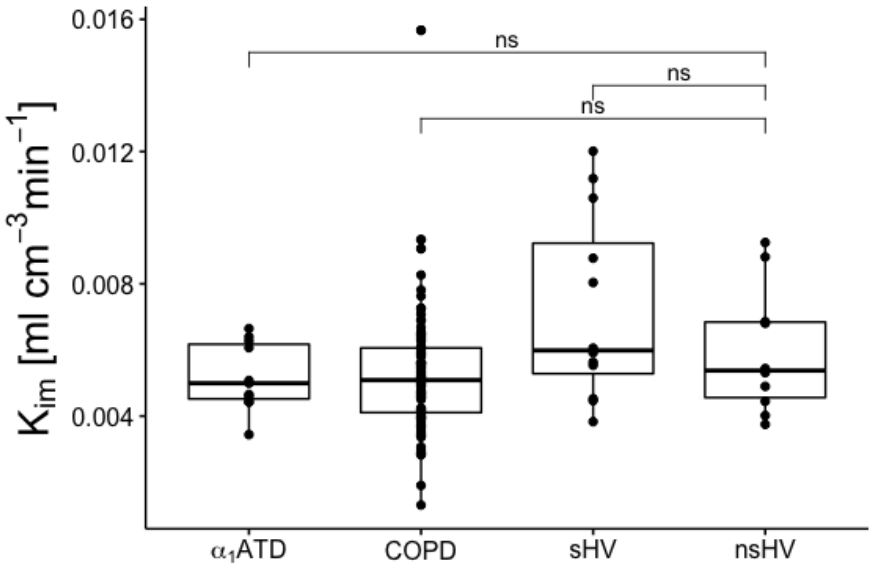

(a) **Whole lung K_{im}.**

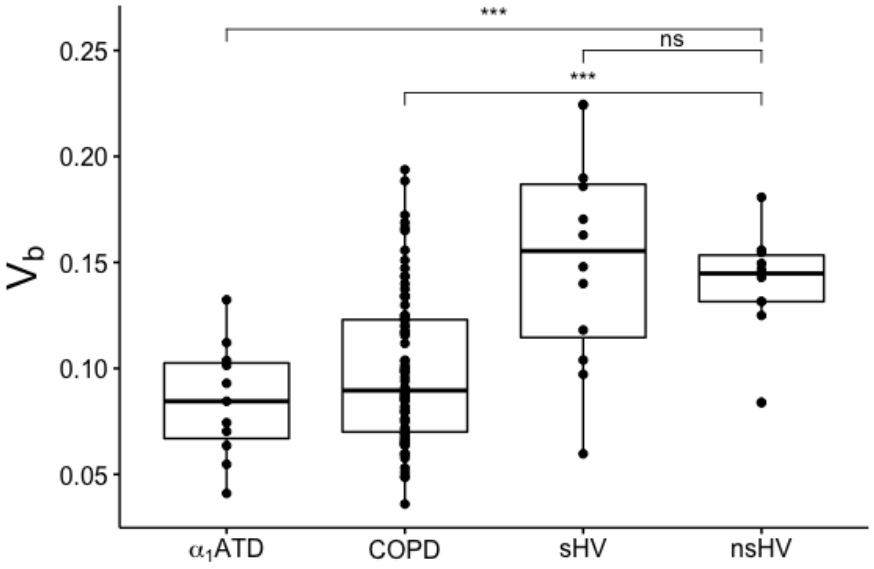

(b) **Whole lung V_b.**

Individual values are shown along with median, first and third quartile values. P-values are indicated by the horizontal lines (for each group compared to the control group of never smokers). *COPD = Chronic Obstructive Pulmonary Disease, α_1ATD = Alpha-1-anti-trypsin deficiency, sHV = Healthy Volunteer smokers, nsHV = Healthy Volunteer never smokers.*
* *p-value* < 0.05, ** *p-value* < 0.01, *** *p-value* < 0.001, **** *p-value* < 0.0001

Figure 4.5: **Whole lung SUV in disease and control groups.**

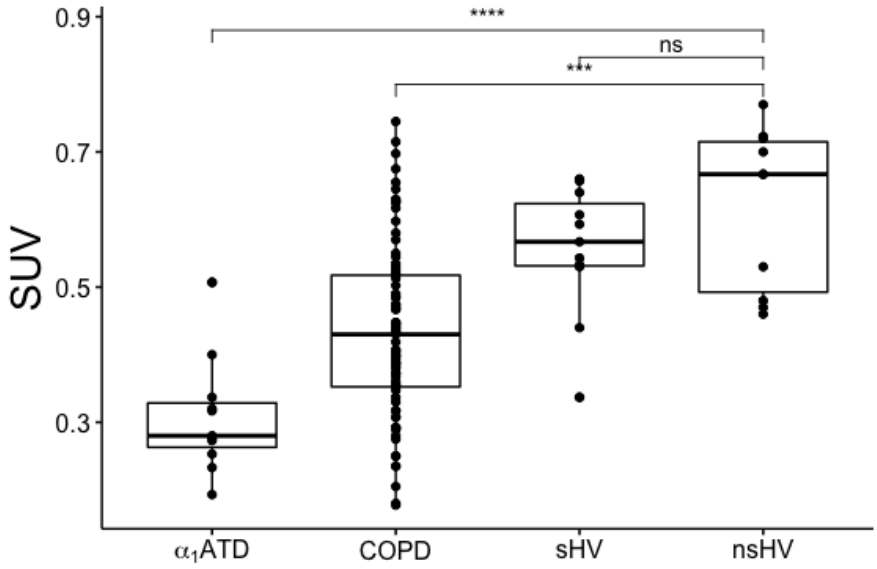

Individual values are shown along with median, first and third quartile values. *COPD = Chronic Obstructive Pulmonary Disease, α_1ATD = Alpha-1-anti-trypsin deficiency, sHV = Healthy Volunteer smokers, nsHV = Healthy Volunteer never smokers.*
* *p-value* < 0.05, ** *p-value* < 0.01, *** *p-value* < 0.001, **** *p-value* < 0.0001

4.5.2 *Regional lung ^{18}F-FDG PET imaging endpoints*

Between group comparison

Table 4.4 shows the results for ^{18}F-FDG PET imaging endpoints assessed in the upper, middle and lower regions of the lung in each of the groups. Notably, COPD participants had increased upper and middle lung nK_i values compared to never smokers. Furthermore, α_1ATD participants and smokers demonstrated a similar increase in upper and middle lung nK_i values compared to never smokers. No differences were found in the lower lung between the cohorts.

In contrast, smokers and never smokers exhibited increased regional K_{ip} values compared to COPD and α_1ATD participants but this did not reach significance. K_{ip} values were elevated in the upper and middle lung in smokers compared to never smokers.

K_{im} values exhibited no statistical differences between the groups when compared to the control group across the upper, middle and lower lung. However, in the upper lung K_{im} values were increased in the smokers when compared to the COPD and α_1ATD participants ($p = 0.002$ and 0.006, respectively). V_b was decreased in the upper, middle and lower lung in α_1ATD and COPD participants compared to never smokers. There was no difference in V_b between smokers and never smokers in any lung region; this was also the case for V_{ss}.

Within-group comparsion

A within group comparison of ^{18}F-FDG PET imaging endpoints found COPD participants had elevated K_{im} values in the upper and middle lung compared to their lower lungs ($p = 2.1 \times 10^{-5}$ and 2.3×10^{-4} , respectively). No within group significant differences were found between the upper, middle or lower regions in the other endpoints measuring uptake (i.e. nK_i, K_{ip}, SUV). In α_1ATD and COPD participants, V_b was greater in the upper lung compared to the lower lung with no other significant within group regional differences.

Table 4.4: Regional lung ^{18}F-FDG PET endpoints in disease and healthy participants.

	COPD			**α_1ATD**		
	Upper	Middle	Lower	Upper	Middle	Lower
$nK_i(\times10^{-3})$ $[ml/cm^3/min^{-1}]$	3.9 ± 1.3*	3.6 ± 1.2*	3.5 ± 1.4	3.8 ± 1.1*	4.2 ± 1.1*	3.8 ± 1.7
$K_{im}(\times10^{-3})$ $[ml/cm^3/min^{-1}]$	5.8 ± 2.1	5.7 ± 2.3	4.5 ± 1.8	5.2 ± 2.3	5.1 ± 1.8	4.2 ± 2.2*
$K_{ip}(\times10^{-4})$ $[ml/cm^3/min^{-1}]$	5.0 ± 1.5	4.8 ± 1.7	4.7 ± 2.3*	4.5 ± 1.2	4.4 ± 1.5	3.9 ± 2.2
V_{ss} $[ml/cm^3]$	0.13 ± 0.047*	0.14 ± 0.035*	0.14 ± 0.041*	0.12 ± 0.034*	0.11 ± 0.034*	0.10 ± 0.038*
V_b	0.11 ± 0.045*	0.10 ± 0.036*	0.087 ± 0.039*	0.11 ± 0.033*	0.084 ± 0.034*	0.052 ± 0.027*
	Smokers healthy volunteers			**Never-smokers healthy volunteers**		
	Upper	Middle	Lower	Upper	Middle	Lower
$nK_i(\times10^{-3})$ $[ml/cm^3/min^{-1}]$	4.5 ± 1.3*	4.3 ± 1.4*	4.0 ± 1.3	2.7 ± 0.8	2.7 ± 0.6	3.3 ± 1.4
$K_{im}(\times10^{-3})$ $[ml/cm^3/min^{-1}]$	8.6 ± 3.4	7.5 ± 3.0	6.4 ± 3.1	7.2 ± 0.3	5.9 ± 1.9	5.4 ± 2.5
$K_{ip}(\times10^{-4})$ $[ml/cm^3/min^{-1}]$	7.9 ± 2.2*	7.7 ± 2.3*	7.6 ± 2.7	5.4 ± 1.6	5.7 ± 1.5	7.3 ± 2.3
V_{ss} $[ml/cm^3]$	0.18 ± 0.030	0.19 ± 0.032	0.20 ± 0.039	0.21 ± 0.025	0.21 ± 0.028	0.23 ± 0.037
V_b	0.16 ± 0.043	0.16 ± 0.053	0.15 ± 0.07	0.15 ± 0.027	0.15 ± 0.027	0.11 ± 0.031

COPD = Chronic Obstructive Pulmonary Disease, α_1ATD = alpha-1 anti-trypsin deficiency
V_b = Fractional blood volume, V_{ss} = steady state partition coefficient of ^{18}F-FDG.
** indicates a p-value < 0.05 as compared to never-smokers.*

4.5.3 *Comparison between ^{18}F-FDG PET endpoints and clinical measurements*

In the COPD group, correlation was observed between whole lung nK_i and fibrinogen ($r = 0.40, p < 0.001$), log_{10}hsCRP ($r = 0.26, p = 0.02$), WCC ($r = 0.24, p = 0.03$) and neutrophils ($r = 0.28, p = 0.01$). A modest inverse correlation was observed between FEV1 (%predicted) ($r = -0.22, p = 0.04$) and whole lung nK_i; however, no correlation was found between nK_i and 6MWD ($r = -0.26, p = 0.15$) or emphysema assessed as Perc15 scores ($r = -0.10, p = 0.42$). There was no correlation found between the total smoking pack years and whole lung nK_i. In contrast to nK_i, there were no significant correlations observed between whole lung K_{im} and clinical measurements. SUV and K_{ip} had modest positive correlations with FEV_1 ($r = 0.64, p = 1.8 \times 10^{-8}$ and $r = 0.40, p = 0.0005$, respectively); no other significant findings were observed.

Given that nK_i demonstrated several significant correlations with clinical measurements, multiple regression analysis was performed for nKi; this demonstrated that fibrinogen was independently associated with nK_i (see table 4.5).

Table 4.5: Variables associated with whole lung nK_i in COPD participants assessed by regression analysis.

	nK_i	
	β	p
Fibrinogen	0.30	0.02
Current Smoking	0.20	0.07
FEV_1 predicted	-0.12	0.37
Neutrophils	0.10	0.41
Log_{10}hsCRP	0.02	0.90

FEV_1 = *Forced expiratory volume in 1 second, hsCRP = high sensitivity C reactive protein.*

4.5.4 *Repeatability of ^{18}F-FDG PET*

In COPD participants who received placebo, where a follow-up scan was available (n= 32), the repeatability of whole lung ^{18}F-FDG PET endpoints were assessed. The

mean difference in nK_i between the baseline and follow-up was $-1.2 \times 10^{-4} ml \cdot cm^{-3} \cdot min^{-1}$ with a coefficient of repeatability (CoR) of 1.8×10^{-3} (see figure 4.6a). The mean difference in K_{ip} and V_{ss} between baseline and follow-up were $-8.7 \times 10^{-6} ml \cdot cm^{-3} \cdot min^{-1}$ and $0.0024 ml \cdot cm^{-3}$, respectively; with CoR of 4.2×10^{-4} and 0.042. The mean difference in K_{im} and V_b between baseline and follow-up was $-1.5 \times 10^{-3} ml \cdot cm^{-3} \cdot min^{-1}$ and -2.9×10^{-3}, respectively; with CoR of 5.0×10^{-3} and 0.057 (see figure 4.6b). The mean difference in SUV was -0.01 with $CoR = 0.14$. Expressing these as percentages to allow for easier comparison, the mean values were -1.2%, 0.84%, 12.0% and 0.72% for nK_i, K_{ip}, K_{im} and the SUV respectively; the CORs were 21.5%, 26.3%, 42.2% and 12.2%.

Interestingly, COPD participants who had an exacerbation in the 3 months following the baseline scan (since study participants had to be exacerbation free for 1 month prior to the follow-up scan) exhibited a modest increase in whole lung nK_i ($p = 0.049$) compared to those who did not experience an exacerbation ($p = 0.59$; see table 4.6). There was no significant change in the other ^{18}F-FDG imaging outcomes in this exacerbation group. V_b exhibited no change between the baseline and follow-up scans.

Figure 4.6: **Bland Altman plots for whole lung ^{18}F-FDG PET outcomes.**

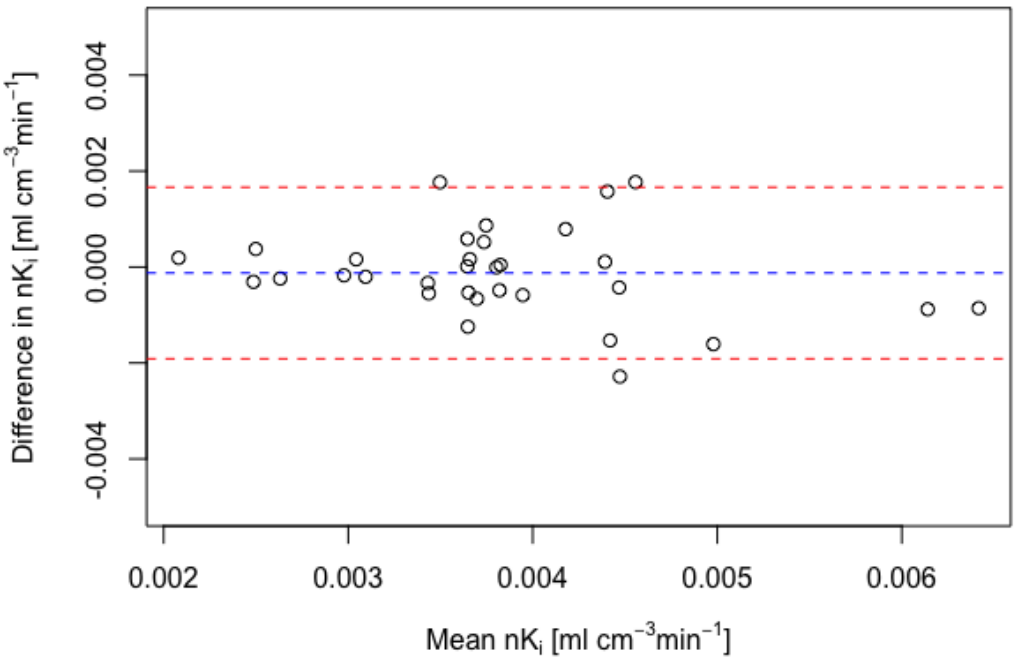

(a) **Bland Altman plot of the repeatability of nK_i.**

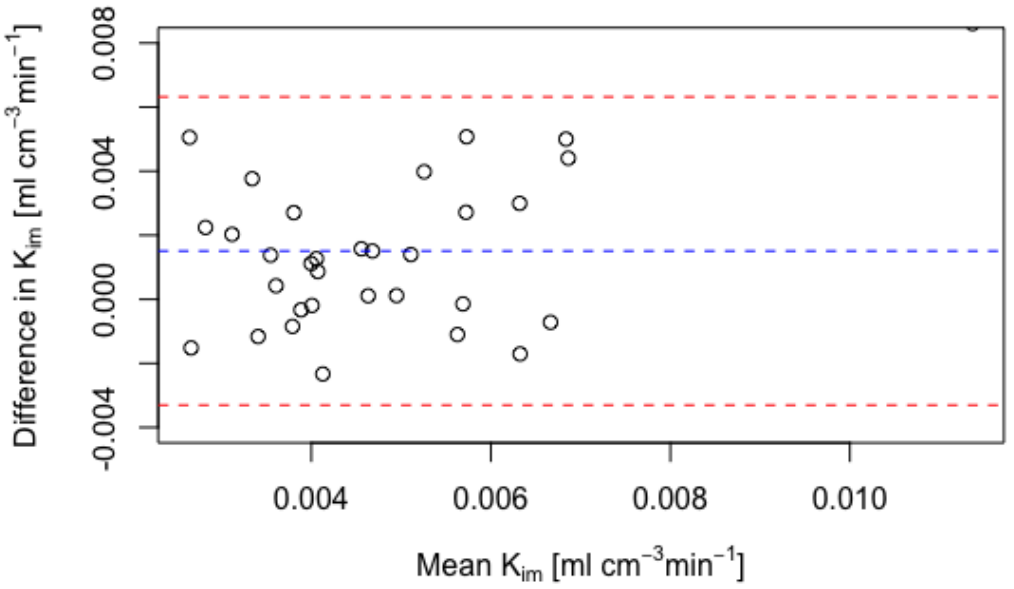

(b) **Bland Altman plot of the repeatability of K_{im}.**

Legend: These data were obtained from the baseline and follow-up ^{18}F-FDG scans of COPD participants in the placebo arm. The interval between scans was approximately 4 months. *Dashed red lines = Upper and lower limits of agreement, dashed blue line = mean of difference.*

Table 4.6: The effect of exacerbation on whole lung ^{18}F-FDG imaging endpoints in COPD participants. Those that experienced an exacerbation (n=10) and those that did not (n=22) between baseline and follow-up scans. These are subjects who were on the placebo arm of the EVOLUTION study.

	Exacerbation		**No exacerbation**	
	Baseline	**Follow-up**	**Baseline**	**Follow-up**
$K_{im}(ml \cdot cm^{-3} \cdot min^{-1})$	$6.0 \pm 1.9 \times 10^{-3}$	$3.9 \pm 1.8 \times 10^{-3}$	$5.0 \pm 1.5 \times 10^{-3}$	$4.3 \pm 1.2 \times 10^{-3}$
V_b	0.12 ± 0.044	0.10 ± 3.8	0.098 ± 0.034	0.095 ± 0.03
$K_{ip}(ml \cdot cm^{-3} \cdot min^{-1})$	$5.0 \pm 2.0 \times 10^{-4}$	$5.7 \pm 2.4 \times 10^{-4}$	$5.0 \pm 1.9 \times 10^{-4}$	$4.9 \pm 1.9 \times 10^{-4}$
$nK_i(ml \cdot cm^{-3} \cdot min^{-1})$	$3.6 \pm 1.1 \times 10^{-3}$	$4.1 \pm 1.3 \times 10^{-3}$	$3.8 \pm 0.88 \times 10^{-3}$	$3.7 \pm 1.1 \times 10^{-3}$
$V_{ss}(ml/cm^3)$	0.14 ± 0.041	0.14 ± 0.046	0.14 ± 0.039	0.13 ± 0.038

V_b = *Fractional blood volume,* V_{ss} = steady state partition coefficient of FDG.

4.5.5 *Reproducibility of analysis*

Pipeline A compared to pipeline B

There was poor agreement between K_{im} values on a subject level between the pipelines: figure 4.7(a) shows the Bland-Altman plot for K_{im}. The mean difference in K_{im} between the two pipelines was 0.0041 $ml \cdot cm^{-3} \cdot min^{-1}$ with upper and lower limits of agreement (uloa and lloa) of 0.00097 and 0.0072 $ml \cdot cm^{-3} \cdot min^{-1}$ respectively; the correlation coefficient was 0.62 ($p < 0.001$). Figure 4.7 (a) indicates a systematic relationship may exist between the difference and the mean values of K_{im} estimated using the two pipelines. These data were log transformed, giving a mean K_{im} of 1.8, lloa of 1.19 and uloa of 2.73 (after transformation back to the original scale). Although the transformation improved the situation, the agreement between pipelines was still poor.

The poor agreement between K_{im} was investigated further, figure 4.8(a) shows the differences in K_{im} between COPD, α_1ATD and controls using the two pipelines. Although a systemic offset was observed between the values obtained between the pipelines, this did not alter the overall group-level conclusions: the Hedge's g factor for the difference between COPD and HV was -0.89 for pipeline A and -0.57 for pipeline B. Further, for pipelines A and B, no significant difference was found between

these groups using the two sample t-test ($p = 0.088$ and $p = 0.26$, respectively). The variance in pipeline B was greater than pipeline A in the α_1ATD group (IQR $= 0.0031$ vs 0.0018, respectively). Figure 4.7(b) shows the Bland-Altman plot for V_b. The mean difference in V_b was -0.0015 (uloa = 0.045, lloa = -0.048); the correlation coefficient was 0.80. The Bland-Altman coefficients of reproducibility were 0.0031 and 0.047 for K_{im} and V_b respectively.

In comparison, the Bland-Altman plots for the ^{18}F-FDG uptake estimated using Patlak analysis are shown in figure 4.9. Both K_{ip} and nK_i have improved reproducibility compared to K_{im}: the coefficients of reproducibility for K_{ip} and nK_i were 0.00092 and 0.00015 and the correlation coefficients were 0.90 and 0.84, respectively ($p < 0.001$ in both cases).

Modified pipeline B

Subsequently, pipeline B was modified to understand the drivers of the difference described above. Since the differences pertained chiefly to compartmental modelling outcomes (i.e. K_{im}), these were used as the main endpoints to improve the reproducibility. Firstly, visual inspection of the lung tissue TACs from pipeline A and B revealed minimal differences. Further, the mean square error (mse) between lung TACs from pipeline A and pipeline B was 0.11 ± 0.040, therefore, the lung TACs were not responsible for the differences.

Next, a visual inspection of the blood TACs revealed slight differences due to the ROI methodology (e.g. size and location) used by the two operators. To improve agreement, the same DA ROI methodology was applied: in pipeline B, the area of each ROI was reduced and the same begin and end axial slice locations as pipeline A were used. This led to an improvement in the visual comparison of the blood TACs and a modest improvement in K_{im} (mean difference between was $0.0037 ml \cdot cm^{-3} \cdot min^{-1}$ compared to the original value of $0.0041 ml \cdot cm^{-3} \cdot min^{-1}$). The modelling of the blood TAC was then compared: the fitting of the input functions differed chiefly in the early stage of the scan (< 5 minutes post-injection) - likely due to the inherent noise due

Figure 4.7: **Bland-Altman plots comparing outcome parameters of a pulmonary compartmental model of ^{18}F-FDG.**

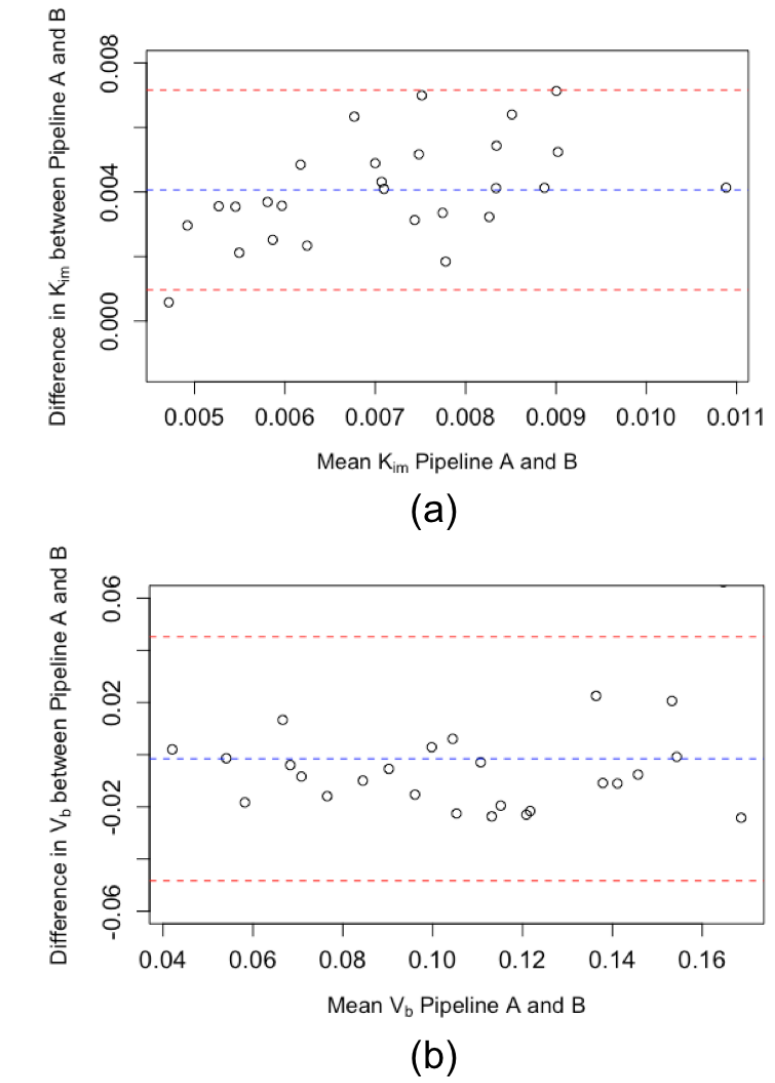

These are the initial results using two different analysis pipelines. Adjustment of pipeline B led to improved agreement between the pipelines (see figure 4.11).

to short frame durations. In pipeline B the input function modelling was altered to match the approach adopted in pipeline A. Firstly, we applied the same fitting function: here the blood TAC is modelled by basis functions [147] with a varying number of exponentials; the exponential model that best fits the blood TAC was found using a least squares algorithm. With both pipelines using this approach, the Bland-Altman coefficients of reproducibility were modestly improved (0.0023 for K_{im} and 0.034 for V_b).

Figure 4.8: **Boxplot of group differences in K_{im} between two independent analysis pipelines.**

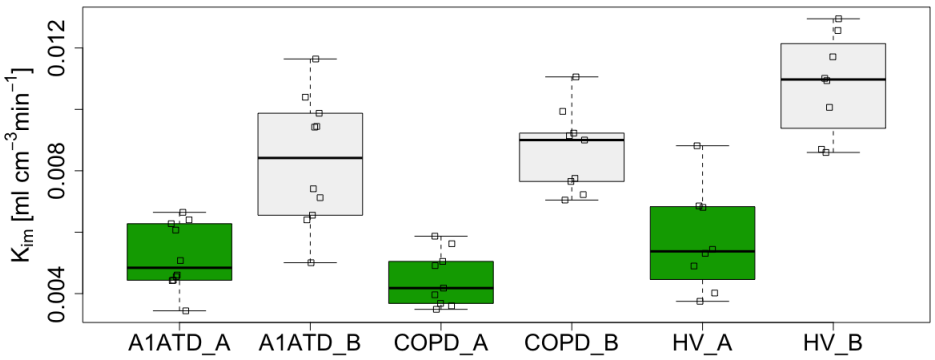

A1ATD = α1-antitrypsin deficiency patients, COPD = Chronic Obstructive Pulmonary Disease, HV = Healthy Volunteer, _A = Pipeline A result, _B = Pipeline B result.

The time delay estimation is also highly dependent on the initial time frames of the input function; an association between the difference in outcome parameters, particularly V_b, and the estimated time delay was found. The mean difference in time delay estimation between pipeline A and B was 3 ± 5.3 second. To improve the agreement between the estimated time delays for each subject, in pipeline B the method outlined in [66] (used in pipeline A) was replicated. Namely, a one compartmental model was fitted to the first 5 minutes of the smoothed blood TAC and lung TAC. Then a delay of $\pm$ 50 seconds in one second increments was introduced and the delay was estimated by finding the minimum value of the residual sum of squares on the model fit. The mean difference in time delay estimation was improved to 0.76 ± 1 second. This improved the Bland-Altman coefficient of reproducibility markedly to 0.016 for K_{im} and 0.028 for V_b.

Various factors were adjusted in the optimisation algorithm including the function, number of iterations, tolerance, initial parameter etc. but these were found to have less influence on outcome parameters. Figure 4.10 summarises the incremental improvement in agreement during each stage of the evaluation as we altered pipeline B. Following all adjustments to pipeline B, the Bland-Altman plots are shown in Figure 4.11; the mean differences were $K_{im} = 9.0 \times 10^{-4} ml \cdot cm^{-3} \cdot min^{-1}$ and $V_b = -0.0014$ with coefficients of reproducibility of 0.0015 and 0.027. The correlation was also improved:

Figure 4.9: **Bland Altman plots comparing ^{18}F-FDG uptake from two independent operators using Patlak analysis.**

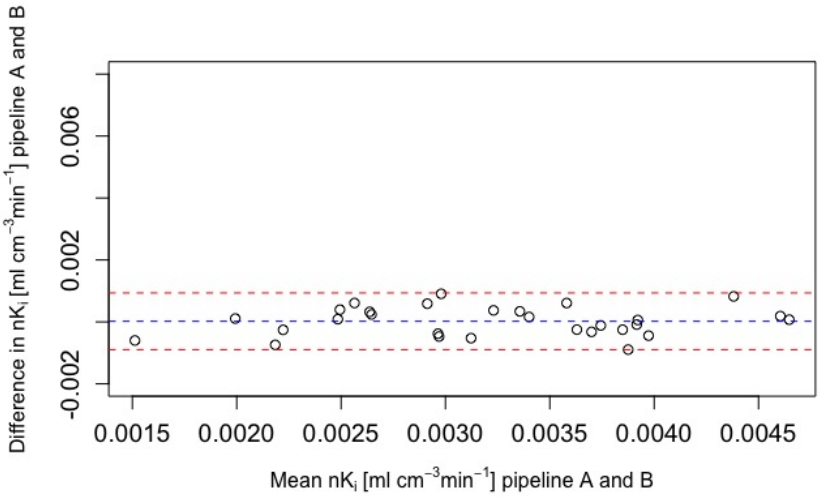

(a) **Bland Altman plot of the reproducibility of nK_i.**

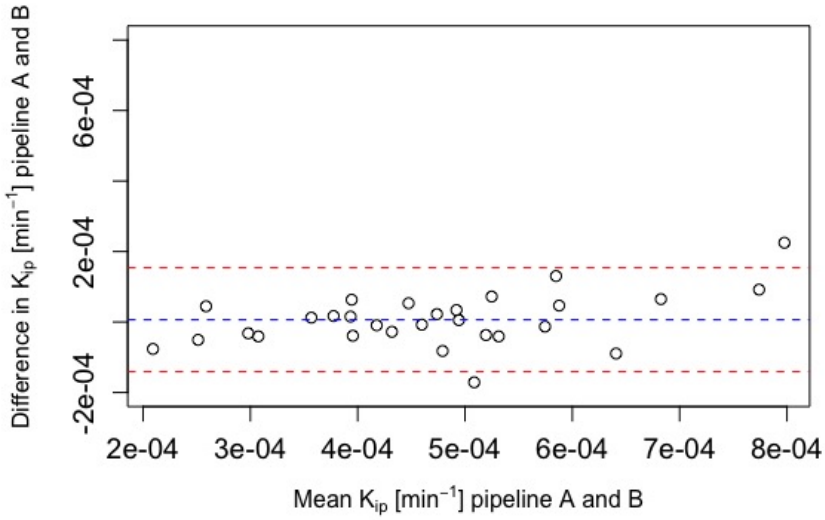

(b) **Bland Altman plot of the reproducibility of K_{ip}.**

These data were obtained from two independent operators and analysis pipelines (A and B). *Dashed red lines = Upper and lower limits of agreement, dashed blue line = mean of difference.*

for K_{im}, $r = 0.86$ and for V_b, $r = 0.94$. Figure 4.12 demonstrates the improvement in agreement on a group level. K_{im} calculated using the adjusted pipeline B had larger variability than pipeline A in the healthy control group (IQR = 0.0031 vs 0.0022, respectively); no notable change was observed in any of the other groups (see figure 4.12).

Figure 4.10: **Cumulative Bland-Altman coefficients of reproducibility for K_{im} during the evaluation of pipeline A and B.**

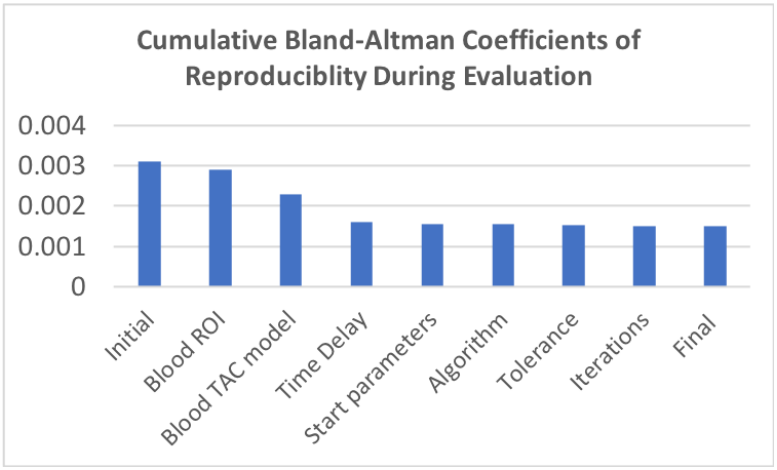

Pipeline B was altered at each stage to improve the agreement in K_{im}, each value represents the cumulative effect of all preceding stages.*ROI = Region of Interest*

Figure 4.11: **Bland-Altman plots comparing outcome parameters of a pulmonary compartmental model of ^{18}F-FDG using two independent analysis pipelines following adjustment of pipeline B.**

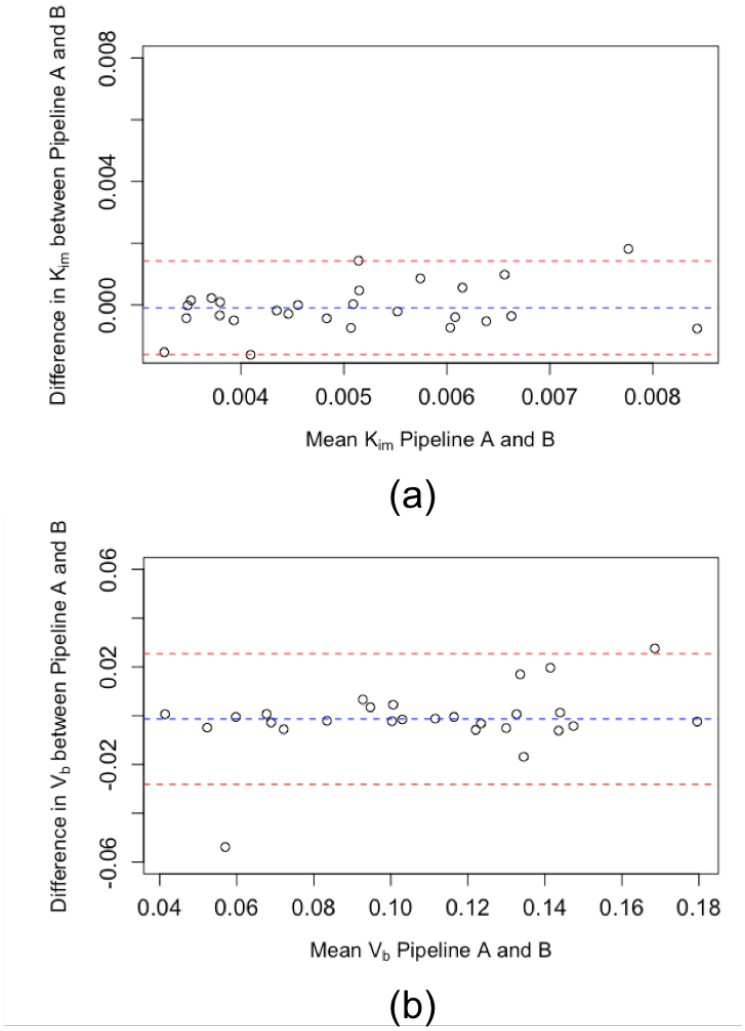

This should be compared to the initial results in figure 4.7.

Figure 4.12: **Boxplot of group differences in K_{im} between two independent analysis pipelines after adjustment of pipeline B.**

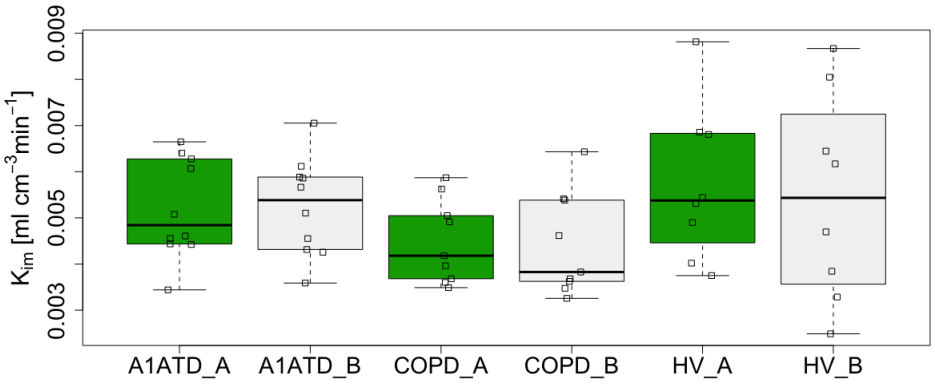

A1ATD = α1-antitrypsin deficiency patients, COPD = Chronic Obstructive Pulmonary Disease, HV = Healthy Volunteer, _A = Pipeline A result, _B = Pipeline B result.

4.6 DISCUSSION

In this study we built on prior small studies [54, 55] to test the hypothesis that ^{18}F-FDG can be used to quantify pulmonary inflammatory burden in COPD patients and investigated the different analysis methods used to quantify the signal. The main finding is that different analysis methods gave disparate results when comparing ^{18}F-FDG uptake in COPD, α_1ATD, healthy smokers and never smokers. Nevertheless, a number of interesting findings were observed which further elucidate the utility of these contending ^{18}F-FDG PET outcomes. Given that there is no gold standard method to assess lung inflammation, these results suggest that nK_i may be a suitable outcome for COPD, corroborating the pathological understanding of this disease. Besides demonstrating an increase in COPD participants compared to healthy never-smokers, nK_i was increased in α_1ATD participants and smokers without COPD. Further, nK_i correlated modestly with other clinical markers with the strongest correlations observed in the upper lung. The recent algebraic proof confirms that nK_i may not be driven predominately by inflammation as previously assumed, but these results suggest it may still be a useful composite measure of disease activity. Indeed, in COPD participants who experienced an exacerbation (1 month prior to the follow-up scan) there was a residual increase in nK_i as detected by ^{18}F-FDG PET. However, further work is needed to explore whether nK_i reflects inflammation.

Previous studies have highlighted that static ^{18}F-FDG PET measurements such as SUVs within the lung may be influenced by radioactivity in the blood vessels and air within lung spaces [24]. In our data, the whole lung SUV was increased in healthy controls compared to patients; indicating that it is unsuitable for evaluating lung disease in the context of COPD. Given that V_b was increased in never smokers and smokers compared to COPD patients, the increased SUV signal may be driven to a large extent by blood volume. The increased V_a found in COPD and α_1ATD due to tissue destruction is likely to be another factor reducing SUVs in the patient groups, and is consistent with previous findings in IPF patients [60]. These two factors likely explain the observed positive correlation between SUVs and FEV_1 in COPD patients. Nevertheless, other investigators found that the SUV was sensitive to low levels of induced

inflammation in healthy volunteers and so response to therapy [30], however, our results suggest in diffuse lung diseases when substantial tissue destruction is present, whole lung SUVs may be inadequate. An air-fraction correction for the SUV has been suggested [53] but the result may still be biased by the concentration of ^{18}F-FDG in the blood and is less sensitive to density mismatches [114]. Similarly, K_{ip} derived using Patlak analysis, showed increased values in the smokers and non-smokers compared to the COPD and α_1ATD participants (see figure 4.4b), these data indicate that as a measure of disease activity, K_{ip} is incongruent with the pathophysiological understanding of these diseases.

Using nK_i, elevated whole lung values were observed in α_1ATD and COPD participants compared to never smokers, consistent with the understanding that lung damage is driven by inflammation. Chronic inflammation is a key trait of smoking and the association of nK_i with smoking agrees with previous early observations [91]. These findings were observed in smokers without airflow limitation (smokers vs never-smokers) despite similar tissue density. Given that ^{18}F-FDG PET signal likely reflects a composite of total immune cell response, this may explain the comparable levels of ^{18}F-FDG in smokers with and without COPD consistent with the poor association between airway neutrophilia and airflow limitation.

nK_i values were elevated in α_1ATD participants compared to the never-smokers group; in contrast to findings previously reported by others [54], but our results are consistent with the understanding of pathological pathways underlying α_1ATD, specifically that lung damage is driven by increased neutrophilic inflammation. There was a modest yet significant correlation between whole lung nK_i values in COPD participants and circulating plasma fibrinogen. Given that previously no strong associations were found between markers of systemic inflammation (including fibrinogen) and vascular inflammation [155], these data do suggest, for the first time, that increased plasma fibrinogen observed in COPD participants may relate to the burden of pulmonary inflammation. Fibrinogen may be more reflective of exacerbation risk than other systemic markers (i.e. hsCRP, WCC and neutrophils) and this further supports its relevance as an FDA and EMA qualified drug development tool assessing risk for exacerbation and mortality in COPD [160]. In vitro studies suggest that pulmonary

epithelium can be an extrahepatic source of fibrinogen in response to local inflammatory mediators [161, 162]. However, fibrinogen is a putative biomarker and there is not currently enough evidence to support its use as a clinical measures of disease. The correlation between nK_i and neutrophil count, although weak, is of particular interest, since it is consistent with the previously held hypothesis that the ^{18}F-FDG signal may be driven primarily by neutrophil migration and activation [163]. However, ^{18}F-FDG uptake is likely to be a composite of the total immune response given previous findings in asthmatic participants that have demonstrated its use as a marker for eosinophilic inflammation [58]. Therefore, care is needed when attributing the origin of the signal to a specific cell line.

In principle compartmental modelling enables isolation of the ^{18}F-FDG PET signal from the influence of V_a and V_b, hence K_{im} is thought to be an accurate estimate of metabolic rate of ^{18}F-FDG in lung cells [30]. Therefore, as an outcome measure it may be more specific to the disease process, namely the inflammatory lung cells. A previous smaller study of COPD using ^{18}F-FDG PET found that compartmental modelling derived imaging endpoints had increased values in the lung compared to healthy controls, whereas Patlak outcomes found no differences [164]. In that study, an alternative methodology was used involving a retrospective correction for pulmonary blood and air; it has been suggested that this method may overestimate values in regions with vanishingly small tissue fractions, which are common in emphysematous disease [66]. Disappointingly, our results showed no significant differences between the groups using K_{im} when compared to the control group in both whole lung and regional analyses. This confirms the recent suggestion that K_{im} may not be sensitive enough to detect underlying metabolic differences in the disease process in COPD patients [66]. Indeed, in the COPD patients there was no evidence of association between K_{im} and clinical measures of disease. Interestingly, it did identify increased metabolic rate in smokers compared to COPD participants but not compared to never smokers, this latter finding is difficult to interpret. Indeed, in the small proportion of subjects who exhibited an exacerbation within 3 months of the baseline scan, K_{im} values exhibited a decrease in the follow-up scan, given the role of inflammation in exacerbations [165] this is another discordant finding. In contrast, nK_i increased, despite no significant

change in V_b or V_a between baseline and follow-up. This was evident despite a minimum one month period prior to the follow-up scan.

Regional differences in lung ^{18}F-FDG PET were identified: the upper lung had increased uptake nK_i in COPD, α_1ATD and healthy smokers compared with the upper lung in healthy non-smokers. In addition, there was a correlation between upper lung emphysema (assessed by perc15) and nK_i in COPD participants. This is consistent with previously reported results which showed a regional predilection for uptake which correlated with disease [54] however, an increase in middle and whole lung nK_i was also observed. This appears to agree with the nascent understanding of the differential regional immune responses in asthmatic patients. No lower lung differences were observed, it is possible that partial volume effects from diaphragm motion were responsible . K_{ip} did not demonstrate any significant regional differences between the groups. Equally, the regional comparison of K_{im} revealed no differences across the groups, in keeping with the findings in the whole lung.

The repeatability of whole lung ^{18}F-FDG PET endpoints in COPD patients on the placebo arm of the EVOLUTION trial was assessed. The Bland-Altman analyses revealed that the compartmental model endpoints (i.e. K_{im} and V_b) demonstrate poorer repeatability than Patlak analysis (i.e. nK_i, K_{ip} and V_{ss}). This is consistent with findings in a smaller study of COPD subjects using ^{18}F-FDG PET which reports the repeatability of the imaging endpoints over a 4 week period [164]. Although in that work the author reports good repeatability for all the outcomes, it is clear from the Bland-Altman plots that the compartmental modelling outcomes have poorer agreement between the two imaging visits. In the results reported here, V_b in particular exhibits a large variance; this may be due to the noise in the initial time frames of the PET scan. The estimation of Patlak outcomes does not require the data points corresponding to these initial time frames and involves fitting fewer parameters. This may also partly explain the improved reproducibility of the analysis methods found in Patlak analysis compared to compartmental modelling. Moreover, Patlak analysis is more easily standardised than compartmental modelling; there are fewer parameters to select and as it is linear model, hence will have only one solution (corresponding to a single minima). The SUV had superior repeatability compared to other outcomes

and is similar to previously reported values using ^{18}F-FDG [166] and other tracers [167].

For compartmental modelling, the initial results of the reproducibility experiment showed a poor subject-level agreement in K_{im} and V_b; despite the application of the same model. Interestingly, this did not change the overall interpretation of the group findings; the effect size between groups was comparable using either pipeline. Further, it did not change the outcome of statistical hypothesis testing between groups. Reproducibility of analysis is an important pre-requisite for an imaging biomarker; the results of this evaluation demonstrate the need for standardisation when applying compartmental modelling to assess lung inflammation. The salient factors in these data were the blood ROI methodology, input function modelling and time delay estimation. By adjusting the blood ROI definitions, the input function fitting method and the time delay calculation in pipeline B, the results demonstrate better agreement between the two pipelines (see figures 4.8, 4.12 and 4.11) and on a similar level to the agreement found using Patlak analysis in the first case. Currently there is no standard method of assessing pulmonary inflammation using compartmental models of ^{18}F-FDG and each centre may undertake such analyses using their own bespoke approach. These findings suggest that despite seemingly similar methodology, individual subject results are sensitive to several factors in the implementation of the methodology, therefore care is needed when reporting the exact methods used.

Limitations

There were limitations in this study including inaccuracies introduced by the alignment of the PET and CT images: CT-AC were acquired under free breathing, this may lead to inaccuracies when quantifying the PET scan due to mismatch between PET and CT. Further, this can be exacerbated by changes in lung density due to respiratory phase [114].

Exacerbations in the COPD participants prior to the study may have confounded the interpretation of the quantitative ^{18}F-FDG PET data, since the recovery period to return to a baseline has yet to be elucidated; this also has implications for the finding that nK_i was increased following an exacerbation. The study was not formally

powered based on secondary endpoints (e.g. 6MWD, Perc15) therefore, it may be underpowered leading to insufficient data to assess these endpoints robustly.

The analyses were performed in retrospective studies, this limited the possible analyses undertaken; for example, it was not possible to estimate the influence of acquisition parameters on imaging endpoints. As mentioned previously, there is no gold standard method to validate the various outcome measures against tissue inflammation, instead the approach adopted here involved evaluating the technical and clinical validity of the outcome measures.

The ^{18}F-FDG PET scans were performed in a heterogenous set of COPD participants with a range of emphysematous burden, the whole lung analyses in particular could have been influenced by the varying severity of emphysema. Further work will be needed to determine the impact of emphysematous changes on ^{18}F-FDG PET analyses.

Estimates of reliability may vary with specific image acquisition parameters, scanner characteristics and data processing; hence, comparisons with other studies is challenging. Nevertheless, by analysis of participants allocated to placebo in the EVOLUTION trial, the repeatability of quantitative ^{18}F-FDG PET outcomes was quantified. Moreover, the reproducibility of the dynamic ^{18}F-FDG outcomes were assessed using two independent pipelines. Since both operators used the same reconstructed datasets, this does not include within subject biological variability or technical factors (e.g. scanner settings & reconstruction algorithms), which would allow the overall reproducibility to be evaluated. Nevertheless, with each operator using identical scans, the systematic variability in ^{18}F-FDG uptake introduced by differences between hardware, reconstruction and acquisition protocols was avoided [168]. Harmonisation of acquisition and analysis protocols in diffuse lung disease should be established for future PET studies.

The POB ratio was calculated for each subject using discrete venous blood samples; this allows the conversion of a blood input function to a plasma input function; this may cause bias in the outcome variables. The POB ratio was found to be very close to

one (1.05 ± 0.03), this agrees with previous findings that ^{18}F-FDG equilibrates between erythrocytes and plasma nearly instantaneously [169]. Further work should determine whether POB corrections are necessary in quantitative ^{18}F-FDG lung studies.

Previous work has demonstrated that the weighting factors chosen to describe the variance of dynamic PET data affects the outcomes of compartmental modelling [170]. In the reproducibility experiments, the impact of different weighting schemes was not explored but this could be another key contributor which may improve reproducibility. The inter-observer effect could not be assessed as results from pipeline A, undertaken by operator A, were retrospectively acquired. Yet, the salient stages of compartmental modelling which were responsible for the low concordance observed between the pipelines were identified.

The findings of this chapter highlight that interpretation of lung ^{18}F-FDG uptake is challenging due to the presence of air and blood which vary with disease burden. Investigators have used SUVs, PGA and CM in previous studies to analyse ^{18}F-FDG uptake. The observation that COPD participants had a sustained signal in the longitudinal study indicates the stability of ^{18}F-FDG uptake. Despite the nascent understanding that nK_i does not represent lung tissue uptake alone, it has shown promise as a composite marker of disease and corroborates previous findings in smaller groups. Interestingly, when comparing the smokers and healthy never smokers, which have no statistical difference in V_a, V_b or airflow limitation, only nK_i found a difference consistent with the understanding of increased inflammation due to smoking [91]. Further, it had a modest, yet significant, correlation with markers of disease severity and a lower variability than K_{im}. Repeatability and reproducibility were also improved in Patlak analysis compared to compartmental modelling. Disappointingly, compartmental modelling - which directly accounts for air and blood- did not reveal any significant differences between groups or associations with clinical measurements. Based on the findings of this chapter, further evidence is required before considering ^{18}F-FDG imaging endpoints as useful biomarkers to assess lung disease in COPD. Indeed, the observations in this chapter demonstrate that investigators using quantitative ^{18}F-FDG in future studies of COPD would need to carefully consider the method of analysing

images and the impact that differences in lung architecture can have on the imaging endpoints. Moreover, there is an assumption that these measures of ^{18}F-FDG uptake relate to underlying inflammation, but further work is needed to validate these measures against lung cell counts in diseased individuals.

4.7 CONCLUSION

There are substantial challenges when using ^{18}F-FDG PET to assess lung disease in COPD, underlined by the disparate findings using different PET analysis outcomes observed in these data. The disparity appears exacerbated in COPD due to the varying severity of emphysema. The observations made here exemplify the need for careful study design when using ^{18}F-FDG PET to assess lung disease in COPD, especially when justifying the image analysis endpoint. There is no gold standard method to assess lung inflammation; nevertheless, our results suggest ^{18}F-FDG uptake quantified by nK_i relates to relevant clinical measures of disease, is consistent with the pathophysiologic understanding of COPD and has good technical validity. However, nK_i should be used judiciously as it is does not reflect ^{18}F-FDG metabolism alone, but is influenced by pulmonary blood and air. For example, when comparing groups with different fractional blood volumes, nK_i should not be considered as a biomarker of inflammation without further supportive evidence such as independent blood volume measures. In addition, tissue validation of the ^{18}F-FDG imaging outcomes will be helpful to further assess their validity in the context of lung inflammation. Further evidence is required to evaluate whether ^{18}F-FDG PET imaging outcomes would be a useful biomarker for COPD; aspects of this will be explored in chapter 5 .

5

SUBTYPES OF COPD BASED ON CT IMAGING: ASSOCIATION WITH DISEASE ACTIVITY USING ^{18}F-FDG

One of the most significant challenges to improving outcomes and quality of life in COPD is clarifying the myriad of underlying phenotypes. Existing classifications such as GOLD, are often based primarily on spirometry, symptoms and exposure to potential pathogens but these have shown poor correspondence for treatment responders. New methods are needed to identify sub-types with similar prognostic and therapeutic benefits [171], better understanding of the heterogeneity of COPD will have important implications for management [172]. There has been growing appreciation of the potential role imaging could play, particularly providing quantitative, regional measures reflective of underlying disease mechanisms [173].

CT imaging and pathologic findings confirm a range of patterns of emphysema are present in COPD, even in patients with similar levels of physical impairment. CT has been validated as a tool for assessment of emphysema with destructive changes detectable in the hounsfield unit (HU). Initial findings suggested that regions with a threshold value of < -910 HU on CT are emphysematous and was confirmed by pathological samples [174]. Subsequently, several investigators have explored the optimal HU threshold, with a value of -950 HU now widely accepted. Alternatively, frequency histograms of the HU values in the lung have been used to quantify emphysema; the 15th percentile value is the most widely reported [175]. In addition, bronchial and small airways disease (SAD) is readily identified from CT either directly or using processing techniques, along with other common features such as bronchiectasis and interstitial lung abnormalities.

Visual and quantitive CT can provide complementary methods to assess COPD and may help to generate sub-types to optimise treatment. To that end, a visual classifi-

cation system was proposed by the Fleischner Society which classifies patients based on the patterns of emphysema, airways disease and associated features; subsequently, the sub-types with severe disease were shown to be associated with increased risk of mortality even after adjusting for quantitative CT measures [176]. Building on this, a recent study confirmed a difference in overall mortality in these groups and further revealed that certain groups were at more risk of progression [177]. The authors suggested that the combination of CT features reflect different underlying pathologic processes.

In this study, the primary aim was to investigate whether these CT subtypes are associated with underlying pulmonary disease activity assessed with ^{18}F-FDG PET. Secondly, using longitudinal ^{18}F-FDG PET scans, treatment response within these imaging subtypes was explored for COPD patients. Finally, to further evaluate ^{18}F-FDG PET outcomes minimising the influence of emphysema, the ^{18}F-FDG uptake in COPD subtypes defined by trace emphysema was compared to healthy smokers without COPD and healthy never smokers.

5.1 HYPOTHESES

COPD subtypes defined by visual and quantitative CT are associated with varying degrees of pulmonary inflammation as assessed by ^{18}F-FDG PET.

5.2 AIMS

The primary aim was to compare lung inflammation (using quantitative ^{18}F-FDG PET) between radiologic sub-types of COPD; the subtypes were based on visual and quantitative assessment of HRCT scans. Associations between emphysema severity and disease activity using ^{18}F-FDG PET were explored. A secondary aim was to investigate if differences in treatment response could be identified in these subtypes of COPD using longitudinal ^{18}F-FDG PET scans. Finally, different ^{18}F-FDG PET outcomes were

assessed in a single subtype defined by the mildest disease- thus minimising the confounding influence of emphysema- and compared to smokers and never-smokers.

5.3 METHODS

5.3.1 *CT subtyping*

HRCT scans were performed as described in chapter 4, the scans were reviewed by a radiology registrar using the HOROS imaging platform [178] after an initial period of training by an experienced thoracic radiologist. Each COPD participant scan was categorised according to the Flesichner society statement [179]; table 5.1 summarises the sub-types. The thoracic radiologist provided oversight by reviewing the resulting classifications.

Table 5.1: Definitions of COPD subtypes using CT*.

Subtype	**Location**	**Appearance**
Trace CLE	Upper lobe predominant	Minimal centrilobular lucencies, occupying $< 0.5\%$ of a lung zone
Mild CLE	Upper lobe predominant	Scattered centrilobular lucencies, involving estimated $0.5 - 5\%$ of a lung zone
Moderate CLE	Upper lobe predominant , diffuse	Many well-defined centrilobular lucencies, $> 5\%$ of any lung zone
Confluent CLE	Upper lobe predominant , diffuse	coalescent centrilobular/lobular lucencies, multiple regions spanning several secondary lobules, but not involving hyperexpansion of secondary lobules or distortion of pulmonary architecture
ADE	Lower lobe predominant , diffuse	panlobular lucencies, with hyperexpansion of secondary lobules and distortion of pulmonary architecture
PLE	Lower lobe predominant	Generealised destruction of all acini more or less equally (associated with α_1ATD)

Emphysema is defined by $> 6\%$ of pixels with < -950HU on CT.
* Condensed version of definitions, full descriptions available from [179].
ADE = Advanced destructive emphysema, CLE = centrilobular emphysema, PLE = panlobular emphysema

5.4 RESULTS

5.4.1 *Overall comparison of CT subtypes*

Baseline HRCT scans were reviewed twice in a total of 69 COPD participants according to the categories in table 5.1. The largest group was ADE with 20 subjects, followed by mild and trace categories both with 15 subjects (see figure 5.1). The demographics, clinical characteristics and imaging data of the groups are shown in table 5.2. There were subjects with predominant airways disease, a secondary pattern of paraseptal emphysema was identified in 16 subjects. Due to the small number of total subjects, only primary patterns are subsequently analysed. Equally, only a small number of subjects with panlobular emphysema (n = 4) were found, these were not included in subsequent analysis.

Figure 5.1: **COPD subtypes defined by CT chest scans using Fleischner guidlines.**

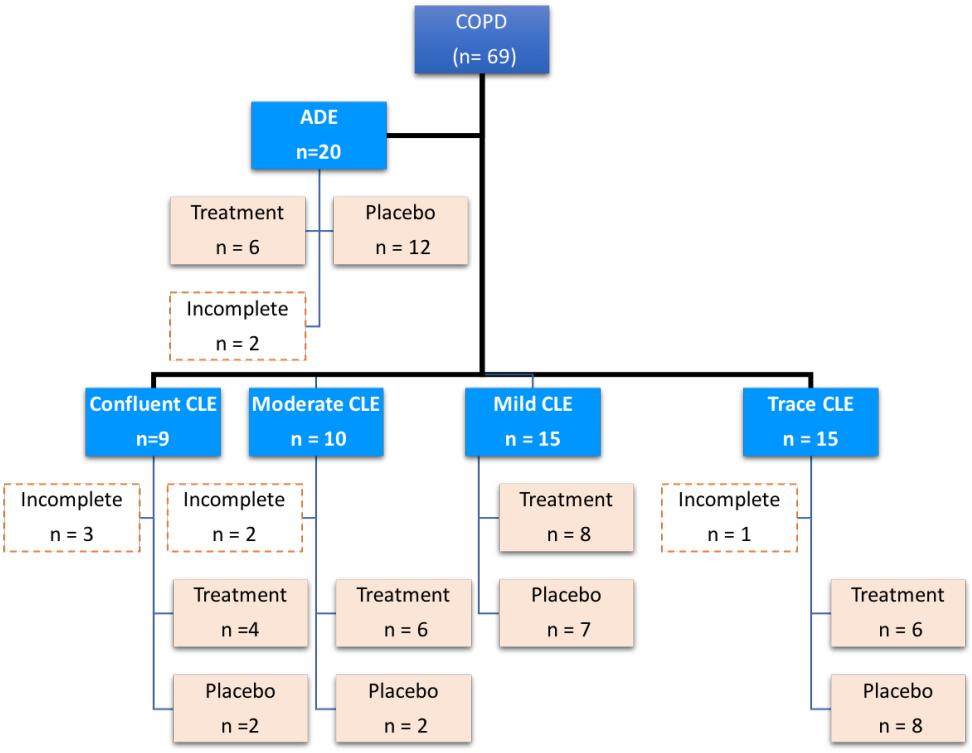

Incomplete indicates that paired baseline and follow-up ^{18}F-FDG PET scans were not available, shown are the number of subjects on placebo or treatment drug, Losmapimod.
ADE = Advanced destructive emphysema, CLE = centrilobular emphysema, light blue box = one of the COPD subtypes

Physical function, characterised by the 6WMD and FEV_1 values, were lowest in the confluent CLE and ADE groups. There was an overlap in some of the clinical

Table 5.2: Demographics, clinical characteristics and whole lung imaging endpoints for sub-types of COPD.

	Trace CLE (n = 15)	**Mild CLE** (n = 15)	**Moderate CLE** (n = 10)	**Confluent CLE** (n = 9)	**ADE** (n = 20)	p-value *
FEV_1 (L)	1.8 ± 0.52	1.4 ± 0.46	1.5 ± 0.73	1.05 ± 0.46	0.99 ± 0.30	< 0.001
Current smoker (%)	7	11	20	11	10	
Pack years (yrs)	35 ± 13	35 ± 11	39 ± 12	44 ± 13	42 ± 6	ns
6MWD (m)	478 ± 115	377 ± 81	375 ± 98	335 ± 145	343 ± 104	< 0.05
Perc15	-833 ± 32	-865 ± 24	-890 ± 35	-918 ± 18	-949 ± 41	< 0.001
V_a	0.75 ± 0.037	0.78 ± 0.027	0.79 ± 0.051	0.82 ± 0.018	0.84 ± 0.033	< 0.001
V_b	0.13 ± 0.038	0.12 ± 0.038	0.11 ± 0.031	0.08 ± 0.018	0.08 ± 0.019	< 0.001
$K_{im}(ml/min^{-1}/cm^{-3})$	5.5 ± 1.3	4.9 ± 1.9	6.8 ± 4.1	5.3 ± 0.67	5.1 ± 1.6	ns
$K_{ip}(ml/min^{-1}/cm^{-3})$	0.61 ± 0.1	0.46 ± 0.12	0.57 ± 0.25	0.48 ± 0.15	0.43 ± 0.19	ns
$nK_i(ml/min^{-1}/cm^{-3})$	3.7 ± 0.8	3.3 ± 0.8	3.9 ± 1.3	4.0 ± 1.3	4.0 ± 1.1	ns
SUV	0.53 ± 0.12	0.47 ± 0.09	0.49 ± 0.14	0.39 ± 0.03	0.34 ± 0.13	< 0.001

* overall comparison between all 5 groups.
6MWD =six minute walk distance.ADE = advanced destructive emphysema, CLE = centrilobular emphysema , FEV_1 *= forced expiratory volume in one second*

characteristics of the groups; for example, 6MWD in mild and moderate sub-types. Consistent with spirometry, CT imaging measures (i.e. V_a and Perc15 values) were significantly different in the confluent CLE and ADE groups compared to the other groups indicating more severe emphysema. The SUV was significantly elevated in the trace, mild and moderate CLE groups when compared to ADE. Additionally, the SUV was increased in the trace CLE group compared to confluent CLE. In contrast, there were no differences between sub-types using K_{im}, nK_i or K_{ip}. V_b values were decreased in the ADE group compared to trace, mild and moderate CLE; they were also decreased in the confluent CLE group when compared to trace or mild CLE.

5.5 TREATMENT EFFECTS

To investigate whether Losmapimod reduced pulmonary inflammation in each of the COPD sub-types, ^{18}F-FDG PET outcomes were adjusted for baseline values and values compared to the placebo group. The number of subjects on treatment and placebo within the CT sub-types were small in some of categories (figure 5.1). Figure 5.2 and 5.3 shows the plots for the effect of treatment on COPD subtypes using the different ^{18}F-FDG PET outcomes. There were no significant differences between the placebo

and treatment cohorts for any of the COPD subtypes using K_{im} or K_{ip}. Notably in the trace COPD sub-type only, the SUV was significantly elevated in the treatment group compared to placebo group ($p = 0.013$), despite no difference in V_b. Moreover, with the exception of the SUV, moderate and confluent subtypes demonstrated the largest differences between placebo and treatment arms in the follow-up imaging endpoints.

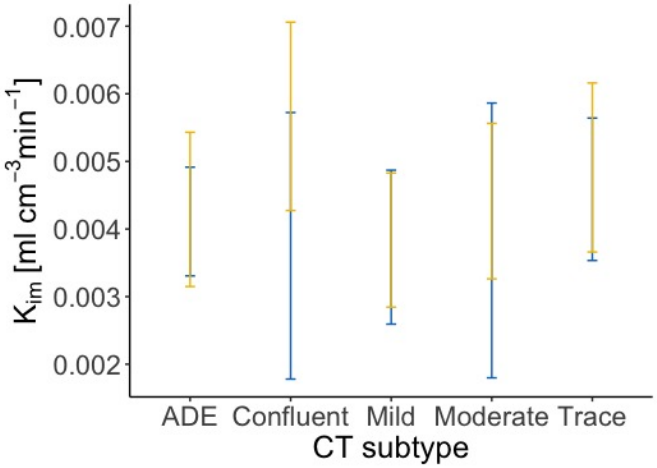

(a) **Treatment effect using K_{im}.**

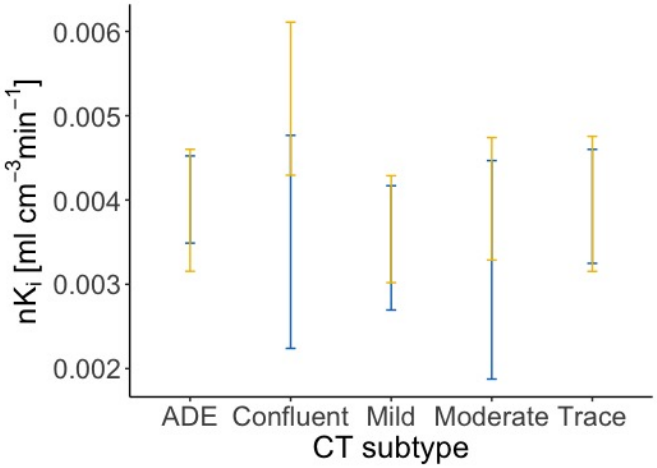

(b) **Treatment effect using nK_i.**

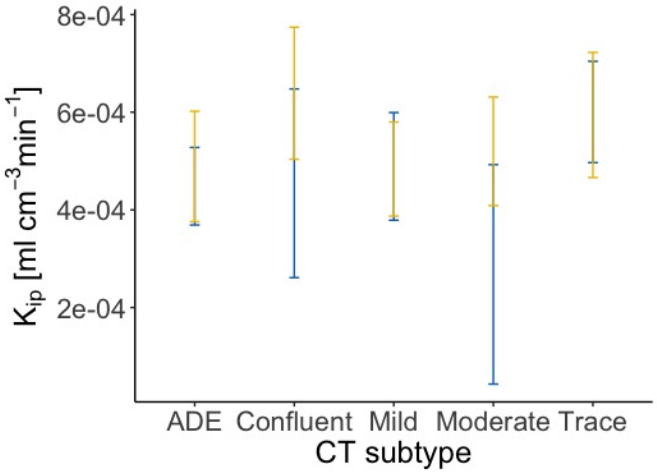

(c) **Treatment effect using K_{ip}.**

Figure 5.2: **Effect of treatment on whole lung dynamic PET endpoints in each COPD subtype.**

The follow-up PET outcome was adjusted for the baseline value using an ANCOVA model. Y-axis is the estimated marginal means for (a) K_{im}, (b) nK_i, (c) K_{ip}, (d) SUV.
ADE = Advanced destructive emphysema, blue line = placebo group, yellow line = treatment group.

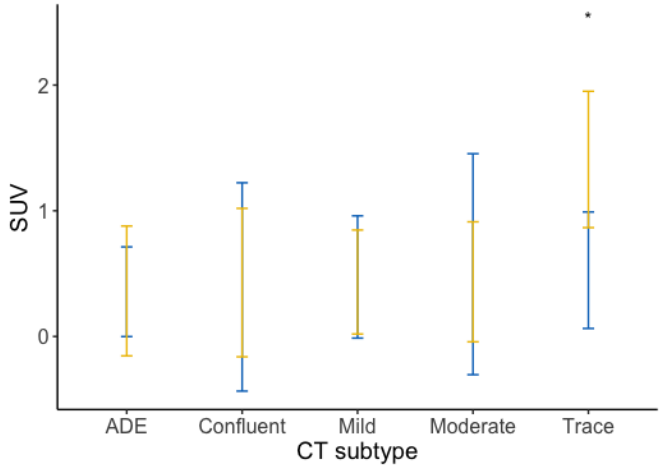

Figure 5.3: **Effect of treatment on whole lung SUV in each COPD subtype.**

The follow-up SUV was adjusted for the baseline value using an ANCOVA model.
Y-axis is the estimated marginal means for SUV.
ADE = Advanced destructive emphysema, blue line = placebo group, yellow line = treatment group
* *p-value* < 0.05, ** *p-value* < 0.01, *** *p-value* < 0.001.

5.5.1 *^{18}F-FDG PET outcomes in trace emphysema compared to controls*

Baseline ^{18}F-FDG PET outcomes were assessed in the trace emphysema group (n =15) compared to the never smokers (n = 10) and smokers without COPD (n = 12). There were no differences in V_b or V_a between the groups ($p = 0.75, 0.45$ and 0.15; see table 5.3). The SUV was highest in the never smokers but there was no significant difference between any of the groups. K_{ip} was elevated in the smokers compared to the trace COPD sub-type ($p = 0.021$) and never smokers ($p = 0.043$). In contrast, nK_i was elevated in the smokers compared to the never smokers ($p = 0.011$), nK_i was modestly increased in the trace group when compared to the never smokers ($p = 0.04$); there was no difference between smokers and trace ($p = 0.25$). K_{im} values exhibited no differences between groups ($p > 0.5$).

Table 5.3: Comparison of PET and CT outcomes in COPD subjects with trace emphysema.

Outcome*	**COPD (trace**)**	**Smokers**	**Never-Smokers**	**P-value*****
V_a	0.75 ± 0.039	0.73 ± 0.040	0.71 ± 0.041	ns
V_b	0.13 ± 0.038	0.15 ± 0.051	0.14 ± 0.025	ns
$K_{im}(ml/min^{-1}/cm^{-3})$	5.3 ± 1.3	7.2 ± 2.8	6.0 ± 1.9	ns
$K_{ip}(ml/min^{-1}/cm^{-3})$	0.59 ± 0.12	0.77 ± 0.21	0.61 ± 0.13	< 0.05
$nK_i(ml/min^{-1}/cm^{-3})$	3.7 ± 0.8	4.1 ± 1.2	2.9 ± 0.54	< 0.05
SUV	0.54 ± 0.11	0.56 ± 0.10	0.62 ± 0.12	ns

* K_{im}, K_{ip} *and* nK_i *values reported as* $\times 10^{-3}$
** *trace emphysema as defined in table 5.1*
*** *P-value reported as difference across all groups*

5.6 DISCUSSION

In this chapter, the clinical, physiologic, and imaging characteristics of COPD sub-types - classified by visual and quantitative chest CT - were investigated. Previously, such categorisation has shown that the presence and degree of emphysema is associated with increased mortality risk in COPD subjects [176]. This work investigated, for the first time, the underlying disease activity in these sub-types of COPD using ^{18}F-FDG PET. Differences were found in clinical and radiological characteristics between the sub-types. Although no differences in disease activity were observed between sub-types using dynamic ^{18}F-FDG PET outcomes, the SUV findings demonstrate that differences between groups are detectable using ^{18}F-FDG PET. Further, these data suggest that when evaluating the performance of novel anti-inflammatory drugs in COPD, understanding the heterogeneity of response using ^{18}F-FDG PET/CT may be enhanced by CT image sub-types.

There were clear differences in air-flow obstruction and functional capacity with increasing emphysema burden, congruent with previous studies in large cohorts of COPD subjects [176]. Previous studies have found that visual classification of emphysema grade in COPD is a valid discriminatory tool. In a large study of 4000 cigarette smokers from COPDgene, direct application of the Fleischner guidelines revealed strong evidence that a worsening grade of emphysema was associated with increased mortality [176], independent of quantitive severity of emphysema, with adjusted hazard ratios increasing from 1.7 for trace emphysema to 4.1 for ADE. Besides using a more precisely defined visual grading system, their findings confirmed previous observations [180, 181] whilst also identifying an independent mortality effect from visual classification. Later work based on the Fleischner grading system evaluated 9080 current and former smokers from the COPDgene study. In addition to confirming that mortality differed between COPD sub-types, the investigators further found distinct discordant subtypes; for example, those with visual but not quantitative emphysema which exhibited greater progression of emphysema [177]. The authors suggest that inflammation of parenchyma or airways may be responsible despite relatively mild

disease.

The finding that SUV was elevated in those groups with milder emphysema indicates that there may be increased pulmonary inflammation compared to sub-types with more severe emphysema. However, it is possible that this signal reflects the differences in fractional tissue and blood volumes rather than inflammatory burden per se. Indeed, the SUV for these milder emphysema sub-types is comparable to that of never-smokers and the *dynamic* ^{18}F-FDG outcomes were unable to detect differences between the sub-types. It is possible that these measures are not sensitive enough to detect subtle differences in inflammation between sub-types. However, in larger COPD cohorts other investigators have suggested that a distinct CT imaging sub-type with visual-only emphysema may be characterised by increased inflammation [177]. Future work that refines CT imaging sub-types may reveal greater inflammatory burden in specific sub-types. Although overall the ^{18}F-FDG PET measurements did not find strong evidence of a difference between groups, measures relating to healthy lung tissue - including V_b, V_{ss} and perc15 - significantly decreased with worsening severity of emphseyma.

To investigate treatment response in the COPD subtypes, ^{18}F-FDG PET scans post treatment with Losmapimod were adjusted for baseline and compared to the placebo group. Previous studies in this COPD cohort found that losmapimod did not attenuate vascular inflammation nor did it improve endothelial function [155]. The SUV analysis revealed that ^{18}F-FDG uptake increased significantly in the treatment group compared to the placebo group for those with minimal emphysema. There were no differences in exacerbations or smoking history between the placebo and treatment cohorts thus, it is difficult to interpret this finding. Importantly, when comparing longitudinal PET/CT scans in the same subject the influence of air volume on SUV is likely to be less important, provided the interval between scans is short compared to emphysematous changes. Nevertheless, the results indicate that when evaluating alternative targeted therapies, imaging sub-types may provide additional value by identifying differences in treatment response.

In the previous chapter, emphysema was found to cause discordant results using the different ^{18}F-FDG PET outcomes. To investigate the relationship between quantitative ^{18}F-FDG whilst minimising the influence of emphysema, COPD patients with trace emphysema were compared to smokers without COPD and never-smokers. Importantly, there were no statistical differences in pulmonary blood volume and air fraction between the trace group, smokers and never-smokers. Consistent with the previous findings (see chapter 4) and the physiological understanding of inflammation, nK_i was elevated in smokers and trace COPD compared to never-smokers. Interestingly, K_{ip} values were increased in smokers compared to trace emphysema COPD subjects, but there was no difference between trace emphysema COPD subjects compared to never smokers. Using K_{im} or the SUV did not reveal a difference between the subtypes. Based on this and previous findings, the SUV appears less reliable when comparing inter-subject differences. The lack of significance found with K_{im} indicates that it may not be sensitive enough in diffuse lung diseases like COPD, similar to observations in chapter 4, K_{im} is more variable than other measures and it is likely that the noise in this parameter estimation is limiting its power to detect the underlying inflammatory signal.

There were limitations in this study. Although the initial cohort of COPD subjects was large for an ^{18}F-FDG PET study, the division into smaller groups led to small subject numbers reducing the statical power to detect changes. Indeed, the study population was too small to identify enough patients with paraseptal emphysema (PSE) or airways disease as the predominant pattern. Nevertheless, it was possible to identify statistical differences between the main CLE sub-types. There was an overlap of clinical features between the sub-types, in particular the mild and moderate groups, indicating that these were not isolated clusters of subjects; this overlap has been observed in similar studies using imaging sub-types [176, 177]. However, in this study there were substantially less current smokers in the trace, mild and moderate groups than previous studies.

5.7 CONCLUSIONS

In conclusion, *dynamic* ^{18}F-FDG PET imaging outcomes did not identify differences in disease activity between sub-types based on CT chest imaging. The SUV demonstrated an increase in disease activity in milder emphysematous disease but this may be driven by underlying tissue volume differences rather than inflammatory activity. These data did show distinct differences in clinical, physiologic and CT imaging characteristics between the COPD subtypes. Treatment with Losmapimod did not reduce pulmonary ^{18}F-FDG uptake in individual sub-types. In addition, when the influence of emphysema on quantitative PET was minimised, Patlak analysis revealed increased uptake between COPD and smokers without COPD compared to never-smokers.

6

EXPLORATION OF DYNAMIC ^{18}F-FDG PET/CT TO ASSESS LUNG INFLAMMATION IN SARCOIDOSIS

6.1 INTRODUCTION

Sarcoidosis is a multi-organ disease of unknown aetiology; the most commonly affected organ is the lung [182]. Sarcoidosis is a disease which is characterised by the formation of inflammatory granulomata and can be complicated by progressive fibrosis and scarring. Despite progress in understanding of the etiopathogensis [183], there are no specific treatments and new treatment strategies are urgently needed [184]. Moreover, biomarkers which can assess disease activity and identify at risk patients have remained elusive. To date, ^{18}F-FDG-PET/CT has had a limited role in the clinical evaluation of sarcoidosis, usually it is reserved for cases where there is diagnostic uncertainty, i.e. suspected cardiac sarcoidosis [185]. Nevertheless, it has been recognised that there is a potentially important role for ^{18}F-FDG-PET in management of sarcoidosis and assessing treatment effect [186–189].

Several studies have identified that ^{18}F-FDG-PET is a useful tool for assessing inflammatory activity in sarcoidosis [187, 188, 190–194]. In a study of 49 newly diagnosed patients, investigators found that ^{18}F-FDG uptake predicted deterioration in lung function in untreated patients [192]. The majority of studies have used SUV_{max} to assess ^{18}F-FDG uptake; recently, other metrics have been investigated such as the total lung glycolysis (TLuG) [195]. However, the TLuG was equivalent to SUV_{max} in predicting response to therapeutics. Other investigators have sought associations between ^{18}F-FDG uptake and serological inflammatory markers, particularly angiotensin converting enzyme (ACE). Results have been mixed: an early study found no correlation between ^{18}F-FDG uptake and ACE [186], later studies found patients with visually confirmed positive ^{18}F-FDG findings had elevated ACE levels compared to to those with negative

results [196]. However, in nearly 50% of those with positive ^{18}F-FDG the ACE levels were normal. Currently there are no reported studies using dynamic measures of ^{18}F-FDG-PET to investigate pulmonary sarcoidosis.

Although quantitative ^{18}F-FDG has been used to assess lung inflammation in diseases such as idiopathic pulmonary fibrosis (IPF) [60], acute lung injury (ALI) [24] and chronic obstructive pulmonary disease (COPD)[55], few studies have provided a measure of clinical validation. This is partly due to the challenge of obtaining a gold standard measure of pulmonary inflammation. In a canine model of ALI, a correlation between rate of ^{18}F-FDG uptake, K_{ip}, using Patlak graphical analysis and [^{3}H]DG uptake in bronchoalveolar fluid (BALf) cells was found [197]. However, they found no correlation between total cell or neutrophil concentration from BAL fluid. Building on this, a few subsequent studies of a human model of ALI used endotoxin instilled into a single lung lobe with the contralateral lung lobe used as a control [23, 24, 65]. However, using cell counts from BALf, there was not strong evidence that the ^{18}F-FDG PET signal in the treated lung was driven by neutrophils alone and further murine studies suggested that other cells were implicated (e.g. macrophages, epitheilal cells) [198]. To our knowledge, no studies have been performed to assess static and dynamic ^{18}F-FDG outcomes against inflammatory cells in a clinically relevant diffuse lung disease.

In this study, pulmonary inflammation was assessed in sarcoidosis patients with clinically active disease using ^{18}F-FDG-PET. The primary aim was to investigate static and dynamic measures of pulmonary ^{18}F-FDG uptake in sarcoidosis compared to age- and gender-matched healthy controls. Secondly, associations between ^{18}F-FDG outcomes, systemic clinical markers of inflammation and pulmonary inflammatory cell counts from BAL fluid were sought. Finally, in a further development for this prospective study only, the impact of respiratory motion on ^{18}F-FDG outcomes was investigated using cine-CT.

6.2 HYPOTHESES

Sarcoidosis patients will have an increased pulmonary ^{18}F-FDG-PET signal compared to healthy controls; outcomes derived from the dynamic acquisition of ^{18}F-FDG will further improve the distinction between these groups.

6.3 AIMS OF THE STUDY

The principal aim of this work was to compare the pulmonary ^{18}F-FDG uptake in sarcoidosis patients to healthy controls; this includes comparing both static and dynamic measures of uptake. Secondly, to compare these quantitative measures against clinical measures of inflammation obtained from inflammatory cell counts in bronchoalveolar lavage fluid (BALf) and plasma biomarkers of inflammation. Finally, to investigate the influence of respiratory motion on quantitative measures of ^{18}F-FDG uptake in sarcoidosis patients.

6.4 METHODS

6.4.1 *Study Participants*

The study aimed to recruit 12 pulmonary sarcoidosis patients with clinically active disease who were eligible for an endobronchial ultrasound (EBUS) procedure with high volume BAL. A further 12 healthy volunteers were age and sex matched to patients; they had no smoking history and were free of any confounding inflammatory disorders; sarcoidosis patients had no history of smoking. Sarcoidosis patients were eligible provided they had confirmed pulmonary sarcoidosis determined by the interstitial lung disease (ILD) multidisciplinary team (MDT), they had no known other pulmonary disease (determined by a recent previous chest CT) or chronic inflammatory disorders. Review of the previous CT scan by the ILD specialist minimised differences in radiologic appearance of sarcoidosis patients. The study consisted of two visits and a follow-up telephone call: the screening visit (V1) included the baseline clinical assess-

ments, the imaging visit (V2) was completed within 6 weeks and included a dynamic ^{18}F-FDG PET scan and cine CT (see figure 6.1).

The study received a favourable ethics opinion and all participants provided written informed consent in-line with the Declaration of Helsinki.

6.4.2 *PET/CT acquisition protocol*

The protocol was as described in chapter 3, a brief description follows highlighting the key differences. Subjects underwent a cine-CT followed by a dynamic ^{18}F-FDG-PET scan. All imaging was performed on the GE 690 PET/CT scanner at Addenbrookes' hospital. Cine-CT was performed with the subjects breathing normally, the FOV was centred on the lungs covering bases to apices, where possible. The Varian respiratory monitoring system was used [199]: a small reflective block was securely placed on the chest at the observed point of maximum displacement, an infra-red camera positioned with full view of the scanner monitored the movement of the block to produce a respiratory trace. The respiratory trace was observed until the breathing period was stable and used to inform the cine-CT acquisition parameters (see table 6.1). Longer respiratory periods required lower tube current, longer cine duration and rotation time. An example of the respiratory trace is shown in figure 6.2; each trace was divided into 10 phases. Cine-CT images consisted of 10 different phases of the respiratory cycle matching the axial field of view of the PET scanner. Following the cine-CT, an administered activity of approximately 200MBq was given. Dynamic ^{18}F-FDG-PET scans were binned into 27 frames of durations $10s \times 12, 60s \times 3, 120s \times 5, 300s \times 5$ and $600s \times 2$; at approximately 50 mins, a single venous blood sample was taken from the contralateral arm.

Table 6.1: Acquisition parameters for CineCT scans of the lungs. Parameters which are subject specific were based on the respiratory period of the subject.

Parameter	**Value**
Tube voltage (kVp)	120
Tube current (mA)	10 to 20 (subject specific)
Rotation (s)	0.5 to 0.8 (subject specific)
Cine duration (s)	2.5 to 9.6 (subject specific)
Reconstruction	Body filter
Slice thickness (mm)	2.5

Figure 6.1: **VERIFY study flow diagram.**

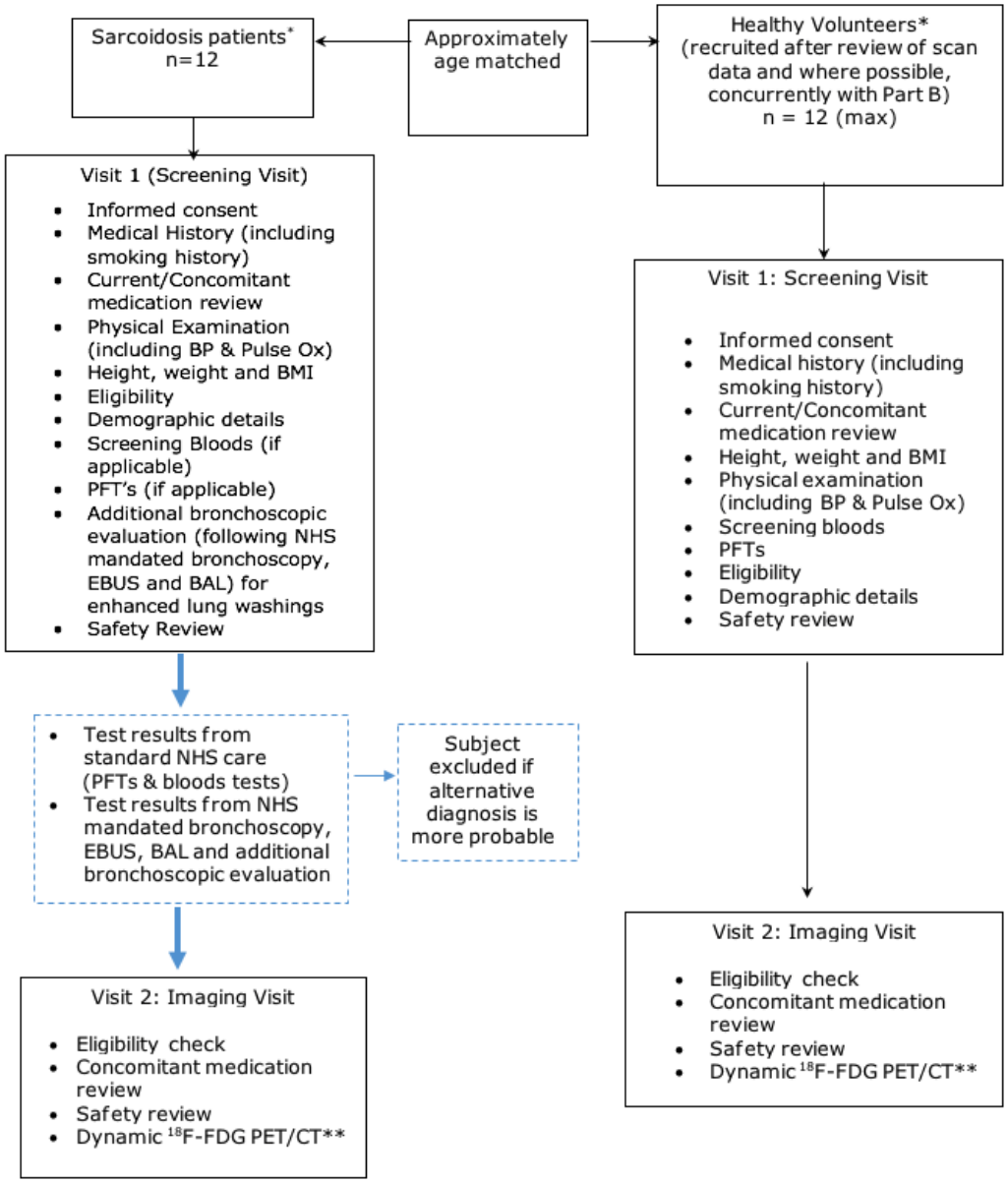

* Twelve evaluable patients and matched controls were required before study completion; evaluable requires both analysable image data and clinical data.
** CT refers to cine-CT.
Part B refers to additional part of study not discussed in this work.
BAL = bronchoalveolar lavage, BMI = body mass index, BP = blood pressure, Ox = oximetry, PFTs = pulmonary function tests, EBUS = endobronchial ultrasound

Figure 6.2: **Example of the respiratory trace used to gate the Cine-CT acquired using the Varian real-time position management software [199].**

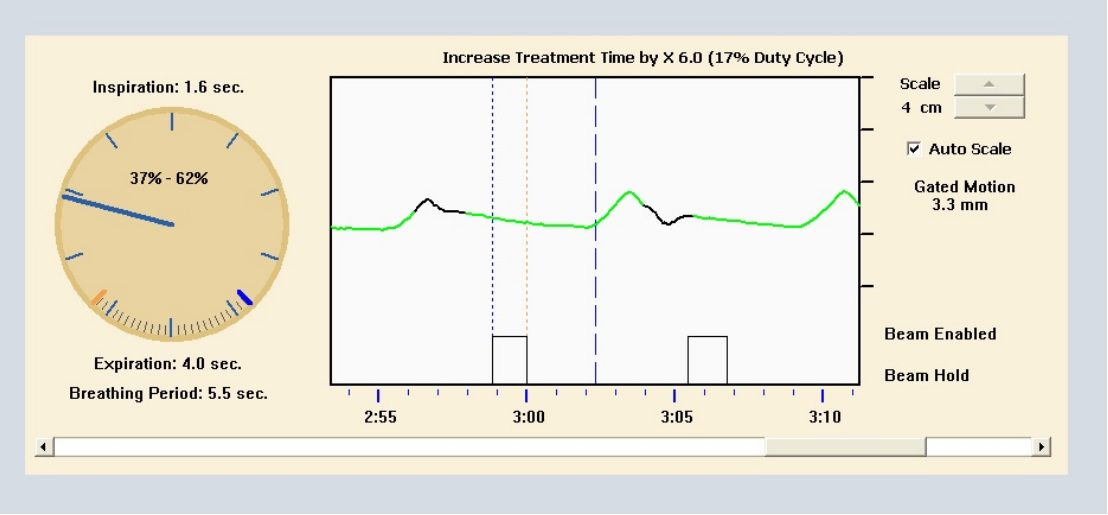

The respiratory cycle was divided into 10 phases and a CT image was reconstructed at each of these points on the trace.

6.4.3 *Bronchoscopy and BAL*

As part of the normal standard of care patients undergo a bronchoscopy procedure including an EBUS. BAL is performed to obtain a differential cell count from within the lung. To ensure a sufficient cell count, a narrower scope than standard practice was used to perform a high volume BAL. Three sequential 50ml volumes of sterile normal saline were instilled through the bronchoscope. BALf was obtained by gentle aspiration and samples pooled, return volume was typically 80-100mL, the samples were gauze filtered and kept on ice for processing. Cell counts and cell differentials were performed independently by two experienced histopathologists.

6.4.4 *Image Analysis - Cine CT and PET*

The image analysis pipeline is described in chapter 3. However, processing of the cine-CT is described here.

Cine-CT images consisted of 10 different phases of the respiratory cycle; these were combined into a single CT representing the average position of the lung. The attenuation correction was performed using the averaged cine-CT during the PET image reconstruction. To investigate the effect of respiration on quantitative ^{18}F-FDG, individual phases in the cine-CT scan were selected and PET images reconstructed using these for attenuation correction. The phases nearest to end expiration and inspiration were chosen as these are likely to represent the largest changes in density and motion. Figure 6.3 shows an example of reconstructed CT images at inspiration and expiration phases. Consistent with the previous chapters, the SUV reported is the mean SUV; in this study it was calculated from the final 25 mins of the scan. All subsequent stages of quantitative PET image analysis are identical to that described in chapter 3. To clarify, the analysis pipeline was identical to that used in chapter 5 and chapter 4 (except section 4.5.5 which used an alternative pipeline).

Figure 6.3: **Example of CT scans of a sarcoidosis subject from two phases of respiration.**

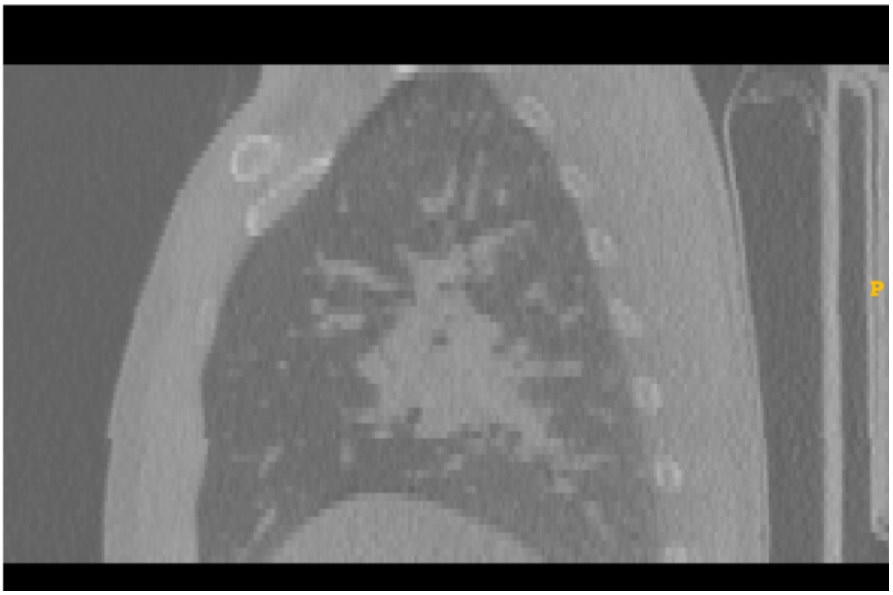

(a) **CT acquired near end expiration.**

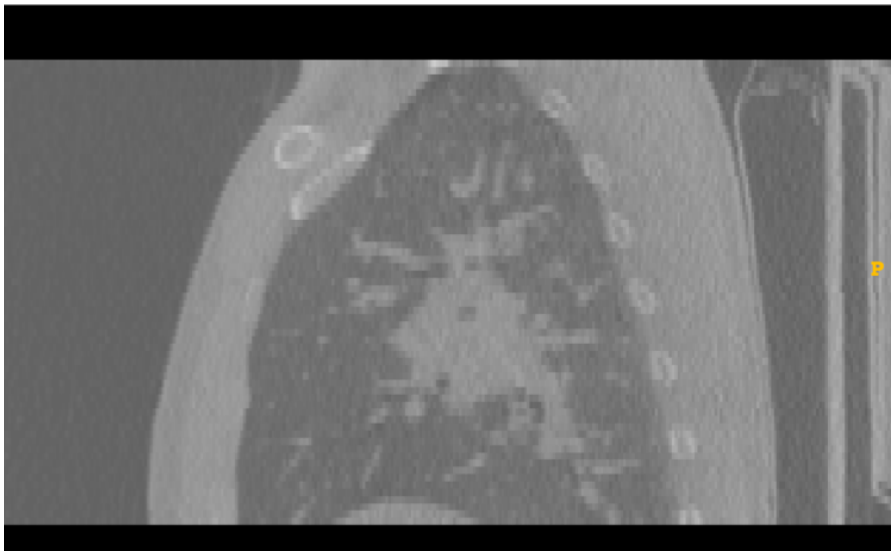

(b) **CT acquired near end inspiration.**
Cine-CT scans provide images from multiple time points, in (a) the nearest point to end expiration is shown, (b) is the point nearest end inspiration.

6.5 RESULTS

6.5.1 *Demographics*

Eleven patients were recruited into the study; seven patients completed the study at the time of writing, the mean age was 46 ± 8.8 yrs old and with a nearly equal male and female split (57% male). A total of 4 were withdrawn from the study; either as

they had another condition (n=2), withdrew voluntarily (n=1) or were ineligible for another reason (n=1). The mean age of the healthy controls was 45 ± 8.5 yrs old (with 57% male). The median time between V1 and V2 was 25 days for the sarcoidosis patients and 22 days for the controls. The demographics and clinical measurements are summarised in table 6.2. There was no statistical difference in FEV_1, age or gender between patients and controls. There were no difference between systemic blood markers of inflammation between sarcoidosis and controls.

Table 6.2: Demographics and clinical measures of the sarcoidosis patients and controls.

	Sarcoidosis (n = 7)	**Controls (n =7)**
Gender (%male)	57	57
Age (years)	46 ± 9	45 ± 9
FEV_1 (L)	2.94 ± 0.47	2.30 ± 0.6
Fibrinogen (g/L)	2.75 ± 1.48	2.62 ± 0.8
WCC ($\times 10^9$ /L)	6.44 ± 2.55	5.2 ± 1.41
Neutrophils ($\times 10^9$ /L)	4.76 ± 2.02	3.23 ± 1.50
Lymphocytes ($\times 10^9$ /L)	1.02 ± 0.6	1.94 ± 0.9
ACE ($\times 10^9$ /L)	80.4 ± 27	NA

FEV_1 = *Forced expiratory volume in 1 second,* ACE = *angiotensin converting enzyme,* WCC = *white cell count.*

6.5.2 *Influence of respiratory motion on ^{18}F-FDG endpoints in Sarcoidosis patients*

The volume change between inspiration and expiration was estimated as $4.1 \pm 0.5\%$, with a maximal displacement of the diaphragm of 13.2 ± 1.2mm. The change in fractional air volume between inspiration and expiration was $1.4 \pm 0.3\%$. ^{18}F-FDG imaging outcomes were estimated using the dynamic PET scans with CT-AC map generated from the inspiration and expiration CT scans. Table 6.3 summarises the percentage change in imaging outcomes between the inspiration and expiration CT derived PET values. Further, the maximum percentage differences in the ^{18}F-FDG imaging outcomes for either expiration or inspiration compared to the time-averaged CT scans are reported. The changes were substantial for imaging outcomes but overall SUV changed the least between inspiration and expiration. With the dynamic measures of ^{18}F-FDG uptake, K_{ip} was least affected but still had a maximum change of 24%. The changes in outcomes between the inspiration CT and expiration CT were greater than either compared to the time averaged CT.

6.5.3 *Comparison of ^{18}F-FDG-PET outcomes in sarcoidosis and controls*

Pulmonary inflammation was assessed by static and dynamic ^{18}F-FDG imaging endpoints in the whole lung, the results are summarised in table 6.4. The patients and

Table 6.3: Percentage differences in ^{18}F-FDG-PET imaging outcomes using CT at different respiratory phases.

Imaging outcome	**% change between exp and insp***	**max % change compared to averaged CT****
SUV	−10.1%	4.2%
K_{ip}	−24.1%	−15.1%
nK_i	−28.3%	−18.4%
K_{im}	−30.5%	−20.1%
V_b	14%	4.5%

* shows the maximum % difference in ^{18}F-FDG PET outcomes between expiration and inspiration.
** shows the maximum % change between either inspiration or expiration and the time-averaged cine-CT.
exp = Expiration, insp = Inspiration, V_b *= fractional blood volume.*

controls exhibited similar values for fractional air and blood volumes (respectively; $p = 0.21$ and $p = 0.56$) hence, the fractional tissue volume in the lung must also be similar between these two groups.

Notably, there was a significant difference in K_{ip} and nK_i values between patients and controls ($p = 0.022$ and 0.025, respectively). In contrast, there was no difference in whole lung SUV or K_{im} values between patients and controls ($p = 0.16$ and 0.62, respectively).

Table 6.4: ^{18}F-FDG-PET whole lung imaging outcomes in sarcoidosis patients and controls.

Imaging outcomes	**Sarcoidosis (n = 7)**	**Controls (n =7)**
SUV	0.60 ± 0.06	0.52 ± 0.05
K_{ip}^{+} $[ml/cm^3/min^{-1}]$	0.92 ± 0.7*	0.69 ± 0.6
$V_{ss}[ml/cm^3]$	0.27 ± 0.09	0.28 ± 0.07
nK_i^{+} $[ml/cm^3/min^{-1}]$	3.4 ± 0.4*	2.4 ± 0.7
K_{im}^{+} $[ml/cm^3/min^{-1}]$	6.5 ± 2.2	5.8 ± 2.1
V_b	0.14 ± 0.06	0.12 ± 0.03
V_a	0.69 ± 0.03	0.71 ± 0.03

* *p-value* < 0.05
$^{+}$ *units are* $\times 10^{-3}$
V_a *= fractional air volume,* V_b *= fractional blood volume*

Regional differences were found within the lungs (see table 6.5). nK_i values were modestly increased in the upper and middle lung of sarcoidosis patients compared to controls ($p = 0.029$ and $p = 0.023$, respectively), further K_{ip} was also increased in the upper and middle lung ($p = 0.020$ and $p = 0.0021$, respectively). There were no differences in V_b, V_{ss} or K_{im} in the upper, middle or lower lungs between the patients and controls. For all ^{18}F-FDG outcomes shown in table 6.5, the healthy control group had very similar values to the never smoking healthy controls in the previous COPD study (see chapter 4).

Table 6.5: Regional lung ^{18}F-FDG-PET endpoints in disease and healthy participants.

	Sarcoidosis			**Heathy controls**		
	Upper	Middle	Lower	Upper	Middle	Lower
SUV	0.62 ± 0.07	0.60 ± 0.04	0.58 ± 0.09	0.55 ± 0.06	0.51 ± 0.05	0.50 ± 0.08
nK_i^+ $[ml/cm^3/min^{-1}]$	3.6 ± 1.3*	3.8 ± 1.1*	3.4 ± 1.4	2.7 ± 1.2	2.3 ± 0.9	3.1 ± 1.7
K_{im}^+ $[ml/cm^3/min^{-1}]$	7.1 ± 3.0	6.8 ± 2.5	5.1 ± 3.3	7.2 ± 2.3	5.6 ± 1.3	5.8 ± 3.7
K_{ip}^+ $[ml/cm^3/min^{-1}]$	0.89 ± 0.21*	0.86 ± 0.21*	0.76 ± 0.33	0.65 ± 0.22	0.63 ± 0.23	0.67 ± 0.28
V_{ss} $[ml/cm^3]$	0.24 ± 0.057	0.23 ± 0.037	0.22 ± 0.043	0.24 ± 0.051	0.27 ± 0.071	0.21 ± 0.10
V_b	0.16 ± 0.045	0.15 ± 0.036	0.12 ± 0.039	0.14 ± 0.036	0.14 ± 0.035	0.10 ± 0.027

$^+$ *units are* $\times 10^{-3}$
* *indicates a p-value < 0.05 as compared to healthy controls.*
V_b = *Fractional blood volume,* V_{ss} = *steady state partition coefficient of* ^{18}*F-FDG.*

6.5.4 *^{18}F-FDG endpoints and inflammatory cell counts*

The BAL cell counts and differentials are shown in table 6.6. The largest proportion of cells in the BALf of the patients were lymphocytes and macrophages, the proportion of eosinophils was negligible. In one patient there was a high proportion of neutrophils (22%), for the remaining subjects neutrophils were negligible. The correlation coefficients between each cell line and whole lung ^{18}F-FDG outcomes were estimated. The correlation between K_{ip} and macrophages was r = 0.76 ($p = 0.048$); the correlation between K_{im} and macrophages was r = 0.73 which was just under the threshold of significance ($p = 0.063$). There was no significant correlations between the other cell lines and any of the ^{18}F-FDG outcomes.

In two patients, additional BAL samples were taken to assess absolute cell counts; the results are summarised in table 6.7. Both patients had similar total number of cells per ml of lavage sample. However, subject 2 had increased macrophages and neutrophils, decreased lymphocytes but similar levels of respiratory epithelial cells compared to subject 1. The ^{18}F-FDG uptake in subject 2 exhibited larger values than subject 1 for all outcomes.

Table 6.6: BAL cell counts and differentials for patients.

BAL measures	Sarcoidosis (n =7)
% Neutrophils	9.2 ± 5.5
% Macrophages	57.8 ± 20.8
% Lymphocytes	22 ± 11.0
% Eosinophils	0.8 ± 0.8

BAL = Bronchoalveolar lavage

Table 6.7: Absolute BAL cell counts and imaging outcomes in Sarcoidosis patients.

	Subject 1	Subject 2
Neutrophils (cells/ml)	0	0.11 ± 0.05
Macrophages (cells/ml)	10.0 ± 0.06	22.2 ± 0.1
Lymphocytes (cells/ml)	15.6 ± 0.08	8.8 ± 0.08
Respiratory Epithelial (cells/ml)	8.8 ± 0.09	6.6 ± 0.08
Squamous (cells/ml)	0.4 ± 0.07	0
Total inflammatory cells (cells/ml)	25.6 ± 0.5	32.2 ± 0.7
nK_i^+ [$ml/cm^3/min^{-1}$]	3.2	3.7
K_{ip}^+ [$ml/cm^3/min^{-1}$]	0.61	0.67
K_{im}^+ [$ml/cm^3/min^{-1}$]	6.2	6.8

* *All BAL measures are* $\times 10^4$
$^+$ *units are* $\times 10^{-3}$
BAL = Bronchoalveolar lavage

6.6 DISCUSSION

In this study, dynamic ^{18}F-FDG PET was used, for the first time, in sarcoidosis patients with clinically active disease to assess lung inflammation. Previous studies have focussed entirely on static measures such as SUV to assess inflammation. Notably, in these data, Patlak analysis revealed a difference in ^{18}F-FDG uptake between sarcoidosis patients and healthy controls which was not evident in static measures (i.e. the SUV_{mean}). On the whole, there was not enough evidence to conclude that pulmonary ^{18}F-FDG uptake in sarcoidosis represents total inflammatory burden; however, there was a high correlation between rate of uptake measured using Patlak analysis and percentage of macrophages. Additionally, compartmental modelling of the ^{18}F-FDG tracer was not able to detect a difference in pulmonary uptake in sarcoidosis patients,

similar to the findings in COPD patients.

Several studies have investigated the potential role of ^{18}F-FDG PET in sarcoidoisis for clinical management and as a predictive tool [200]. Specifically, there have been numerous studies which have evaluated ^{18}F-FDG as a marker of disease activity [186, 192, 196, 201]. All of these previous studies have been based on SUV_{max} as a tool for indirectly measuring pulmonary inflammation. In this study, there was no difference in whole lung SUV between healthy controls and sarcoidosis patients. This is consistent with the previous observation that ^{18}F-FDG uptake calculated using dynamic scans may be more sensitive to low levels of pulmonary uptake [202] and this appears to be the case in sarcoidosis. Both normalised and unnormalised Patlak outcomes demonstrated an increase in whole lung ^{18}F-FDG compared to healthy volunteers. Further, regional analyses found that the upper and middle lung ^{18}F-FDG uptake also appear elevated. Importantly, the fractional air and blood volumes did not significantly differ between these groups thus, there should be more confidence that the SUV, K_{ip} and nK_i better reflect underlying FDG metabolism than in conditions such as COPD. In contrast, ^{18}F-FDG uptake determined from compartmental modelling did not show elevated activity in the sarcoidosis patients either in the whole or regional lung analyses. This is consistent with the earlier observations in COPD patients (see chapter 4).

Despite its limitations, serum ACE is considered a marker of inflammation in sarcoidosis patients. Despite high levels of measured ACE, there was no correlation between serum ACE and ^{18}F-FDG uptake assessed by any method in these patients. Indeed, peripheral blood markers of inflammation in the patients did not show any correlation with ^{18}F-FDG-uptake. To obtain a more specific relationship to pulmonary inflammation, cells from within the lung were assessed using BAL. The BALf analysis revealed high proportions of lymphocytes and macrophages, consistent with previously reported values in clinically active sarcoidosis patients [203]. A previous study of sarcoidosis patients demonstrated higher lymphocytosis and total cell count in BALf in clinically active compared to asymptomatic patients [203]. In another study, uptake of ^{18}F-FDG in endotoxin challenged healthy volunteers was found to be elevated in BALf containing cells compared to BALf without cells [23], indicating that 80% of ^{18}F-

FDG signal was associated with cells. Further, autoradiography revealed that specific uptake of [^{3}H]-deoxyglucose was confined to the neutrophils, this is consistent with other early studies [43, 204, 205]. However, there was only a weak correlation between concentration of neutrophils and K_{ip} ($R^2 = 0.21$). In this study, the proportion of neutrophils and eosinophils was low or negligible in most patients but there was modest evidence of correlation between macrophages and K_{ip} suggesting that macrophages may be responsible for elevated ^{18}F-FDG uptake. However, due to the small sample size, this should be confirmed in larger subject numbers. On the whole, the current findings in sarcoidosis patients agree with those earlier observations, as there were no strong associations with any particular cell type and ^{18}F-FDG outcomes.
In a small subset of patients absolute cell counts were calculated and compared to ^{18}F-FDG uptake to elucidate if a particular cell is driving the underlying ^{18}F-FDG signal. It is not possible to make any firm conclusions since the number of subjects was too small (due to recruitment issues). Clearly, upon study completion the analyses of absolute cell counts may provide further insight into the origin of the ^{18}F-FDG signal.

Respiratory motion leads to anatomical mismatch and density variations between CT and PET scans; these manifest as inaccuracies in the attenuation correction (AC) map of the PET scan. One method to limit these errors is to use an averaged CT scan to more closely match the temporal blurring of the PET lung image [112, 113]. Errors in AC correction lead to over- or underestimation of the radioactivity concentration; for dynamic data analyses, these manifest as inaccuracies in the time activity curves (TAC) and subsequent parameter estimation (e.g. K_{ip}, K_{im}). In a previous study, density and motion mismatches led to significant errors estimating ^{18}F-FDG outcomes using simulations and real data from idiopathic pulmonary fibrosis (IPF) patients [114]. In that study, K_{ip} was shown to be more accurate and stable than the equivalent compartmental modelling outcome. Yet, the errors could still be substantial. The findings presented here in sarcoidosis patients agree with these earlier observations, although the maximum differences were slightly smaller (K_{ip} : -24.1% compared to -30.8%). It would be expected that the largest mismatches between PET and CT would occur with CT scans at either end inspiration or expiration. In these data, the maximum change was indeed greater between expiration and inspiration compared to the differ-

ence between the time averaged CT and either inspiration or expiration (e.g. change in K_{ip}: 24% compared to 15%). This shows that time averaging the cine-CT may reduce the variation in ^{18}F-FDG outcomes due to mismatch compared to using a CT from a random point in the respiratory cycle. These findings show that K_{ip} exhibited less variation than K_{im} when estimated using AC maps from different respiratory phases; this suggests that estimation of K_{ip} may be less prone to errors due to respiratory motion than other dynamic outcomes. However, it is hoped that future studies will include protocols designed to mitigate these errors through techniques such as shallow breathing, gated PET or cine-CT [68] .

Only a relatively small sample size was recruited into this study at the time of writing due to recruitment delays (subsequently worsened by the coronavirus pandemic); nevertheless, it was shown that ^{18}F-FDG can be used to non-invasively assess disease activity in sarcoidosis patients. Autoradiography of the BALf was not performed therefore those cells with a higher affinity for ^{18}F-FDG could not be identified; however, other studies have demonstrated that ^{18}F-FDG labels inflammatory cells. The assumption that the cell proportions in a BALf sample is representative of the whole lung and this is uniform throughout may also be too simplistic; however BAL is often taken as the gold standard method in pulmonary inflammation [65]. Pulmonary sarcoidosis has a varying appearance on chest CT between patients, these difference could result in different patterns of ^{18}F-FDG uptake. Since recent previous CT scans were reviewed prior to entry into the study by an ILD specialist, these differences are likely to be minimal.

6.7 CONCLUSION

In summary, quantitative dynamic ^{18}F-FDG demonstrated increased values compared to healthy controls. It can only be speculated that this is due to pulmonary inflammation; indeed, the similarity in fractional air and blood volumes between patient and control groups is suggestive that the increase is related inflammation, but further data is required before any firm conclusions are made. Patlak graphical analysis demonstrated increased uptake of ^{18}F-FDG uptake compared to controls, whereas static and

compartmental modelling analyses found no difference between the groups. The results suggest that Patlak analyses may be the most suitable method to detect the low levels of pulmonary ^{18}F-FDG uptake typically present in clinically active sarcoidosis. Considerable errors in ^{18}F-FDG uptake can be introduced by mismatches between CT and PET due to respiratory motion underlining the importance of correction methods.

7

CONCLUSIONS AND FUTURE DIRECTIONS

Inflammation is a characteristic feature of several lung diseases and is thought to be an important factor in their pathogenesis and progression. Existing markers which are used as indirect measures of lung inflammation such as pulmonary function tests (PFTs) have a number of limitations, particularly in the research setting. For example, PFTs do not relate directly to lung dysfunction and exhibit long intervals before changes in disease manifest in the measurements. Imaging techniques can fulfil many of the requirements of an improved biomarker for lung inflammation.

Although other imaging modalities are used to assess diffuse lung disease, PET imaging techniques are capable of evaluating disease activity and improving our understanding of the molecular basis of disease. Whilst ^{18}F-FDG is not a specific marker of inflammation, to date, it is the PET tracer which has formed the foundation of pulmonary inflammation assessment. There are several quantitative ^{18}F-FDG imaging outcomes which have been disparately applied as endpoints in studies of pulmonary inflammation. Notwithstanding the low signal-to-noise ratio of ^{18}F-FDG lung images and errors introduced by respiratory motion, there has been nascent recognition of a significant knowledge gap regarding the utility of these outcomes as a research tool and in understanding their biologic interpretation [30]. This work sought to clarify these issues, by scrutinising these imaging outcomes in different clinical and experimental conditions with the hope it will improve confidence in PET imaging endpoints. Of course, these issues are not restricted to ^{18}F-FDG; they will exist to a varying extent for other PET tracers targeting lung inflammation.

Using retrospective data from two complementary imaging studies, pulmonary ^{18}F-FDG uptake was investigated in COPD patients, α_1-ATD patients, smokers without COPD and heathy non-smokers. This was performed in a substantially larger cohort

than previous ^{18}F-FDG imaging studies of COPD [55]. Indeed, in the literature, there are no comparably sized studies investigating different ^{18}F-FDG outcomes in relevant human diseases. The results demonstrate that the contending ^{18}F-FDG outcomes produce disparate findings which are exacerbated by the presence of varying blood and air volumes due to emphysema. Nevertheless, normalised rate of ^{18}F-FDG uptake, nK_i, derived from Patlak analysis revealed elevated uptake consistent with the pathophysiological understanding of the disease process. Further, nK_i demonstrated correlation with fibrinogen; another putative marker of inflammation. Indeed, increased nKi values were found in a subset of COPD patients with similar pulmonary blood and air volumes to healthy controls, suggesting that the PET signal was related to increased pulmonary ^{18}F-FDG metabolism. Further, Patlak analysis was shown to be more reliable than compartmental modelling; both in terms of repeatability assessed in longitudinal scans of COPD patients and in reproducibility of analysis performed by two independent operators. This latter observation is due to the wide range of parameters that can be chosen during implementation of compartmental modelling, whereas Patlak analysis is better standardised.

In a further development, PET and CT were used synergistically to evaluate associations between disease severity and disease activity. Sub-typing based on CT features has identified clear differences in progression of COPD subtypes [176]. Although no strong evidence of an association was found, new studies continue to refine the CT subtypes and may identify treatment responders [177]; ^{18}F-FDG PET may have a role in assessing efficacy of novel anti-inflammatory therapies.

Finally, in a prospective study, dynamic ^{18}F-FDG PET scans were used to evaluate pulmonary inflammation in sarcoidosis patients and healthy controls. These patients underwent bronchoscopy and BAL allowing inflammatory cell counts within the lung to be compared to ^{18}F-FDG uptake. Importantly, there was no difference in fractional blood and air volumes between the patient and control groups. Despite small numbers, there was evidence that ^{18}F-FDG uptake was increased in sarcoidosis using Patlak analysis; this was not apparent using static measures such as SUV, one can speculate that the increased signal was predominately related to inflammation. In-

terestingly, there was a significant correlation between the proportion of macrophages and ^{18}F-FDG uptake assessed with Patlak analysis. However, these initial observations and the relationship between ^{18}F-FDG and pulmonary inflammation will need to be confirmed upon study completion. Consistent with previous findings [114], mismatch in CT and PET lung images had a substantial effect on the quantitative ^{18}F-FDG imaging outcomes; notably, Patlak outcomes were less influenced than compartmental modelling. This effect will be less pronounced in solid tissues in the lung such as malignant lesions, but is important in diffuse lung diseases.

Overall, these data suggest that SUV may be inadequate for studies of diffuse lung disease, especially when large differences in blood and air volume may be present; in the COPD study this led to non-physiological findings (i.e. healthy controls had increased uptake). Further, the SUV was insensitive to differences between disease and healthy groups when this confounder was not present. Equally, the consistent inability of compartmental modelling outcome, K_{im}, to discern differences in ^{18}F-FDG uptake between disease and control groups suggests that compartmental modelling may have poor utility in studies of diffuse lung disease. This may be due to the inherent noise of PET imaging; Patlak analysis uses linear modelling which mitigate the issues with parameter estimation in noisy PET lung data better than non-linear compartmental modelling. However, in this work, the sample sizes were small when comparing groups with similar pulmonary air and blood volumes, therefore it is possible that an effect may be observed using compartment modelling with larger sample sizes. All parameters in this work were estimated using indirect methods - that is, the images were reconstructed prior to fitting linear and non-linear models. Direct estimation methods (i.e. parameter estimation from PET emission data prior to reconstruction) has favourable noise characteristics and this may improve the sensitivity of both Patlak methods and compartmental modelling [206]. Further, improvements in PET scanner technology - such as whole body PET scanners - will also lead to improved SNR and better parameter estimation [207].

Across this project, Patlak outcomes, K_{ip} and nK_i, were the most valuable and reliable measures of pulmonary ^{18}F-FDG uptake in diffuse disease. However, it is now

known that Patlak outcomes are biased by pulmonary air and blood [66] hence they reflect a composite measure of ^{18}F-FDG metabolism, V_b and V_a. Therefore, in circumstances where V_b and V_a are similar or not expected to change such as in the sarcoidosis patient study (chapter 6) or investigating intra-subject treatment effects, then one can speculate that Patlak outcomes may provide a measure which better relates to underlying inflammation. If V_b and V_a are significantly different in subjects then differences in Patlak outcomes could be driven by these variables rather than inflammation per se, hence may not be a suitable biomarker for pulmonary inflammation but may be useful as a marker of disease activity. Further, the poor signal-to-noise ratio in pulmonary ^{18}F-FDG images appears to limit the application of compartmental modelling derived putative biomarkers of pulmonary inflammation. Future studies which incorporate independent measures of pulmonary blood volume (such as ^{15}O-CO PET) alongside ^{18}F-FDG would be desirable to provide further insight and instill confidence.

Given the findings of this work, it it evident that meticulous planning is required when using ^{18}F-FDG PET to study diffuse lung diseases. It is incumbent on the investigators to give due consideration to the acquisition and analysis of data from such studies. As is clear from the preceding discussion, the choice of imaging endpoint has the potential to lead to different conclusions, hence the chosen endpoint should be rigorously justified. Indeed, this has implications for the selection of subjects; for example, thought needs to be given to the heterogeneity of disease within a single patient group and its implications on the imaging outcome (as shown in chapter 5). Another related factor will be comparisons between groups with different lung tissue fractions, which could lead to different conclusions depending on the imaging endpoint (as shown in chapter 4). Methods to mitigate respiratory motion ought be considered prior to a study of diffuse lung disease to minimise the differences in PET imaging outcomes between scans (see findings from chapter 6). Further, all steps in the analysis should be kept consistent throughout and clearly documented as seemingly minor changes can result in bias in imaging endpoints (as shown by the poor reproducibility of compartmental modelling outcomes).

An important limitation when evaluating biomarkers of lung inflammation is the lack of a gold standard. Indeed, it is difficult to assess the accuracy of one outcome against another without this comparator. Instead this work has evaluated the reliability of the different outcomes against established clinical markers, and through assessment of repeatability, reproducibility and dependence on technical factors. One route to address this problem is the design and fabrication of more realistic lung phantoms capable of assessing quantitative ^{18}F-FDG [68]; another related method is through computerised simulation studies [114].

The lack of specificity could be recognised as a limitation of ^{18}F-FDG. However, ^{18}F-FDG provides a measure of integrated inflammatory response and therefore may be useful in diseases where a specific inflammatory pathway has yet to be identified. Nonetheless, the development of more specific PET probes capable of targeting individual immune cells or other molecules thought to be important to the disease (such as cytokines [208]) would be beneficial; for example, in efficacy studies of novel therapeutics. Although there are several tracers on the horizon which have been used to evaluate pulmonary inflammation, these are at the very early stages of development, most have not yet been tested in human models of disease [50]. These candidate PET tracers have shown promise in distinguishing animal models of pulmonary inflammation. Further studies in humans are needed to investigate whether these encouraging results translate into humans. Questions regarding clinical validity and utility will also need to be addressed. Yet by adopting well designed preclinical studies early, strong evidence of a relationship to meaningful biological features can be identified. Nonetheless, it is probable that ^{18}F-FDG will remain the most widely utilised tracer in inflammatory lung diseases; the existing literature is compelling and supports continued use of ^{18}F-FDG for monitoring inflammation in a variety of diseases.

In summary, there is an existing platform of evidence, built on previous studies, that suggests ^{18}F-FDG PET is a valuable tool for evaluating lung inflammation in diffuse lung diseases. In these data, although there was increased pulmonary FDG metabolism in diseased groups compared to healthy controls ostensibly supporting its continued use, one can only speculate that this is related primarily to underlying

inflammation. Importantly, the findings reported here demonstrate that different analysis methods may produce disparate results. Overall, the results suggest that Patlak analysis may have the most utility when assessing diffuse lung diseases. However, differences in Patlak outcomes should be interpreted judiciously, as they may be driven by differences in pulmonary blood and air along with inflammation. These findings underlie the need for careful design, analysis and interpretation of studies using ^{18}F-FDG PET to assess lung inflammation which may make it challenging to implement as a widespread tool to accurately assess inflammation.

I believe that PET has a potentially useful role in future proof-of-concept studies and drug efficacy trials. Yet, further work is needed to improve the catalogue of other PET tracers available to prospective researchers of diffuse lung disease. It is hoped that through increasing the number of targeted tracers, improving the noise characteristics of the estimation methods and multiplexed tracer studies will help improved understanding of the pathophysiology of lung disease, phenotype patients and facilitate the discovery of effective therapies.

BIBLIOGRAPHY

[1] G J. Gibson et al., eds. *European Lung White Book*. 2019. ISBN: 978-1-84984-042-2.

[2] C. P Adams and V. V Brantner. "Estimating the cost of new drug development: is it really 802 million dollars?" eng. In: *Health affairs (Project Hope)* 25.2 (2006), pp. 420–428. ISSN: 1544-5208 0278-2715. DOI: 10.1377/hlthaff.25.2.420.

[3] M. G. Netea et al. "A guiding map for inflammation." In: *Nature Immunology* 18.8 (2017), pp. 826–831. ISSN: 15292916. DOI: 10.1038/ni.3790. URL: http://dx.doi.org/10.1038/ni.3790.

[4] D. L Chen et al. "PET imaging approaches for inflammatory lung diseases: Current concepts and future directions." In: *European Journal of Radiology* 86 (2017), pp. 371–376. ISSN: 0720048X. DOI: 10.1016/j.ejrad.2016.09.014. URL: https://linkinghub.elsevier.com/retrieve/pii/S0720048X16302832.

[5] T. J. Craig et al. "Aeroallergen sensitization correlates with PC20 and exhaled nitric oxide in subjects with mild-to-moderate asthma." In: *Journal of Allergy and Clinical Immunology* 121.3 (2008), pp. 671–677. ISSN: 0091-6749. DOI: 10.1016/J.JACI.2007.12.1153. URL: https://www.sciencedirect.com/science/article/pii/S0091674907035804.

[6] M. E Kuruvilla, F Eun-Hyung Lee, and Gerald B Lee. "Understanding Asthma Phenotypes, Endotypes, and Mechanisms of Disease." eng. In: *Clinical reviews in allergy & immunology* 56.2 (2019), pp. 219–233. ISSN: 1559-0267 (Electronic). DOI: 10.1007/s12016-018-8712-1.

[7] C. Bostantzoglou et al. "Clinical asthma phenotypes in the real world: opportunities and challenges." In: *Breathe* 11.3 (2015), 186 LP –193. DOI: 10.1183/20734735.008115. URL: http://breathe.ersjournals.com/content/11/3/186.abstract.

[8] B Moldoveanu et al. "Inflammatory mechanisms in the lung." In: *Journal of inflammation research* 2 (2009), pp. 1–11. ISSN: 1178-7031. URL: http://www.ncbi.nlm.nih.gov/pubmed/22096348http://www.pubmedcentral.nih.gov/articlerender.fcgi?artid=PMC3218724.

[9] N. Snell et al. "Burden of lung disease in the UK; findings from the British Lung Foundation's 'respiratory health of the nation' project." In: *European Respiratory Journal* 48.suppl 60 (2016), PA4913. DOI: 10.1183/13993003.congress-2016.PA4913. URL: http://erj.ersjournals.com/content/48/suppl{_}60/PA4913.abstract.

[10] J.C Hogg et al. "The Nature of Small-Airway Obstruction in Chronic Obstructive Pulmonary Disease." In: *New England Journal of Medicine* 350.26 (2004), pp. 2645–2653. ISSN: 0028-4793. DOI: 10.1056/NEJMoa032158. URL: https://doi.org/10.1056/NEJMoa032158.

[11] P. J Barnes. "Immunology of asthma and chronic obstructive pulmonary disease." In: *Nature Reviews Immunology* 8 (2008), p. 183. URL: https://doi.org/10.1038/nri2254http://10.0.4.14/nri2254.

[12] G. G Brusselle, G. F Joos, and K. R Bracke. "New insights into the immunology of chronic obstructive pulmonary disease." In: *Lancet (London, England)* 378.9795 (2011), pp. 1015–26. ISSN: 1474-547X. DOI: 10.1016/S0140-6736(11)60988-4. URL: http://www.ncbi.nlm.nih.gov/pubmed/21907865.

[13] C. J Galbán et al. "Computed tomography?based biomarker provides unique signature for diagnosis of COPD phenotypes and disease progression." In: *Nature Medicine* 18 (2012), p. 1711. URL: https://doi.org/10.1038/nm.2971http://10.0.4.14/nm.2971https://www.nature.com/articles/nm.2971{\#}supplementary-information.

[14] B. L. Barker and C. E. Brightling. "Phenotyping the heterogeneity of chronic obstructive pulmonary disease." In: *Clinical Science* 124.6 (2013), pp. 371–387. ISSN: 01435221. DOI: 10.1042/CS20120340.

[15] F. Garcia-Rio et al. "Systemic inflammation in chronic obstructive pulmonary disease: a population-based study." eng. In: *Respiratory research* 11.1 (2010), p. 63. ISSN: 1465-993X. DOI: 10.1186/1465-9921-11-63. URL: https://pubmed.ncbi.nlm.nih.gov/20500811https://www.ncbi.nlm.nih.gov/pmc/articles/PMC2891677/.

[16] C. Viniol and C. F Vogelmeier. "Exacerbations of COPD." In: *European Respiratory Review* 27.147 (2018), p. 170103. DOI: 10.1183/16000617.0103-2017. URL: http://err.ersjournals.com/content/27/147/170103.abstract.

[17] "Statement on Sarcoidosis." In: *American Journal of Respiratory and Critical Care Medicine* 160.2 (1999), pp. 736–755. DOI: 10.1164/ajrccm.160.2.ats4-99. URL: https://doi.org/10.1164/ajrccm.160.2.ats4-99.

[18] J. E Gottlieb et al. "Outcome in Sarcoidosis: The Relationship of Relapse to Corticosteroid Therapy." In: *Chest* 111.3 (1997), pp. 623–631. ISSN: 0012-3692. DOI: https://doi.org/10.1378/chest.111.3.623. URL: http://www.sciencedirect.com/science/article/pii/S0012369215468138.

[19] R P Baughman et al. "Presenting characteristics as predictors of duration of treatment in sarcoidosis." In: *QJM: An International Journal of Medicine* 99.5 (2006), pp. 307–315. ISSN: 1460-2725. DOI: 10.1093/qjmed/hcl038. URL: https://doi.org/10.1093/qjmed/hcl038.

[20] P R Studdy et al. "Biochemical findings in sarcoidosis." eng. In: *Journal of clinical pathology* 33.6 (1980), pp. 528–533. ISSN: 0021-9746. DOI: 10.1136/jcp.33.6.528. URL: https://pubmed.ncbi.nlm.nih.gov/6249857https://www.ncbi.nlm.nih.gov/pmc/articles/PMC1146136/.

[21] G M AINSLIE and S R BENATAR. "Serum Angiotensin Converting Enzyme in Sarcoidosis: Sensitivity and Specificity in Diagnosis: Correlations with Disease Activity, Duration, Extra-thoracic Involvement, Radiographic Type and Therapy." In: *QJM: An International Journal of Medicine* 55.3-4 (1985), pp. 253–270. ISSN: 1460-2725. DOI: 10.1093/oxfordjournals.qjmed.a067873. URL: https://doi.org/10.1093/oxfordjournals.qjmed.a067873.

[22] DL Chen and PE Kinahan. "Multimodality molecular imaging of the lung." In: *Journal of Magnetic Resonance Imaging* 32.6 (2010), pp. 1409–1420. DOI: 10.1002/jmri.22385.Multimodality. URL: http://onlinelibrary.wiley.com/doi/10.1002/jmri.22385/full.

[23] D. L Chen et al. "FDG-PET imaging of pulmonary inflammation in healthy volunteers after airway instillation of endotoxin." In: 63110 (2006), pp. 1602–1609. DOI: 10.1152/japplphysiol.01429.2005..

[24] D. L. Chen et al. "The peroxisome proliferator-activated receptor agonist pioglitazone and 5-lipoxygenase inhibitor zileuton have no effect on lung inflammation in healthy volunteers by positron emission tomography in a single-blind placebo-controlled cohort study." In: *PLoS ONE* 13.2 (2018), pp. 1–17. ISSN: 19326203. DOI: 10.1371/journal.pone.0191783. URL: http://dx.doi.org/10.1371/journal.pone.0191783.

[25] P. Chanez et al. "Sputum induction." In: *European Respiratory Journal* 20.37 suppl (2002), 3s–8s. ISSN: 0903-1936. DOI: 10.1183/09031936.02.00000302. eprint: https://erj.ersjournals.com/content/20/37_suppl/3s.full.pdf. URL: https://erj.ersjournals.com/content/20/37_suppl/3s.

[26] D. M Mannino et al. "Plasma Fibrinogen as a Biomarker for Mortality and Hospitalized Exacerbations in People with COPD." eng. In: *Chronic obstructive pulmonary diseases (Miami, Fla.)* 2.1 (2015), pp. 23–34. ISSN: 2372-952X (Print). DOI: 10.15326/jcopdf.2.1.2014.0138.

[27] Y. Peng et al. "Understanding the controversy surrounding the correlation between fibrinogen level and prognosis of coronary artery disease?The role of the subtypes of coronary artery disease." In: *International Journal of Cardiology* 222 (2016), pp. 968–972. ISSN: 0167-5273. DOI: https://doi.org/10.1016/j.ijcard.2016.07.160. URL: https://www.sciencedirect.com/science/article/pii/S0167527316315558.

[28] Ke Z. et al. "The association between plasma fibrinogen levels and lung cancer: a meta-analysis." In: *Journal of Thoracic Disease* 11.11 (2019). ISSN: 2077-6624. URL: https://jtd.amegroups.com/article/view/33473.

[29] S Loukides et al. "Exhaled Breath Condensate in Asthma: From Bench to Bedside." In: 18.10 (2011), pp. 1432–1443. DOI: http://dx.doi.org/10.2174/092986711795328418. URL: http://www.eurekaselect.com/node/73762/article.

[30] D. L. Chen et al. "Quantification of Lung PET Images: Challenges and Opportunities." In: *Journal of Nuclear Medicine* 58.2 (2017), pp. 201–207. ISSN: 0161-5505. DOI: 10.2967/jnumed.116.184796. URL: http://jnm.snmjournals.org/lookup/doi/10.2967/jnumed.116.184796.

[31] R. Sharma and E. Aboagye. "Development of radiotracers for oncology - The interface with pharmacology." In: *British Journal of Pharmacology* 163.8 (2011), pp. 1565–1585. ISSN: 00071188. DOI: 10.1111/j.1476-5381.2010.01160.x. URL: http://files/280/developmentofradiotracers.pdf.

[32] D. L Chen et al. "PET imaging approaches for inflammatory lung diseases: Current concepts and future directions." In: *European Journal of Radiology* 86 (2017), pp. 371–376. ISSN: 0720048X. DOI: 10.1016/j.ejrad.2016.09.014. URL: https://linkinghub.elsevier.com/retrieve/pii/S0720048X16302832http://files/303/chenandvanbeek2016-reviewofpetimaginginlunginflammation.pdf.

[33] S. F. Nemec, R. L Eisenberg, and A. A Bankier. "Noninfectious Inflammatory Lung Disease: Imaging Considerations and Clues to Differential Diagnosis." In: *American Journal of Roentgenology* 201.2 (2013), pp. 278–294. ISSN: 0361-803X. DOI: 10.2214/AJR.12.9772. URL: https://doi.org/10.2214/AJR.12.9772.

[34] D. J Lederer et al. "Cigarette Smoking Is Associated with Subclinical Parenchymal Lung Disease." In: *American Journal of Respiratory and Critical Care Medicine* 180.5 (2009), pp. 407–414. ISSN: 1073-449X. DOI: 10.1164/rccm.200812-1966OC. URL: https://doi.org/10.1164/rccm.200812-1966OC.

[35] L. Lonzetti et al. "Magnetic resonance imaging of interstitial lung diseases: A state-of-the-art review." In: *Respiratory Medicine* 155 (2019), pp. 79–85. ISSN: 0954-6111. DOI: https://doi.org/10.1016/j.rmed.2019.07.006. URL: http://www.sciencedirect.com/science/article/pii/S095461111930229X.

[36] C. A. Yi et al. "3-T MRI for differentiating inflammation- and fibrosis-predominant lesions of usual and nonspecific interstitial pneumonia: Comparison study with pathologic correlation." In: *American Journal of Roentgenology* 190.4 (2008), pp. 878–885. ISSN: 0361803X. DOI: 10.2214/AJR.07.2833.

[37] L. P Lavelle et al. "Pulmonary fibrosis: tissue characterization using late-enhanced MRI compared with unenhanced anatomic high-resolution CT." eng. In: *Diagnostic and interventional radiology (Ankara, Turkey)* 23.2 (2017), pp. 106–111. ISSN: 1305-3612 (Electronic). DOI: 10.5152/dir.2016.15331.

[38] C. Romei et al. "The use of chest magnetic resonance imaging in interstitial lung disease: a systematic review." eng. In: *European respiratory review : an official journal of the European Respiratory Society* 27.150 (2018). ISSN: 1600-0617 (Electronic). DOI: 10.1183/16000617.0062-2018.

[39] R. J Theilmann et al. "Quantitative MRI measurement of lung density must account for the change in T(2) (*) with lung inflation." eng. In: *Journal of magnetic resonance imaging : JMRI* 30.3 (2009), pp. 527–534. ISSN: 1053-1807. DOI: 10.1002/jmri.21866. URL: https://www.ncbi.nlm.nih.gov/pubmed/19630079https://www.ncbi.nlm.nih.gov/pmc/articles/PMC3354915/.

[40] J. Ley-Zaporozhan, S. Ley, and HU Kauczor. "Morphological and functional imaging in COPD with CT and MRI: present and future." In: *European Radiology* 18.3 (2008), pp. 510–521. ISSN: 1432-1084. DOI: 10.1007/s00330-007-0772-1. URL: https://doi.org/10.1007/s00330-007-0772-1.

[41] C Bekerman et al. "Gallium-67 citrate imaging studies of the lung." In: *Seminars in Nuclear Medicine* 10.3 (1980), pp. 286–301. ISSN: 0001-2998. DOI: 10.1016/S0001-2998(80)80007-9. URL: https://www.sciencedirect.com/science/article/pii/S0001299880800079.

[42] H. Susskind and W. N Rom. "Lung Inflammation in Coal Miners Assessed by Uptake of 67Ga-Citrate and Clearance of Inhaled 99mTc-labeled Diethylenetriamine Pentaacetate Aerosol." In: *American Review of Respiratory Disease* 146.1 (1992), pp. 47–52. ISSN: 0003-0805. DOI: 10.1164/ajrccm/146.1.47. URL: https://doi.org/10.1164/ajrccm/146.1.47.

[43] H A Jones et al. "Dissociation of neutrophil emigration and metabolic activity in lobar pneumonia and bronchiectasis." In: *European Respiratory Journal* 10.4 (1997), pp. 795–803. ISSN: 0903-1936 (Print)\no903-1936 (Linking). DOI: 10.1183/09031936.97.10040795. URL: http://files/214/197-Jones-1997.pdf.

[44] N. Tregay et al. "Use of autologous ^{99m}Technetium-labelled neutrophils to quantify lung neutrophil clearance in COPD." In: *Thorax* 74.7 (2019), 659 LP –666. DOI: 10.1136/thoraxjnl-2018-212509. URL: http://thorax.bmj.com/content/74/7/659.abstract.

[45] N. Farahi et al. "In vivo imaging reveals increased eosinophil uptake in the lungs of obese asthmatic patients." In: *Journal of Allergy and Clinical Immunology* 142.5 (2018), 1659–1662.e8. ISSN: 0091-6749. DOI: 10.1016/j.jaci.2018.07.011. URL: https://doi.org/10.1016/j.jaci.2018.07.011.

[46] K. Ostridge and T. M.A. Wilkinson. "Present and future utility of computed tomography scanning in the assessment and management of COPD." In: *European Respiratory Journal* 48.1 (2016), pp. 216–228. ISSN: 13993003. DOI: 10.1183/13993003.00041-2016. URL: http://dx.doi.org/10.1183/13993003.00041-2016.

[47] R. Golestani et al. "Matrix metalloproteinase-Targeted imaging of lung inflammation and remodeling." In: *Journal of Nuclear Medicine* 58.1 (2017), pp. 138–143. ISSN: 2159662X. DOI: 10.2967/jnumed.116.176198.

[48] R. Golestani et al. "Imaging vessel wall biology to predict outcome in abdominal aortic aneurysm." In: *Circulation. Cardiovascular imaging* 8.1 (2015). ISSN: 1942-0080. DOI: 10.1161/CIRCIMAGING.114.002471. URL: http://www.ncbi.nlm.nih.gov/pubmed/25550400http://www.pubmedcentral.nih.gov/articlerender.fcgi?artid=PMC4284949.

[49] JJ. Jung et al. "Multimodality and molecular imaging of matrix metalloproteinase activation in calcific aortic valve disease." In: *Journal of nuclear medicine : official publication, Society of Nuclear Medicine* 56.6 (2015), pp. 933–8. ISSN: 1535-5667. DOI: 10.2967/jnumed.114.152355. URL: http://www.ncbi.nlm.nih.gov/pubmed/25908827http://www.pubmedcentral.nih.gov/articlerender.fcgi?artid=PMC4454445.

[50] L. Vass et al. "Advances in PET to assess pulmonary inflammation: A systematic review." In: *European Journal of Radiology* 130 (2020), p. 109182. ISSN: 0720-048X. DOI: https://doi.org/10.1016/j.ejrad.2020.109182. URL: http://www.sciencedirect.com/science/article/pii/S0720048X20303715.

[51] D. L Chen, Jeffrey J Atkinson, and Thomas W Ferkol. "FDG PET Imaging in Cystic Fibrosis." In: *Non-Oncology PET (Part II)* 43.6 (2013), pp. 412–419. ISSN: 0001-2998. DOI: 10.1053/j.semnuclmed.2013.06.002. URL: http://www.sciencedirect.com/science/article/pii/S000129981300055X.

[52] Y. Umeda et al. "Prognostic value of dual-time-point 18F-FDG PET for idiopathic pulmonary fibrosis." In: *Journal of Nuclear Medicine* 56.12 (2015), pp. 1869–1875. DOI: 10.2967/jnumed.115.163360. URL: http://files/296/Umedaetal2015-IPFdualtimepointSUV.pdf.

[53] T. Lambrou et al. "The importance of correction for tissue fraction effects in lung PET: Preliminary findings." In: *European Journal of Nuclear Medicine and Molecular Imaging* 38.12 (2011), pp. 2238–2246. ISSN: 16197070. DOI: 10.1007/s00259-011-1906-x.

[54] D. R. Subramanian et al. "Assessment of pulmonary neutrophilic inflammation in emphysema by quantitative positron emission tomography." In: *American Journal of Respiratory and Critical Care Medicine* 186.11 (2012), pp. 1125–1132. ISSN: 1073449X. DOI: 10.1164/rccm.201201-0051OC. arXiv: arXiv:1011.1669v3.

[55] H.A. Jones et al. "In vivo assessment of lung inflammatory cell activity in patients with COPD and asthma." In: *European Respiratory Journal* 21.4 (2003), pp. 567–573. ISSN: 0903-1936. DOI: 10.1183/09031936.03.00048502.

[56] D. A Torigian et al. "In vivo quantification of pulmonary inflammation in relation to emphysema severity via partial volume corrected (18)F-FDG-PET using computer-assisted analysis of diagnostic chest CT." In: *Hellenic Journal of Nuclear Medicine* 16.1 (2013), pp. 12–18. ISSN: 1790-5427. DOI: 10.1967/s0024499100066. URL: http://ovidsp.ovid.com/ovidweb.cgi?T=JS{\&}CSC=Y{\&}NEWS=N{\&}PAGE=fulltext{\&}D=medl{\&}AN=23529388{\%}5Cnhttp://sfx.bibl.ulaval.ca:9003/sfx{_}local?sid=OVID:medline{\&}id=pmid:23529388{\&}id=doi:10.1967/s0024499100066{\&}issn=1790-5427{\&}isbn={\&}volume=16{\&}issue=1{\&}spage=12{\&}pages=12-8{\&}dahttp://files/194/84-Torigian-2013.pdf.

[57] I K Taylor et al. "Imaging allergen-invoked airway inflammation in atopic asthma with [18F]-fluorodeoxyglucose and positron emission tomography." In: *Lancet* 347.9006 (1996), pp. 937–940. URL: http://www.ncbi.nlm.nih.gov/pubmed/8598758http://files/284/TheLancet1996Taylor.pdf.

[58] R S Harris et al. "18F-FDG Uptake Rate Is a Biomarker of Eosinophilic Inflammation and Airway Response in Asthma." en. In: *Journal of Nuclear Medicine* 52.11 (2011), pp. 1713–1720. ISSN: 0161-5505. DOI: 10.2967/jnumed.110.086355. URL: http://jnm.snmjournals.org/cgi/doi/10.2967/jnumed.110.086355http://files/127/Harris-fdguptakebiomarkerforeosinophilicinflammation.pdf.

[59] A. M Groves et al. "Idiopathic pulmonary fibrosis and diffuse parenchymal lung disease: implications from initial experience with 18F-FDG PET/CT." In: *Journal of nuclear medicine : official publication, Society of Nuclear Medicine* 50.4 (2009), pp. 538–545. ISSN: 0161-5505 (Print)\r0161-5505 (Linking). DOI: 10.2967/jnumed.108.057901. URL: http://files/292/JournalofNuclearMedicine2009Groves.pdf.

[60] B. Holman et al. "Improved correction for the tissue fraction effect in lung PET/CT imaging." In: *Physics in Medicine and Biology* 60.18 (2015), pp. 7387–7402. ISSN: 0031-9155. DOI: 10.1088/0031-9155/60/18/7387. URL: http://dx.doi.org/10.1088/0031-9155/60/18/7387.

[61] T Win et al. "18F-Fluorodeoxyglucose positron emission tomography pulmonary imaging in idiopathic pulmonary fibrosis is reproducible: Implications for future clinical trials." In: *European Journal of Nuclear Medicine and Molecular Imaging* 39.3 (2012), pp. 521–528. ISSN: 1619-7089 (Electronic)\r1619-7070 (Linking). DOI: 10.1007/s00259-011-1986-7. URL: http://files/290/Winetal(2011)-FDGPETinIPFisreproducible.pdf.

[62] T Win et al. "Areas of normal pulmonary parenchyma on HRCT exhibit increased FDG PET signal in IPF patients." In: *European Journal of Nuclear Medicine and Molecular Imaging* 2 (), pp. 337–342. ISSN: 1619-7070. DOI: 10.1007/s00259-013-2514-8.

[63] M. Klein et al. "^{18}F-FDG-PET/CT imaging of lungs in patients with cystic fibrosis." In: *Chest* 136.5 (2009), pp. 1220–1228. DOI: 10.1378/chest.09-0610. URL: http://files/152/139-Klein-2009.pdf.

[64] R. Amin et al. "Cystic fibrosis: Detecting changes in airway inflammation with FDG PET/CT." In: *Radiology* 264.3 (2012), pp. 868–875. DOI: 10.1148/radiol.12111873. URL: http://files/294/AminRadiology2012{_}264{_}868CFFDGPET.pdf.

[65] D. L. Chen et al. "[18F]fluorodeoxyglucose positron emission tomography for lung antiinflammatory response evaluation." In: *American Journal of Respiratory and Critical Care Medicine* 180.6 (2009), pp. 533–539. ISSN: 1073449X. DOI: 10.1164/rccm.200904-0501OC.

[66] C. Coello et al. "Quantitative analysis of dynamic 18F-FDG PET/CT for measurement of lung inflammation." In: *EJNMMI Research* 7.1 (2017), p. 47. ISSN: 2191-219X. DOI: 10.1186/s13550-017-0291-2. URL: http://ejnmmires.springeropen.com/articles/10.1186/s13550-017-0291-2.

[67] L. D Vass et al. "Reproducibility of compartmental modelling of 18F-FDG PET/CT to evaluate lung inflammation." In: *EJNMMI Physics* 6.1 (2019), p. 26. ISSN: 2197-7364. DOI: 10.1186/s40658-019-0265-8. URL: https://doi.org/10.1186/s40658-019-0265-8.

[68] D. L Chen et al. "Consensus recommendations on the use of (18)F-FDG PET/CT in lung disease." eng. In: *Journal of nuclear medicine : official publication, Society of Nuclear Medicine* (2020). ISSN: 1535-5667 (Electronic). DOI: 10.2967/jnumed.120.244780.

[69] D. Zhou et al. "Design and synthesis of 2-amino-4-methylpyridine analogues as inhibitors for inducible nitric oxide synthase and in vivo evaluation of [18F]6-(2-fluoropropyl)-4-methyl-pyridin-2-amine as a potential PET tracer for inducible nitric oxide synthase." eng. In: *Journal of medicinal chemistry* 52.8 (2009), pp. 2443–2453. ISSN: 1520-4804. DOI: 10.1021/jm801556h. URL: https://www.ncbi.nlm.nih.gov/pubmed/19323559https://www.ncbi.nlm.nih.gov/pmc/articles/PMC2782628/.

[70] P Herrero et al. "Feasibility and Dosimetry Studies for 18F-NOS as a Potential PET Radiopharmaceutical for Inducible Nitric Oxide Synthase in Humans." In: *Journal of Nuclear Medicine* 53.6 (2012), pp. 994–1001. ISSN: 1535-5667 (Electronic)\no161-5505 (Linking). DOI: 10.2967/jnumed.111.088518. URL: http://jnm.snmjournals.org/cgi/doi/10.2967/jnumed.111.088518http://files/138/104-Herrero-2012.pdf.

[71] H J Huang et al. "Imaging Pulmonary Inducible Nitric Oxide Synthase Expression with PET." In: *Journal of Nuclear Medicine* 56.1 (2015), pp. 76–81. DOI: 10.2967/jnumed.114.146381. URL: http://jnm.snmjournals.org/cgi/doi/10.2967/jnumed.114.146381http://files/174/49-Huang-2015.pdf.

[72] S. Wagner et al. "Novel Fluorinated Derivatives of the Broad-Spectrum MMP Inhibitors N-Hydroxy-2(R)-[[(4-methoxyphenyl)sulfonyl](benzyl)- and (3-picolyl)-amino]-3-methyl-butanamide as Potential Tools for the Molecular Imaging of Activated MMPs with PET." In: *Journal of Medicinal Chemistry* 50.23 (2007), pp. 5752–5764. ISSN: 0022-2623. DOI: 10.1021/jm0708533. URL: https://doi.org/10.1021/jm0708533.

[73] N. Matusiak et al. "MicroPET Evaluation of a Hydroxamate-Based MMP Inhibitor, [18F]FB-ML5, in a Mouse Model of Cigarette Smoke-Induced Acute Airway Inflammation." In: *Molecular Imaging and Biology* 17.5 (2015), pp. 680–687. DOI: 10.1007/s11307-015-0847-3. URL: http://files/132/45-Matusiak-2015.pdf.

[74] N. Kondo et al. "Development of matrix metalloproteinase-targeted probes for lung inflammation detection with positron emission tomography." In: *Scientific Reports* 8.1 (2018), p. 1347. ISSN: 2045-2322. DOI: 10.1038/s41598-018-19890-1. URL: https://doi.org/10.1038/s41598-018-19890-1.

[75] A. Churg, D. D Sin, and J. L Wright. "Everything prevents emphysema: are animal models of cigarette smoke-induced chronic obstructive pulmonary disease any use?" eng. In: *American journal of respiratory cell and molecular biology* 45.6 (2011), pp. 1111–1115. ISSN: 1535-4989 1044-1549. DOI: 10.1165/rcmb.2011-0087PS.

[76] A Churg, S Zhou, and J L Wright. "Matrix metalloproteinases in COPD." In: *European Respiratory Journal* 39.1 (2012), p. 197. DOI: 10.1183/09031936.00121611. URL: http://erj.ersjournals.com/content/39/1/197.abstract.

[77] R B Banati, R Myers, and G W Kreutzberg. "The peripheral benzodiazepine binding sites in the CNS indicate early and discrete brain lesions: microautoradiographic detection of [3H]PK 11195 binding to activated microglia." In: *Journal of Neurocytology* 26.2 (1997), pp. 77–82. ISSN: 1573-7381. DOI: 10.1023/A:1018567510105. URL: https://doi.org/10.1023/A:1018567510105.

[78] D. L Chen, M. A Mintun, and D. P Schuster. "Comparison of methods to quantitate 18F-FDG uptake with PET during experimental acute lung injury." In: *Journal of Nuclear Medicine* 45.9 (2004), pp. 1583–1590. URL: http://eutils.ncbi.nlm.nih.gov/entrez/eutils/elink.fcgi?dbfrom=pubmed{\&}id=15347728{\&}retmode=ref{\&}cmd=prlinks{\&}holding=uwisclib{\&}otool=uwwisclib{\%}5Cnpapers3://publication/uuid/5FD37B7B-C73E-4DF5-B4B8-268E6AECA5A8.

[79] A. C Kuhlmann and T. R Guilarte. "The peripheral benzodiazepine receptor is a sensitive indicator of domoic acid neurotoxicity." In: *Brain Research* 751.2 (1997), pp. 281–288. ISSN: 0006-8993. DOI: 10.1016/S0006-8993(96)01409-6. URL: http://www.sciencedirect.com/science/article/pii/S0006899396014096.

[80] A C Kuhlmann and T R Guilarte. "Regional and temporal expression of the peripheral benzodiazepine receptor in MPTP neurotoxicity." In: *Toxicological Sciences* 48.1 (1999), pp. 107–116. ISSN: 1096-6080. DOI: 10.1093/toxsci/48.1.107. URL: https://doi.org/10.1093/toxsci/48.1.107.

[81] A. C Kuhlmann and T. R Guilarte. "Cellular and Subcellular Localization of Peripheral Benzodiazepine Receptors After Trimethyltin Neurotoxicity." In: *Journal of Neurochemistry* 74.4 (2000), pp. 1694–1704. ISSN: 0022-3042. DOI: 10.1046/j.1471-4159.2000.0741694.x. URL: https://doi.org/10.1046/j.1471-4159.2000.0741694.x.

[82] J. L Mankowski et al. "Elevated Peripheral Benzodiazepine Receptor Expression in Simian Immunodeficiency Virus Encephalitis." In: *Journal of Neurovirology* 9.1 (2003), pp. 94–100. ISSN: 1355-0284. DOI: 10.1080/13550280390173283. URL: http://link.springer.com/10.1080/13550280390173283.

[83] M. J Hardwick et al. "In vivo imaging of peripheral benzodiazepine receptors in mouse lungs: a biomarker of inflammation." In: *Molecular imaging* 4.4 (2005), pp. 432–438. ISSN: 1535-3508. URL: http://eutils.ncbi.nlm.nih.gov/entrez/eutils/elink.fcgi?dbfrom=pubmed{\&}id=16285905{\&}retmode=ref{\&}cmd=prlinks{\%}5Cnpapers3://publication/uuid/D3C456AA-01F8-42A6-B32C-7372A5B65833http://files/172/176-Hardwick-2005.pdf.

[84] J. Maeda et al. "Novel peripheral benzodiazepine receptor ligand [11C]DAA1106 for PET: An imaging tool for glial cells in the brain." In: *Synapse* 52.4 (2004), pp. 283–291. ISSN: 0887-4476. DOI: 10.1002/syn.20027. URL: https://doi.org/10.1002/syn.20027.

[85] K. Kumata et al. "Synthesis and evaluation of novel carbon-11 labeled oxopurine analogues for positron emission tomography imaging of translocator protein (18 kDa) in peripheral organs." In: *Journal of Medicinal Chemistry* 54.17 (2011), pp. 6040–6049. ISSN: 0022-2623. DOI: 10.1021/jm200516a. URL: http://files/218/114-Kumuata-2011.pdf.

[86] K. Yanamoto et al. "[18F]FEAC and [18F]FEDAC: Two novel positron emission tomography ligands for peripheral-type benzodiazepine receptor in the brain." In: *Bioorganic & Medicinal Chemistry Letters* 19.6 (2009), pp. 1707–1710. ISSN: 0960-894X. DOI: 10.1016/j.bmcl.2009.01.093. URL: http://www.sciencedirect.com/science/article/pii/S0960894X09001280.

[87] J. Yui et al. "18F-FEAC and 18F-FEDAC: PET of the Monkey Brain and Imaging of Translocator Protein (18 kDa) in the Infarcted Rat Brain." In: *Journal of Nuclear Medicine* 51.8 (2010), pp. 1301–1309. ISSN: 0161-5505. DOI: 10.2967/jnumed.109.072223. URL: http://jnm.snmjournals.org/cgi/doi/10.2967/jnumed.109.072223.

[88] K. Yanamoto et al. "In vivo imaging and quantitative analysis of TSPO in rat peripheral tissues using small-animal PET with [18F]FEDAC." In: *Nuclear Medicine and Biology* 37.7 (2010), pp. 853–860. ISSN: 0969-8051. DOI: 10.1016/j.nucmedbio.2010.04.183. URL: http://www.sciencedirect.com/science/article/pii/S0969805110002738.

[89] A. Hatori et al. "PET Imaging of Lung Inflammation with [18F]FEDAC, a Radioligand for Translocator Protein (18 kDa)." In: *PLoS ONE* 7.9 (2012). ISSN: 1932-6203. DOI: 10.1371/journal.pone.0045065. URL: http://files/134/98-Hatori-2012.pdf.

[90] N. de Prost et al. "Effects of ventilation strategy on distribution of lung inflammatory cell activity." In: *Critical Care* 17.4 (2013), R175–R175. ISSN: 1466-609X (Electronic)\r1364-8535 (Linking). DOI: 10.1186/cc12854. URL: http://ccforum.com/content/17/4/R175http://files/186/72-DeProst-2013.pdf.

[91] L H Brudin et al. "Regional lung density and blood volume in nonsmoking and smoking subjects measured by PET." In: *J Appl Physiol* 63.4 (1987), pp. 1324–1334. ISSN: 8750-7587. DOI: 10.1152/jappl.1987.63.4.1324. URL: http://files/270/Brudinetal(1987)-RegionallungdensitymeasuredbyPET.pdf.

[92] SJ Chung et al. "Invivo imaging of activated macrophages by 18F-FEDAC, a TSPO targeting PET ligand, in the use of biologic disease-modifying antirheumatic drugs (bDMARDs)." In: *Biochemical and Biophysical Research Communications* 506.1 (2018), pp. 216–222. ISSN: 0006-291X. DOI: 10.1016/j.bbrc.

2018.10.083. URL: http://www.sciencedirect.com/science/article/pii/S0006291X18322393.

[93] A. Hatori et al. "Utility of Translocator Protein (18?kDa) as a Molecular Imaging Biomarker to Monitor the Progression of Liver Fibrosis." eng. In: *Scientific reports* 5 (2015), p. 17327. ISSN: 2045-2322. DOI: 10.1038/srep17327. URL: https://www.ncbi.nlm.nih.gov/pubmed/26612465https://www.ncbi.nlm.nih.gov/pmc/articles/PMC4661446/.

[94] A. K Brown et al. "Radiation dosimetry and biodistribution in monkey and man of 11C-PBR28: a PET radioligand to image inflammation." eng. In: *Journal of nuclear medicine : official publication, Society of Nuclear Medicine* 48.12 (2007), pp. 2072–2079. ISSN: 0161-5505 0161-5505. DOI: 10.2967/jnumed.107.044842.

[95] M. Schain and W.C. Kreisl. "Neuroinflammation in Neurodegenerative Disorders?a Review." In: *Current Neurology and Neuroscience Reports* 17.3 (2017), p. 25. ISSN: 1534-6293. DOI: 10.1007/s11910-017-0733-2. URL: https://doi.org/10.1007/s11910-017-0733-2.

[96] D. R Owen et al. "Two binding sites for [3H]PBR28 in human brain: implications for TSPO PET imaging of neuroinflammation." eng. In: *Journal of cerebral blood flow and metabolism : official journal of the International Society of Cerebral Blood Flow and Metabolism* 30.9 (2010), pp. 1608–1618. ISSN: 1559-7016. DOI: 10.1038/jcbfm.2010.63. URL: https://www.ncbi.nlm.nih.gov/pubmed/20424634https://www.ncbi.nlm.nih.gov/pmc/articles/PMC2949260/.

[97] J C Mak and P J Barnes. "Peripheral type benzodiazepine receptors in human and guinea pig lung: characterization and autoradiographic mapping." In: *Journal of Pharmacology and Experimental Therapeutics* 252.2 (1990), p. 880. URL: http://jpet.aspetjournals.org/content/252/2/880.abstract.

[98] J W Babich, Q Dong, and W Graham. "A novel high affinity chemotactic peptide antagonist for infection imaging." In: *Journal of Nuclear Medicine* 38 (1997), 268P.

[99] Y. Zhang et al. "Synthesis of novel neutrophil-specific imaging agents for Positron Emission Tomography (PET) imaging." In: *Bioorganic and Medicinal Chemistry Letters* 17.24 (2007), pp. 6876–6878. DOI: 10.1016/j.bmcl.2007.10.013. URL: http://files/166/155-Zhang-2007.pdf.

[100] L W Locke et al. "A Novel Neutrophil-Specific PET Imaging Agent: cFLFLFK-PEG-64Cu." In: *Journal of Nuclear Medicine* 50.5 (2009), pp. 790–797. DOI: 10.2967/jnumed.108.056127. URL: http://jnm.snmjournals.org/cgi/doi/10.2967/jnumed.108.056127http://files/160/144-Locke-2009.pdf.

[101] Y. Zhang et al. "PET imaging detection of macrophages with a formyl peptide receptor antagonist." eng. In: *Nuclear medicine and biology* 42.4 (2015), pp. 381–386. ISSN: 1872-9614. DOI: 10.1016/j.nucmedbio.2014.12.001. URL: https://pubmed.ncbi.nlm.nih.gov/25532700https://www.ncbi.nlm.nih.gov/pmc/articles/PMC4405787/.

[102] I. F Charo and R. M Ransohoff. "The Many Roles of Chemokines and Chemokine Receptors in Inflammation." In: *New England Journal of Medicine* 354.6 (2006), pp. 610–621. ISSN: 0028-4793. DOI: 10.1056/NEJMra052723. URL: https://doi.org/10.1056/NEJMra052723.

[103] T. Tomankova, E. Kriegova, and M. Liu. "Chemokine receptors and their therapeutic opportunities in diseased lung: Far beyond leukocyte trafficking." In: *American Journal of Physiology-Lung Cellular and Molecular Physiology* 308.7 (2015), pp. L603–L618. ISSN: 1040-0605. DOI: 10.1152/ajplung.00203.2014. URL: https://doi.org/10.1152/ajplung.00203.2014.

[104] S L Traves et al. "Increased levels of the chemokines GROalpha and MCP-1 in sputum samples from patients with COPD." eng. In: *Thorax* 57.7 (2002), pp. 590–595. ISSN: 0040-6376. DOI: 10.1136/thorax.57.7.590. URL: https://www.ncbi.nlm.nih.gov/pubmed/12096201https://www.ncbi.nlm.nih.gov/pmc/articles/PMC1746378/.

[105] W.I de Boer et al. "Monocyte chemoattractant protein 1, interleukin 8, and chronic airways inflammation in COPD." In: *The Journal of Pathology* 190.5 (2000), pp. 619–626. ISSN: 0022-3417. DOI: 10.1002/(SICI)1096-9896(200004)190:5<619::AID-PATH555>3.0.CO;2-6. URL: https://doi.org/10.1002/(SICI)1096-9896(200004)190:5{\%}3C619::AID-PATH555{\%}3E3.0.COhttp://2-6.

[106] C. Auvynet et al. "ECL1i, d(LGTFLKC), a novel, small peptide that specifically inhibits CCL2-dependent migration." In: *The FASEB Journal* 30.6 (2016), pp. 2370–2381. ISSN: 0892-6638. DOI: 10.1096/fj.201500116. URL: https://doi.org/10.1096/fj.201500116.

[107] Y Liu et al. "Noninvasive Imaging of CCR2+ Cells in Ischemia-Reperfusion Injury After Lung Transplantation." In: *American Journal of Transplantation* 16.10 (2016), pp. 3016–3023. ISSN: 1600-6135. DOI: 10.1111/ajt.13907. URL: https://doi.org/10.1111/ajt.13907.

[108] Y. Liu et al. "PET-based Imaging of Chemokine Receptor 2 in Experimental and Disease-related Lung Inflammation." In: *Radiology* 283.3 (2017), pp. 758–768. DOI: 10.1148/radiol.2016161409. URL: http://pubs.rsna.org/doi/10.1148/radiol.2016161409http://files/176/4-Liu-2017.pdf.

[109] K. F Rabe and H. Watz. "Chronic obstructive pulmonary disease." In: *The Lancet* 389.10082 (2017), pp. 1931–1940. DOI: 10.1016/S0140-6736(17)31222-9. URL: https://www.tandfonline.com/doi/full/10.1080/15412555.2018.1464551http://files/51/Rabe-copdlancet2017.pdf.

[110] M. Defrise, P. E Kinahan, and C. J Michel. "Image Reconstruction Algorithms in PET BT - Positron Emission Tomography: Basic Sciences." In: ed. by Dale L Bailey et al. London: Springer London, 2005, pp. 63–91. ISBN: 978-1-84628-007-8. DOI: 10.1007/1-84628-007-9_4. URL: https://doi.org/10.1007/1-84628-007-9{_}4.

[111] J. J. Vaquero and P. Kinahan. "Positron Emission Tomography: Current Challenges and Opportunities for Technological Advances in Clinical and Preclinical Imaging Systems." In: *Annual Review of Biomedical Engineering* 17.1 (2015), pp. 385–414. ISSN: 1523-9829. DOI: 10.1146/annurev-bioeng-071114-040723.

[112] T. Pan et al. "Attenuation correction of PET images with respiration-averaged CT images in PET/CT." eng. In: *Journal of nuclear medicine : official publication, Society of Nuclear Medicine* 46.9 (2005), pp. 1481–1487. ISSN: 0161-5505 (Print).

[113] A. M Alessio et al. "Cine CT for attenuation correction in cardiac PET/CT." eng. In: *Journal of nuclear medicine : official publication, Society of Nuclear Medicine* 48.5 (2007), pp. 794–801. ISSN: 0161-5505. DOI: 10.2967/jnumed.106.035717. URL: https://pubmed.ncbi.nlm.nih.gov/17475969https://www.ncbi.nlm.nih.gov/pmc/articles/PMC2585486/.

[114] B. F Holman et al. "The effect of respiratory induced density variations on non-TOF PET quantitation in the lung." In: *Physics in medicine and biology* 61.8 (2016), pp. 3148–3163. ISSN: 1361-6560 (Electronic). DOI: 10.1088/0031-9155/61/8/3148. URL: http://dx.doi.org/10.1088/0031-9155/61/8/3148.

[115] S. A. Nehmeh and Y.E. Erdi. "Respiratory Motion in Positron Emission Tomography/Computed Tomography: A Review." In: *Seminars in Nuclear Medicine* 38.3 (2008), pp. 167–176. ISSN: 00012998. DOI: 10.1053/j.semnuclmed.2008.01.002.

[116] R. Boellaard et al. "FDG PET/CT: EANM procedure guidelines for tumour imaging: version 2.0." In: *European Journal of Nuclear Medicine and Molecular Imaging* 42.2 (2014), pp. 328–354. ISSN: 16197089. DOI: 10.1007/s00259-014-2961-x.

[117] V. J Lowe et al. "Optimum scanning protocol for FDG-PET evaluation of pulmonary malignancy." In: *Lung Cancer* 13.2 (2004), p. 204. ISSN: 01695002. DOI: 10.1016/0169-5002(95)90601-0.

[118] K R Zasadny and R L Wahl. "Standardized uptake values of normal tissues at PET with 2-[fluorine-18]-fluoro-2-deoxy-D-glucose: variations with body weight and a method for correction." In: *Radiology* 189.3 (1993), pp. 847–850. ISSN: 0033-8419. DOI: 10.1148/radiology.189.3.8234714. URL: https://doi.org/10.1148/radiology.189.3.8234714.

[119] D. L Chen, M. A Mintun, and D.P Schuster. "Comparison of methods to quantitate 18F-FDG uptake with PET during experimental acute lung injury." In: *Journal of Nuclear Medicine* 45.9 (2004), pp. 1583–1590. ISSN: 01615505. URL: http://www.scopus.com/inward/record.url?eid=2-s2.0-6944226158{\&}partnerID=40{\&}md5=57271b9df9e1f70db21327cd61e8ccf2.

[120] R N Gunn, S R Gunn, and V J Cunningham. "Positron emission tomography compartmental models." In: *Journal of cerebral blood flow and metabolism : official journal of the International Society of Cerebral Blood Flow and Metabolism* 21.6 (2001), pp. 635–652. ISSN: 0271-678X. DOI: 10.1097/00004647-200106000-00002.

[121] L Sokoloff, M Reivich, and C Kennedy. "The [14C]deoxyglucose method for the measurement of local cerebral glucose utilization: theory, procedure, and normal values in the conscious and anesthetized albino rat." In: *Journal of Neurochemistry* 28.5 (1977), pp. 897–916. ISSN: 0022-3042. URL: http://www.scopus.com/inward/record.url?eid=2-s2.0-0017368491{\&}partnerID=40{\&}md5=3158d54b116f5df1ed0d9f00f07e6ac9{\%}5Cnhttp://www.embase.com/search/results?subaction=viewrecord{\&}from=export{\&}id=L8098854{\%}5Cnhttp://sfx.library.uu.nl/utrecht?sid=EMBASE{\&}issn=002230.

[122] Tobias S. et al. "Modelling pulmonary kinetics of 2-deoxy-2-[18F]fluoro-D-glucose during acute lung injury." In: *Anat Rec (Hoboken_* 15.6 (2008), pp. 763–775. ISSN: 1097-4164. DOI: 10.1002/ar.20849.3D. arXiv: NIHMS150003.

[123] R. E. Carson. "Precision and Accuracy Considerations of Physiological Quantitation in PET." In: *Journal of Cerebral Blood Flow & Metabolism* 11.1_suppl (2011), A45–A50. ISSN: 0271-678X. DOI: 10.1038/jcbfm.1991.36.

[124] L.F. De Geus-Oei et al. "Comparison of Image-Derived and Arterial Input Functions for Estimating the Rate of Glucose Metabolism in Therapy-Monitoring 18F-FDG PET Studies." In: *Journal of Nuclear Medicine* 47.6 (2006), pp. 945–949. ISSN: 0161-5505. DOI: 47/6/945[pii]. URL: http://jnm.snmjournals.org/content/47/6/945.abstract.

[125] A P van der Weerdt et al. "Image-derived input functions for determination of MRGlu in cardiac (18)F-FDG PET scans." In: *Journal of nuclear medicine : official publication, Society of Nuclear Medicine* 42.11 (2001), pp. 1622–9. ISSN: 0161-5505. URL: http://www.ncbi.nlm.nih.gov/pubmed/11696630.

[126] B. Holman, B. Hutton, and K Thielemans. "Method to determine the voxel-wise blood volume in the lung from dynamic PET data." In: *The Journal of Nuclear Medicine* 58.Supplement 1 (2017), p. 1310.

[127] T. Schroeder et al. "Image-Derived Input Function for Assessment of 18F-FDG Uptake by the Inflamed Lung." In: *Journal of Nuclear Medicine* 48.11 (2007), pp. 1889–1896. ISSN: 0161-5505. DOI: 10.2967/jnumed.107.041079. URL: http://jnm.snmjournals.org/cgi/doi/10.2967/jnumed.107.041079.

[128] D. Vriens et al. "A Curve-Fitting Approach to Estimate the Arterial Plasma Input Function for the Assessment of Glucose Metabolic Rate and Response to Treatment." In: *Journal of Nuclear Medicine* 50.12 (2009), pp. 1933–1939. ISSN: 0161-5505. DOI: 10.2967/jnumed.109.065243.

[129] Y. Hori et al. "Noninvasive quantification of cerebral metabolic rate for glucose in rats using 18 F-FDG PET and standard input function." In: *Journal of Cerebral Blood Flow and Metabolism* 35.10 (2015), pp. 1664–1670. ISSN: 15597016. DOI: 10.1038/jcbfm.2015.104. URL: http://dx.doi.org/10.1038/jcbfm.2015.104.

[130] H. Guo, R. A. Renaut, and K. Chen. "An input function estimation method for FDG-PET human brain studies." In: *Nuclear Medicine and Biology* 34.5 (2007), pp. 483–492. ISSN: 09698051. DOI: 10.1016/j.nucmedbio.2007.03.008. eprint: NIHMS150003. URL: https://linkinghub.elsevier.com/retrieve/pii/S0969805107000868.

[131] J. E M Mourik et al. "Partial volume corrected image derived input functions for dynamic PET brain studies: Methodology and validation for [11C]flumazenil." In: *NeuroImage* 39.3 (2008), pp. 1041–1050. ISSN: 10538119. DOI: 10.1016/j.neuroimage.2007.10.022.

[132] Y. Kimura et al. "Extraction of a Plasma Time-Activity Curve From Dynamic Brain PET Images Based on Independent Component Analysis." In: *IEEE Transactions on Biomedical Engineering* 52.2 (2005), pp. 201–210. ISSN: 0018-9294. DOI: 10.1109/tbme.2004.840193.

[133] S. Zhou et al. "A method for generating image-derived input function in quantitative 18F-FDG PET study based on the monotonicity of the input and output function curve." In: *Nuclear Medicine Communications* 33.4 (2012), pp. 362–370. ISSN: 0143-3636. DOI: 10.1097/MNM.0b013e32834f262e. URL: https://insights.ovid.com/crossref?an=00006231-201204000-00003.

[134] P Herscovitch, J Markham, and M E Raichle. "Brain blood flow measured with intravenous H2(15)O. I. Theory and error analysis." In: *Journal of nuclear medicine : official publication, Society of Nuclear Medicine* 24.9 (1983), pp. 782–9. ISSN: 0161-5505. URL: http://www.ncbi.nlm.nih.gov/pubmed/6604139.

[135] E Meyer. "Simultaneous correction for tracer arrival delay and dispersion in CBF measurements by the H215O autoradiographic method and dynamic PET." In: *Journal of Nuclear Medicine* 30.6 (1989), pp. 1069–78. ISSN: 0161-5505. URL: http://www.ncbi.nlm.nih.gov/pubmed/2786948.

[136] J Van den Hoff et al. "Accurate local blood flow measurements with dynamic PET: fast determination of input function delay and dispersion by multilinear minimization." In: *Journal of Nuclear Medicine* 34.10 (1993), pp. 1770–7. ISSN: 0161-5505. URL: http://www.ncbi.nlm.nih.gov/pubmed/8410297.

[137] M. F. Alf et al. "FDG kinetic modeling in small rodent brain PET: Optimization of data acquisition and analysis." In: *EJNMMI Research* 3.1 (2013), pp. 1–14. ISSN: 2191219X. DOI: 10.1186/2191-219X-3-61.

[138] T. J. Wellman, T. Winkler, and M. F. Vidal Melo. "Modeling of Tracer Transport Delays for Improved Quantification of Regional Pulmonary 18F-FDG Kinetics, Vascular Transit Times, and Perfusion." In: *Annals of Biomedical Engineering* 43.11 (2015), pp. 2722–2734. ISSN: 0090-6964. DOI: 10.1007/s10439-015-1327-2. URL: http://link.springer.com/10.1007/s10439-015-1327-2.

[139] A. R Blais and TY Lee. "Simulating the effect of venous dispersion on distribution volume measurements from the Logan plot." In: *Biomedical Physics & Engineering Express* 1.4 (2015), p. 45102. ISSN: 2057-1976. DOI: 10.1088/2057-1976/1/4/045102. URL: http://dx.doi.org/10.1088/2057-1976/1/4/045102.

[140] C. R. O'Donnell et al. "Comparison of plethysmographic and helium dilution lung volumes: Which is best for COPD?" In: *Chest* 137.5 (2010), pp. 1108–1115. ISSN: 00123692. DOI: 10.1378/chest.09-1504.

[141] C. S. Patlak, R. G. Blasberg, and J. D. Fenstermacher. "Graphical evaluation of blood-to-brain transfer constants from multiple-time uptake data." In: *Journal of Cerebral Blood Flow and Metabolism* 3.1 (1983), pp. 1–7. ISSN: 0271678X. DOI: 10.1038/jcbfm.1983.1.

[142] J. Wanger et al. "Standardisation of the measurement of lung volumes." In: *European Respiratory Journal* 26.3 (2005), pp. 511–522. ISSN: 09031936. DOI: 10.1183/09031936.05.00035005.

[143] R. Boellaard et al. "FDG PET and PET/CT: EANM procedure guidelines for tumour PET imaging: version 1.0." eng. In: *European journal of nuclear medicine and molecular imaging* 37.1 (2010), pp. 181–200. ISSN: 1619-7089. DOI: 10.1007/s00259-009-1297-4. URL: https://pubmed.ncbi.nlm.nih.gov/19915839https://www.ncbi.nlm.nih.gov/pmc/articles/PMC2791475/.

[144] R. Boellaard, Arthur van Lingen, and Adriaan A Lammertsma. "Experimental and Clinical Evaluation of Iterative Reconstruction (OSEM) in Dynamic PET: Quantitative Characteristics and Effects on Kinetic Modeling." In: *Journal of Nuclear Medicine* 42.5 (2001), 808 LP –817. URL: http://jnm.snmjournals.org/content/42/5/808.abstract.

[145] MATLAB. *version 7.10.0 (R2010a)*. Natick, Massachusetts: The MathWorks Inc., 2010.

[146] P. A Yushkevich et al. "User-guided 3D active contour segmentation of anatomical structures: Significantly improved efficiency and reliability." In: *NeuroImage* 31.3 (2006), pp. 1116–1128. ISSN: 1053-8119 (Print). DOI: 10.1016/j.neuroimage.2006.01.015. URL: http://files/228/ITK-snapalgorithm.pdf.

[147] V. J. Cunningham et al. "Positron Emission Tomography Compartmental Models: A Basis Pursuit Strategy for Kinetic Modeling." In: *Journal of Cerebral Blood Flow & Metabolism* 22.12 (2015), pp. 1425–1439. ISSN: 0271-678X. DOI: 10.1097/01.wcb.0000045042.03034.42.

[148] R Core Team. *R: A Language and Environment for Statistical Computing*. R Foundation for Statistical Computing. Vienna, Austria, 2017. URL: https://www.R-project.org/.

[149] P. J. Barnes. "Cellular and molecular mechanisms of chronic obstructive pulmonary disease." In: *Clinics in Chest Medicine* 35.1 (2014), pp. 71–86. ISSN: 02725231. DOI: 10.1016/j.ccm.2013.10.004. URL: http://dx.doi.org/10.1016/j.ccm.2013.10.004.

[150] R. Faner, T. Cruz, and A. Agusti. "Immune response in chronic obstructive pulmonary disease." In: *Expert Review of Clinical Immunology* 9.9 (2013), pp. 821–833. DOI: 10.1586/1744666X.2013.828875. URL: https://doi.org/10.1586/1744666X.2013.828875.

[151] P Gutierrez et al. "Macrophage activation in exacerbated COPD with and without community-acquired pneumonia." In: *European Respiratory Journal* 36.2 (2010), pp. 285–291. ISSN: 0903-1936. DOI: 10.1183/09031936.00118909. URL: https://erj.ersjournals.com/content/36/2/285.

[152] P. W. Jones and A. G.N. Agusti. "Outcomes and markers in the assessment of chronic obstructive pulmonary disease." In: *European Respiratory Journal* 27.4 (2006), pp. 822–832. ISSN: 09031936. DOI: 10.1183/09031936.06.00145104.

[153] K. Jörgensen et al. "Reduced intrathoracic blood volume and left and right ventricular dimensions in patients with severe emphysema: An MRI study." In: *Chest* 131.4 (2007), pp. 1050–1057. ISSN: 00123692. DOI: 10.1378/chest.06-2245.

[154] M. Fisk et al. "Evaluation of losmapimod in patients with chronic obstructive pulmonary disease (COPD) with systemic inflammation stratified using fibrinogen ('EVOLUTION'): RATIONALE and protocol." In: *Artery Research* 8.1 (2014), pp. 24–34. ISSN: 18729312. DOI: 10.1016/j.artres.2013.10.380.

[155] M. Fisk et al. "The p38 mitogen activated protein kinase inhibitor losmapimod in chronic obstructive pulmonary disease patients with systemic inflammation, stratified by fibrinogen: A randomised double-blind placebo-controlled trial." In: *PLoS ONE* 13.3 (2018), pp. 1–17. ISSN: 19326203. DOI: 10.1371/journal.pone.0194197.

[156] J D Newell, J C Hogg, and G L Snider. "Report of a workshop: Quantitative computed tomography scanning in longitudinal studies of emphysema." In: *European Respiratory Journal* 23.5 (2004), pp. 769–775. ISSN: 0903-1936 (Print) 0903-1936 (Linking). DOI: 10.1183/09031936.04.00026504.

[157] MIAKAT. *version 4.2.6*. Hammersmith Hospital: Invicro ltd, 2010.

[158] Paul A. Y. et al. "User-Guided 3D Active Contour Segmentation of Anatomical Structures: Significantly Improved Efficiency and Reliability." In: *Neuroimage* 31.3 (2006), pp. 1116–1128.

[159] J M. Bland and D. G. Altman. "STATISTICAL METHODS FOR ASSESSING AGREEMENT BETWEEN TWO METHODS OF CLINICAL MEASUREMENT." In: *The Lancet* 327.8476 (1986), pp. 307–310. ISSN: 0140-6736. DOI: https://doi.org/10.1016/S0140-6736(86)90837-8. URL: http://www.sciencedirect.com/science/article/pii/S0140673686908378.

[160] B. E. Miller et al. "Plasma fibrinogen qualification as a drug development tool in chronic obstructive pulmonary disease: Perspective of the chronic obstructive pulmonary disease biomarker qualification consortium." In: *American Journal of Respiratory and Critical Care Medicine* 193.6 (2016), pp. 607–613. ISSN: 15354970. DOI: 10.1164/rccm.201509-1722PP.

[161] P. J S. Haidaris. "Induction of Fibrinogen Biosynthesis and Secretion from Cultured Pulmonary Epithelial Cells." In: *Blood* 89 (1997), pp. 873–882.

[162] S. O Lawrence and P. J Simpson-Haidaris. "Regulated de novo biosynthesis of fibrinogen in extrahepatic epithelial cells in response to inflammation." In: *Thrombosis and Haemostasis* 92.2 (2004), pp. 234–243. ISSN: 03406245. DOI: 10.1160/TH04-01-0024. URL: http://files/47/fibrinogensynethesis.pdf.

[163] H.A Jones et al. "Dissociation Between Respiratory Burst Activity and Deoxyglucose Uptake in Human Neutrophil Granulocytes : Implications for Interpretation of 18F-FDG PET Images." In: *Journal of Nuclear Medicine* 43.5 (2002), pp. 652–657.

[164] C. Gourab. "Role of 18F-FDG PET/CT as a novel non-invasive biomarker of inflammation in Chronic Obstructive Pulmonary Disease." PhD thesis. PhD thesis. University of Edinburgh, 2018.

[165] S. Santos et al. "Treatment of patients with COPD and recurrent exacerbations: the role of infection and inflammation." eng. In: *International journal of chronic obstructive pulmonary disease* 11 (2016), pp. 515–525. ISSN: 1178-2005. DOI: 10.2147/COPD.S98333. URL: https://pubmed.ncbi.nlm.nih.gov/27042040https://www.ncbi.nlm.nih.gov/pmc/articles/PMC4795571/.

[166] T. J Fraum et al. "Measurement Repeatability of (18)F-FDG PET/CT Versus (18)F-FDG PET/MRI in Solid Tumors of the Pelvis." eng. In: *Journal of nuclear medicine : official publication, Society of Nuclear Medicine* 60.8 (2019), pp. 1080–1086. ISSN: 1535-5667 (Electronic). DOI: 10.2967/jnumed.118.218735.

[167] C. Lin et al. "Repeatability of Quantitative 18F-NaF PET: A Multicenter Study." eng. In: *Journal of nuclear medicine : official publication, Society of Nuclear Medicine* 57.12 (2016), pp. 1872–1879. ISSN: 1535-5667 (Electronic). DOI: 10.2967/jnumed.116.177295.

[168] R. K. Doot et al. "Instrumentation factors affecting variance and bias of quantifying tracer uptake with PET/CT." In: *Medical Physics* 37.11 (2010), pp. 6035–6046. ISSN: 00942405. DOI: 10.1118/1.3499298. arXiv: NIHMS150003.

[169] C. Nahmias et al. "Equilibration of 6-[18F]Fluoro-L-m-Tyrosine Between Plasma and Erythrocytes." In: *Journal of Nuclear Medicine* 41.10 (2000), pp. 1636–1641.

[170] M. Yaqub et al. "Optimization algorithms and weighting factors for analysis of dynamic PET studies." In: *Physics in medicine and biology* 51.17 (2006), pp. 4217–4232. ISSN: 0031-9155. DOI: 10.1088/0031-9155/51/17/007. URL: http://stacks.iop.org/0031-9155/51/.

[171] M. K Han et al. "Chronic obstructive pulmonary disease phenotypes: the future of COPD." eng. In: *American journal of respiratory and critical care medicine* 182.5 (2010), pp. 598–604. ISSN: 1535-4970 (Electronic). DOI: 10.1164/rccm.200912-1843CC.

[172] J. L. Lopez-Campos et al. "Moving Towards Patient-Centered Medicine for COPD Management: Multidimensional Approaches versus Phenotype-Based Medicine?A Critical View." In: *COPD: Journal of Chronic Obstructive Pulmonary Disease* 11.5 (2014), pp. 591–602. ISSN: 1541-2555. DOI: 10.3109/15412555.2014.898035. URL: https://doi.org/10.3109/15412555.2014.898035.

[173] M. Kirby et al. "Management of COPD: Is there a role for quantitative imaging?" In: *European Journal of Radiology* 86 (2017), pp. 335–342. ISSN: 18727727. DOI: 10.1016/j.ejrad.2016.08.022.

[174] G A Gould et al. "CT Measurements of Lung Density in Life Can Quantitate Distal Airspace Enlargement?An Essential Defining Feature of Human Emphysema." In: *American Review of Respiratory Disease* 137.2 (1988), pp. 380–392. ISSN: 0003-0805. DOI: 10.1164/ajrccm/137.2.380. URL: https://doi.org/10.1164/ajrccm/137.2.380.

[175] D G Parr et al. "Validation of computed tomographic lung densitometry for monitoring emphysema in alpha1-antitrypsin deficiency." eng. In: *Thorax* 61.6 (2006), pp. 485–490. ISSN: 0040-6376. DOI: 10.1136/thx.2005.054890. URL: https://pubmed.ncbi.nlm.nih.gov/16537666https://www.ncbi.nlm.nih.gov/pmc/articles/PMC2111224/.

[176] D. A. Lynch et al. "CT-based visual classification of emphysema: Association with mortality in the COPDGene study." In: *Radiology* 288.3 (2018), pp. 859–866. ISSN: 15271315. DOI: 10.1148/radiol.2018172294.

[177] J. Park et al. "Subtyping COPD by Using Visual and Quantitative CT Imaging Features." In: *Chest* 157.1 (2020), pp. 47–60. ISSN: 19313543. DOI: 10.1016/j.chest.2019.06.015.

[178] Horos software. Annapolis, MD USA. URL: https://www.Horosproject.org/.

[179] D.A. Lynch et al. "CT-definable subtypes of chronic obstructive pulmonary disease: A statement of the fleischner society." In: *Radiology* 277.1 (2015), pp. 192–205. ISSN: 15271315. DOI: 10.1148/radiol.2015141579.

[180] A. Johannessen et al. "Mortality by Level of Emphysema and Airway Wall Thickness." In: *American Journal of Respiratory and Critical Care Medicine* 187.6 (2013), pp. 602–608. ISSN: 1073-449X. DOI: 10.1164/rccm.201209-1722OC. URL: https://doi.org/10.1164/rccm.201209-1722OC.

[181] E. C Oelsner et al. "Per cent emphysema is associated with respiratory and lung cancer mortality in the general population: a cohort study." In: *Thorax* 71.7 (2016), 624 LP –632. DOI: 10.1136/thoraxjnl-2015-207822. URL: http://thorax.bmj.com/content/71/7/624.abstract.

[182] J. Grunewald et al. eng. In: *Nature reviews. Disease primers* 1 (). ISSN: 2056-676X (Electronic). DOI: 10.1038/s41572-019-0096-x.

[183] R. P Baughman, Daniel A Culver, and Marc A Judson. "A Concise Review of Pulmonary Sarcoidosis." In: *American Journal of Respiratory and Critical Care Medicine* 183.5 (2011), pp. 573–581. ISSN: 1073-449X. DOI: 10.1164/rccm.201006-0865CI. URL: https://doi.org/10.1164/rccm.201006-0865CI.

[184] D. Valeyre et al. "Sarcoidosis." In: *The Lancet* 383.9923 (2014), pp. 1155–1167. ISSN: 0140-6736. DOI: https://doi.org/10.1016/S0140-6736(13)60680-7. URL: http://www.sciencedirect.com/science/article/pii/S0140673613606807.

[185] S. Barrington, P. Blower, and G. Cook. "New horizons in multimodality molecular imaging and novel radiotracers." In: *Clinical Medicine* 17.5 (2017), 444 LP –448. DOI: 10.7861/clinmedicine.17-5-444. URL: http://www.rcpjournals.org/content/17/5/444.abstract.

[186] R G M Keijsers et al. "18F-FDG PET in sarcoidosis: an observational study in 12 patients treated with infliximab." eng. In: *Sarcoidosis, vasculitis, and diffuse lung diseases : official journal of WASOG* 25.2 (2008), pp. 143–149. ISSN: 1124-0490 (Print).

[187] J. J. Braun et al. "18F-FDG PET/CT in sarcoidosis management: review and report of 20 cases." eng. In: *European journal of nuclear medicine and molecular imaging* 35.8 (2008), pp. 1537–1543. ISSN: 1619-7070 (Print). DOI: 10.1007/s00259-008-0770-9.

[188] "Consensus conference: activity of sarcoidosis. Third WASOG meeting, Los Angeles, USA, September 8-11, 1993." eng. In: *The European respiratory journal* 7.3 (1994), pp. 624–627. ISSN: 0903-1936 (Print).

[189] A Balan et al. "Multi-technique imaging of sarcoidosis." eng. In: *Clinical radiology* 65.9 (2010), pp. 750–760. ISSN: 1365-229X (Electronic). DOI: 10.1016/j.crad.2010.03.014.

[190] G Treglia, S Taralli, and A Giordano. "Emerging role of whole-body ^{18}F-FDG positron emission tomography as a marker of disease activity in patients with sarcoidosis: a systematic review." eng. In: *Sarcoidosis, vasculitis, and diffuse lung diseases : official journal of WASOG* 28.2 (2011), pp. 87–94. ISSN: 1124-0490 (Print).

[191] G. Youssef et al. "The use of 18F-FDG PET in the diagnosis of cardiac sarcoidosis: a systematic review and metaanalysis including the Ontario experience." eng. In: *Journal of nuclear medicine : official publication, Society of Nuclear Medicine* 53.2 (2012), pp. 241–248. ISSN: 1535-5667 (Electronic). DOI: 10.2967/jnumed.111.090662.

[192] R G Keijsers et al. "Imaging the inflammatory activity of sarcoidosis: sensitivity and inter observer agreement of (67)Ga imaging and (18)F-FDG PET." eng. In: *The quarterly journal of nuclear medicine and molecular imaging : official publication of the Italian Association of Nuclear Medicine (AIMN) [and] the International Association of Radiopharmacology (IAR), [and] Section of the Society of...* 55.1 (2011), pp. 66–71. ISSN: 1824-4785 (Print).

[193] Y. Nishiyama et al. "Comparative evaluation of 18F-FDG PET and 67Ga scintigraphy in patients with sarcoidosis." eng. In: *Journal of nuclear medicine : official publication, Society of Nuclear Medicine* 47.10 (2006), pp. 1571–1576. ISSN: 0161-5505 (Print).

[194] A. S Teirstein et al. "Results of 188 whole-body fluorodeoxyglucose positron emission tomography scans in 137 patients with sarcoidosis." eng. In: *Chest* 132.6 (2007), pp. 1949–1953. ISSN: 0012-3692 (Print). DOI: 10.1378/chest.07-1178.

[195] M. C Schimmelpennink et al. "Quantification of pulmonary disease activity in sarcoidosis measured with F-FDG PET / CT : SUVmax versus total lung glycolysis." In: (2019), pp. 1–7.

[196] D. Sobic-Saranovic et al. "The utility of 18F-FDG PET/CT for diagnosis and adjustment of therapy in patients with active chronic sarcoidosis." eng. In: *Journal of nuclear medicine : official publication, Society of Nuclear Medicine* 53.10 (2012), pp. 1543–1549. ISSN: 1535-5667 (Electronic). DOI: 10.2967/jnumed.112.104380.

[197] D. L Chen and D. P Schuster. "Positron emission tomography with [18F]FDG to evaluate neutrophil kinetics during acute lung injury." In: *American journal of physiology. Lung cellular and molecular physiology* 286 (2004), pp. L834–L840. ISSN: 1040-0605 (Print). DOI: 10.1152/ajplung.00339.2003.

[198] Z. Zhou et al. "Molecular imaging of lung glucose uptake after endotoxin in mice." In: *American journal of physiology. Lung cellular and molecular physiology* 289.5 (2005), pp. L760–L768. ISSN: 1040-0605 (Print)\r1040-0605 (Linking). DOI: 10.1152/ajplung.00146.2005. URL: http://www.ncbi.nlm.nih.gov/pubmed/15980036http://files/204/180-Zhou-2005.pdf.

[199] . URL: https://www.varian.com/products/radiotherapy/real-time-tracking-motion-management/real-time-position-management.

[200] G. Treglia et al. "The role of 18F-FDG-PET and PET/CT in patients with sarcoidosis: An updated evidence-based review." In: *Academic Radiology* 21.5 (2014), pp. 675–684. ISSN: 18784046. DOI: 10.1016/j.acra.2014.01.008. URL: http://dx.doi.org/10.1016/j.acra.2014.01.008.

[201] R L M Mostard et al. "Inflammatory activity assessment by F18 FDG-PET/CT in persistent symptomatic sarcoidosis." In: *Respiratory Medicine* 105.12 (2011), pp. 1917–1924. ISSN: 0954-6111. DOI: https://doi.org/10.1016/j.rmed.2011.08.012. URL: http://www.sciencedirect.com/science/article/pii/S0954611111002897.

[202] D L Chen and P E Kinahan. "Multimodality molecular imaging of the lung." In: *Journal of Magnetic Resonance Imaging* 6 (), pp. 1409–1420. DOI: 10.1002/jmri.22385.Multimodality.

[203] E. Danila et al. "BAL fluid cells in newly diagnosed pulmonary sarcoidosis with different clinical activity." eng. In: *Upsala journal of medical sciences* 114.1 (2009), pp. 26–31. ISSN: 2000-1967 (Electronic). DOI: 10.1080/03009730802579729.

[204] H A Jones et al. "In vivo measurement of neutrophil activity in experimental lung inflammation." In: *Am J Respir Crit Care Med* 149.6 (1994), pp. 1635–1639. URL: http://eutils.ncbi.nlm.nih.gov/entrez/eutils/elink.fcgi?dbfrom=pubmed{\&}id=7516252{\&}retmode=ref{\&}cmd=prlinks{\%}5Cnpapers2://publication/doi/10.1164/ajrccm.149.6.7516252http://files/220/200-jones-1994.pdf.

[205] H. A Jones et al. "Pulmonary fibrosis correlates with duration of tissue neutrophil activation." In: *American Journal of Respiratory and Critical Care Medicine* 158.2 (1998), pp. 620–628. ISSN: 1073-449X. DOI: 10.1164/ajrccm.158.2.9711075.

[206] C. Tsoumpas, F. E Turkheimer, and K. Thielemans. "Study of direct and indirect parametric estimation methods of linear models in dynamic positron emission tomography." In: *Medical Physics* 35.4 (2008), pp. 1299–1309. ISSN: 0094-2405. DOI: 10.1118/1.2885369. URL: https://doi.org/10.1118/1.2885369.

[207] X. Zhang et al. "Total-Body Dynamic Reconstruction and Parametric Imaging on the uEXPLORER." eng. In: *Journal of nuclear medicine : official publication, Society of Nuclear Medicine* 61.2 (2020), pp. 285–291. ISSN: 1535-5667 (Electronic). DOI: 10.2967/jnumed.119.230565.

[208] W. Wei et al. "ImmunoPET: Concept, Design, and Applications." In: *Chemical Reviews* 120.8 (2020), pp. 3787–3851. ISSN: 0009-2665. DOI: 10.1021/acs.chemrev.9b00738. URL: https://doi.org/10.1021/acs.chemrev.9b00738.